Coordination Chemistry Reviews 523 (2025) 216250

Contents lists available at ScienceDirect

Coordination Chemistry Reviews

journal homepage: www.elsevier.com/locate/ccr

Revisiting gold nanoshells as multifunctional biomedical nanotools

Antonio Topete [a,b,*,1], Alejandro Varela [a,1], Mariana Navarro-Real [b], Ramón Rial [c], Alberto Pardo [a,*], Pablo Taboada [a]

[a] Colloids and Polymers Physics Group, Particle Physics Department, Materials Institute (iMATUS) and Health Research Institute (IDIS), University of Santiago de Compostela, 15782 Santiago de Compostela, Spain
[b] Immunology Laboratory, Department of Physiology, University Center for Health Sciences (CUCS), University of Guadalajara, 44340 Guadalajara, Mexico
[c] Soft Matter and Molecular Biophysics Group, Applied Physics Department and Materials Institute (iMATUS), University of Santiago de Compostela, 15782 Santiago de Compostela, Spain

ARTICLE INFO

Keywords:
Gold nanoshells
Gold nanoparticles
Biological interactions
Photothermal therapy
Bioimaging
Biosensing
Theragnosis

ABSTRACT

The application of gold nanoparticles in the biomedical field has been widely explored in the last decades owing to their high biocompatibility, easy functionalization, and their structurally highly dependent optical properties. Among the different types of gold-based nanostructures, gold nanoshells (GNSs) are a particularly interesting option due to their complex dual structure, which allows the integration of several functionalities and a wide tunability of their optical response. Despite the remarkable progress made for the design of GNSs with the optimal characteristics for the intended application, the development of nanosystems that display the desired functionalities and preserve them in biological environments while showing effective targeting capability is still a challenge. In this review, the different synthetic routes proposed for the design of GNSs, their most remarkable optical properties, and the most relevant concerns associated with their interaction with biological systems are discussed. The application of these nanostructures for different diagnostic and/or therapeutic purposes is also reviewed. Finally, major remaining barriers to the clinical translation of GNSs and potential future directions of research in this field are critically commented.

1. Introduction

Over the last decades, metallic nanoparticles (NPs) have been widely proposed for many different applications, ranging from catalysis, cosmetics, or environmental remediation to more sophisticated uses in the biomedical field. In contrast to their bulk counterparts, nanoscale metallic structures show unique optical and physical features, which include high X-ray absorption coefficient, easy synthetic manipulation, and highly tunable electronic, magnetic and/or optical properties [1]. Among the different types of nanostructured metallic materials explored so far, gold nanoparticles (GNPs) have attracted a special attention in the scientific community due to their controllable synthesis, uncomplicated surface modification, and outstanding electrical conductivity. However, the main characteristics that make GNPs preferred over other

Abbreviations and acronyms: ATP, adenosine triphosphate; C_{abs}, absorption cross section; CAR, chimeric antigen receptor; CD44, cluster of differentiation 44, homing cell adhesion molecule; C_{ext}, extinction cross section; Ce6, chlorine6, photosensitizer; CISI, cerebral ischemia reperfusion injury; cLABL, Cyclo-(1,12)-Pen-ITDGEATDSGC peptide; CPPs, cell penetrating peptides; C_{sca}, scattering cross section; CT, computed tomography; DAMPs, damage associated molecular patterns; EGFR, epidermal growth factor receptor; EpCAM, epithelial cell adhesion molecule; FDA, Food and Drug Administration; FoM, figure of merit; FRα, folate receptor alpha; GM, Goeppert Mayer units; GNPs, gold nanoparticles; GNSs, gold nanoshells; HER2, human epidermal growth factor receptor 2; HER3, human epidermal growth factor receptor 3; ICAM-1, intercellular adhesion molecule 1; IGF1R, insulin-like growth factor 1 receptor; IgG, immunoglobulin G; LSPR, localized surface plasmon resonance; MRI, magnetic resonance imaging; mRNA, messenger RNA; NIR, near infrared; NPs, nanoparticles; $^1O_2$, singlet oxygen; OCT, optical coherence tomography; PAI, photoacoustic imaging; p-AKT, protein kinase B; PBS, phosphate buffer saline; PD-L1, programmed death ligand 1; PDT, photodynamic therapy; PEG, poly(ethylene glycol); PLGA, poly(lactic-co-glycolic); PNIPAM, poly(N-isopropylacrylamide); PTT, photothermal therapy; R_1, inner radius; R_2, outer radius; RIS, refractive index sensitivity; ROS, reactive oxygen species; SAX, small angle X ray diffraction; SERS, surface enhanced Raman spectroscopy; siRNA, small interfering RNA; T_1, longitudinal relaxation time; T_2, transversal relaxation time; TAMs, tumor associated macrophages; TPI, two-photon imaging..

* Corresponding authors at: Colloids and Polymers Physics Group, Particle Physics Department, Materials Institute (iMATUS) and Health Research Institute (IDIS), University of Santiago de Compostela, 15782 Santiago de Compostela, Spain.
E-mail addresses: antonio.topete.camacho@usc.es (A. Topete), alberto.pardo.montero@usc.es (A. Pardo).
[1] These authors contributed equally to this work.

https://doi.org/10.1016/j.ccr.2024.216250
Received 27 June 2024; Received in revised form 6 September 2024; Accepted 25 September 2024
Available online 11 October 2024

metallic nanostructures such as silver, palladium, or platinum NPs, especially for their application in the biomedical field, are their highly tunable optical properties, high stability, and excellent biocompatibility. In this way, the plasmonic response of GNPs can be adjusted over a wider range than those of other metallic nanosystems by carefully varying their physico-chemical properties. On the other hand, researchers have typically used gold over other metals for the design of their nanoplatforms as it is chemically stable and so less prone to induce negative effects in the body. Although other metallic nanostructures such as silver NPs have demonstrated slightly higher efficiency than GNPs in, for example, antimicrobial applications [2], gold-based nanosystems have showed lower toxicity degrees, allowing the use of higher doses to achieve the desired effect in different biomedical applications [3–5].

The use of GNPs has been documented for centuries, when their capability to display different colors depending on the angle of the incident light were exploited for ornamental purposes, such as those observed on the Lycurgus' cup in Roman culture or the stained glasses of gothic churches throughout Europe [6]. However, the controlled synthesis and the systematic analysis of colloidal dispersions of GNPs with well-defined physicochemical features was not initiated until the 19th century with the research carried out by Michael Faraday [7]. From those early studies up to the present time, an extensive body of knowledge on the synthesis, structural characterization, properties evaluation, and application of GNPs has been developed.

One of the most relevant features of metallic NPs, including GNPs, are their unique optical properties, which are based on the localized surface plasmon resonance (LSPR) phenomenon. It consists of the displacement and coherent oscillation of conduction electrons on the surface of the NPs when excited by an incident light with a particular frequency. Thus, LSPR results in an extinction (absorption + scattering) spectral peak, being the resonant frequency strongly dependent on several factors including the morphology and composition of the metallic nanostructures, the interparticle distance, or the refractive index of the surrounding dielectric medium, among others [8]. In contrast to other metals like led, mercury, indium, tin, or cadmium, that show plasma frequencies in the UV of the electromagnetic spectrum, the plasma frequency of gold is displaced to larger wavelengths, allowing the tuning of the LSPR peaks of GNPs in the visible and near infrared (NIR) regions of the spectrum [9]. As well, other metallic NPs like silver and copper which also have plasma frequencies in the visible region, are considerably more reactive and, thus, less bioinert. In this way, the LSPR can be modified by controlling the aforementioned parameters, opening a wide range of potential applications of GNPs (Fig. 1) [10].

In the most simplistic approach, spherical-shaped GNPs can be easily synthesized through chemical, thermal, electrochemical, or sonochemical pathways [11–15]. However, the optical properties of GNPs with spherical morphology have very limited sensitivity to changes on their size, structure, or modifications in the dielectric function of the surrounding media. Consequently, their LSPR peak cannot be displaced to wavelengths beyond the visible region of the electromagnetic spectrum, thus limiting their range of potential applications. In this point, the design of GNPs with anisotropic and/or asymmetric morphologies has emerged as an effective strategy to solve this limitation of their spherical-shaped counterparts (Fig. 2) [16]. Gold nanostars, nanorods, nanoprisms, nanocages or nanoshells have shown a strong dependence between the displayed optical properties and their size, morphology and/or core/shell and aspect ratios. These anisotropic GNPs can be properly designed to displace its LSPR to the NIR or infrared regions of the spectrum, where biological molecules and tissues have lower light extinction coefficients. This enables a larger number of photons to interact with GNPs upon their incorporation within cells or living organisms, making them valuable nanotools for many biomedical applications [10]. For example, gold nanostars with multiple sharp branches have demonstrated superior tip-enhanced plasmonic properties in the NIR tissue optical window. This typology of GNPs can enhance the electromagnetic field at their plasmonic tips by acting as an antenna, being the intensity and plasmon frequency of gold nanostars highly influenced by the arrangement and number of spikes [17]. On the other hand, the anisotropic structure of rod-shaped GNPs led to independent electron collective vibrations in the diameter and long axis directions, thus allowing a high control over their optical properties by adjusting their aspect ratio [18–20].

However, despite the intriguing properties of star- and rod-shaped GNPs, gold nanoshells (GNSs) hold particular interest among the different typologies of anisotropic gold-based nanostructures due to their unique combination of outstanding optical properties, complex dual structure, low cytotoxicity, and ease of functionalization with molecules of interest. Moreover, their container-like structure allows their use for the transport of drugs and/or bioactive molecules not only on their surface, but also within their inner cavity, enabling the controlled spatial-temporal delivery of the cargos [21]. The tunable optical resonance of GNSs in the NIR region (700–1100 nm) further enhances their applicability since, as mentioned, this wavelength range coincides with optimal light penetration into tissues with minimal associated toxicity. Thus, GNSs with resonances in the NIR region can be designed and synthesized to have specific absorbing and scattering cross sections for various applications in the biomedical field, ranging from biosensing and cellular and tissue imaging to cancer treatment [22].

Motivated by the great and still unexplored potential of GNSs as biomedical tools, this review firstly discusses the optical properties of GNSs and the available design strategies to manipulate their optical

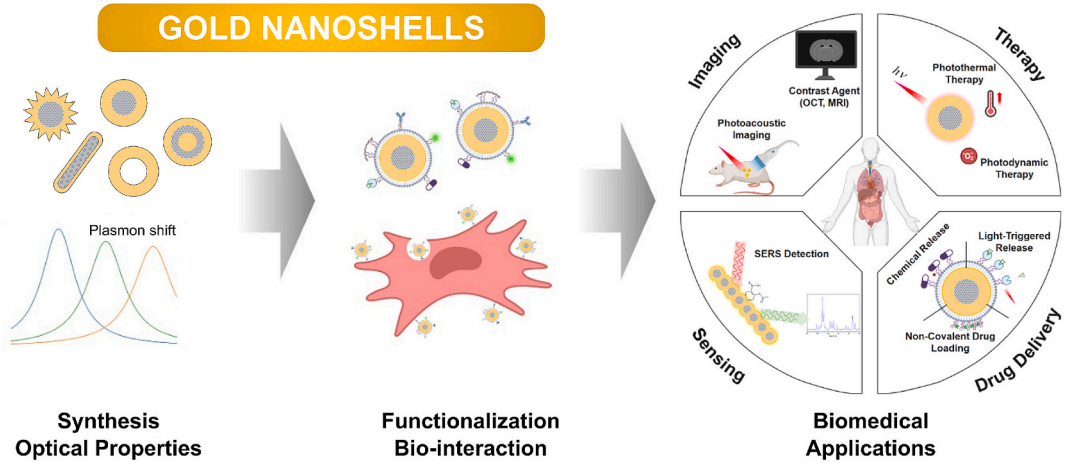

Fig. 1. Schematic illustration: design, biological evaluation, and biomedical application of GNSs.

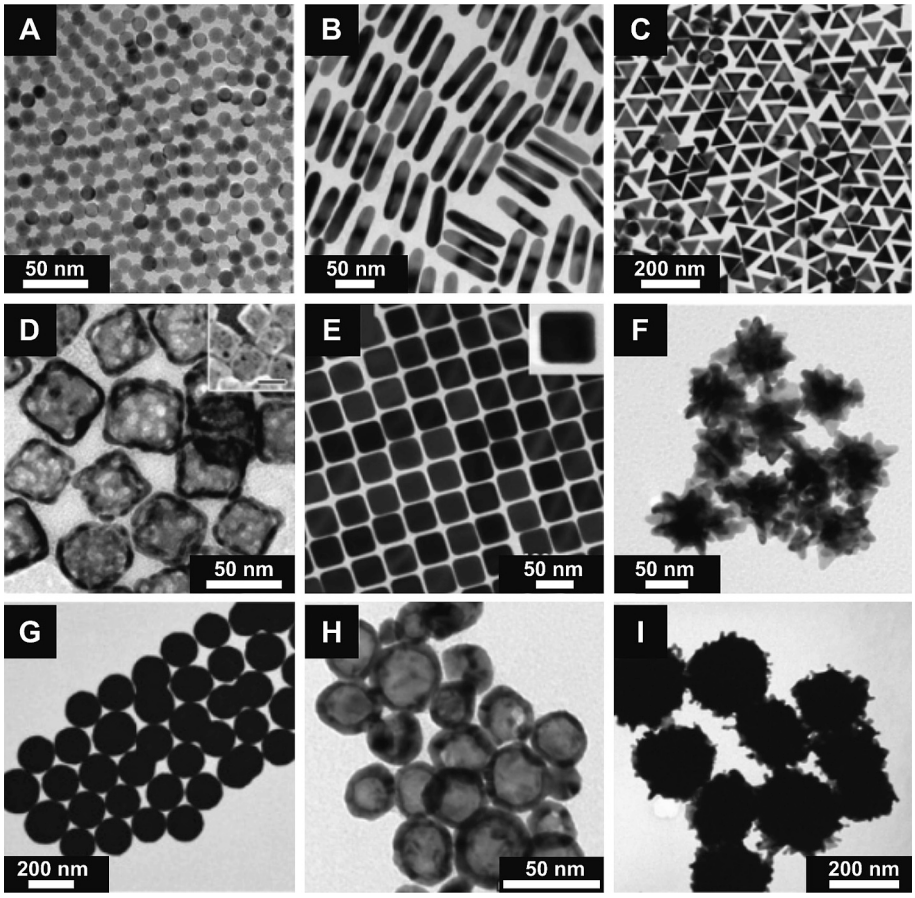

Fig. 2. Transmission electron microscopy images of GNPs with different geometries and morphologies: A) Nanospheres (Reproduced with permission [23] Copyright 2021, American Chemical Society). B) Nanorods (Reproduced with permission [24] Copyright 2021, American Chemical Society, CC-BY-NC-ND 4.0). C) Triangular nanoprisms (Reproduced with permission [25] Copyright 2014, American Chemical Society). D) Nanocages (Reproduced with permission [26] Copyright 2008, American Chemical Society). E) Cubic nanoprisms (Reproduced with permission [27] Copyright 2018, American Chemical Society). F) Nanostars (Reproduced with permission [28] Copyright 2010, American Chemical Society). G) Silica-core GNSs (Reproduced with permission [29] Copyright 2014, Elsevier). H) Hollow GNSs (Reproduced with permission [30] Copyright 2024, American Chemical Society). I) Branched GNSs (Reproduced with permission [31] Copyright 2014, American Chemical Society).

absorption/scattering ratio. The most common synthetic methods used for the preparation of GNSs are also reviewed, as well as their interactions with biological environments/elements in basis to the seminal works that have paved the way for present and future specialized applications. Furthermore, we examine the current experimental, preclinical, and clinical evidence for the potential real-life applications of GNSs, with special attention to disruptive and novel approaches to human health management. In this way, we expect to provide a valuable guide for the properly design of this typology of gold nanostructures for their application in the biomedical field. Further, the review ends by providing our perspectives on future developments in the field.

2. Optical properties of GNSs

As described above, the resonance effect is originated from the collective oscillation of conduction electrons in the metallic nanoshells, which efficiently couple to the incident electromagnetic field at a given frequency and propagate along the surface of the particle [32]. At this resonant frequency, some incident photons are dispersed in all directions through a process known as scattering, while others photons are converted into lattice vibrations in the termed absorption process [32]. In the specific case of GNSs, it has been demonstrated that they display enhanced optical properties when compared to GNPs with other morphologies, including large extinction cross-sections, resistance to photobleaching, tunable scattering/absorption ratios, electromagnetic near-field enhancement, or improved luminescence [33]. These properties are primarily associated with the interaction between GNSs and the incident electromagnetic field, being significantly magnified by the LSPR [34].

The high intricacy of modeling the electromagnetic behavior of nanostructures with complex geometries through Maxwell's equations has motivated the use of numerical approximations to analyze the optical response of GNSs, such as finite difference time domain [35], discrete dipole approximation [32], or computing codes utilizing Mie theory [36]. These methods have allowed an accurate estimation of the correlation between the extinction cross-section (C_{ext}; an equivalent cross-sectional area of the particle that contributes to the extinction of the incident light), the wavelength of the incident light, the dielectric properties of the dispersion medium, and the geometrical characteristics of the analyzed GNSs [37]. The obtained results showed a remarkable dependence of the resonant wavelength with the physicochemical characteristics of the GNSs.

In this way, the position of the LSPR can be shifted to longer or shorter wavelengths by modifying the size, the core/shell ratio and/or the surface roughness of the GNSs, among other features. The thickness of the nanoshells, that is, the difference between the radii of the outer (R_2) and inner (R_1) surfaces, also has a very strong influence on the resonant wavelength and the relative contributions of absorption and scattering to the total extinction (Fig. 3). For example, simulation data indicated that a variation in GNSs thickness from 20 nm to 5 nm while

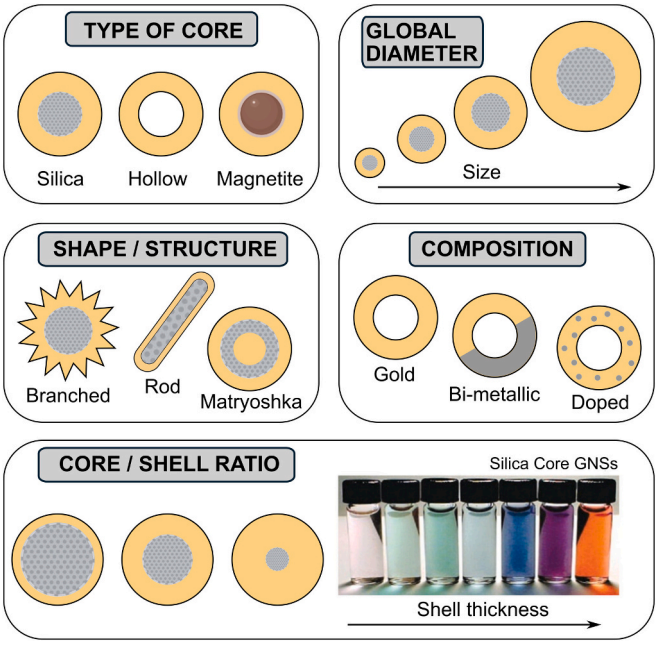

Fig. 3. Schematic representation of the most commonly explored design strategies to modify the optical properties of GNSs: variations on the typology of core, global diameter, morphology/structure, composition, and/or core/shell ratio of GNSs. The image of the colour dependence of silica-core GNSs on their thickness was reproduced with permission [68] Copyright 2023, Wiley-VCH.

keeping R_1 constant resulted in a red-shift of the LSPR peak by approximately 300 nm (Fig. 4A) [38]. In another work, discrete dipole approximation calculations were performed to demonstrate that the LSPR peak of GNSs shifts from 870 nm to 1000 nm when the shell thickness decreases from 3 nm to 2 nm for a fixed R_1 = 60 nm. Interestingly, the position of LSPR can also be displaced by modifying the R_1 value while the shell thickness remains constant, thus being possible the selective tuning of the LSPR peak wavelength between *ca.* 600 nm and 1000 nm by controlling the structural characteristics of the GNSs [39]. As mentioned, this range of wavelengths falls in the NIR regions, within the "biological windows" (NIR-I: 700–950 nm; NIR-II: 1000–1350 nm; NIR-III: 1550–1870 nm) [40], thus allowing the potential use of GNSs in multiple *in vivo* applications (Fig. 4B).

This highly tunable optical properties of GNSs constitutes a remarkable advantage when compared with the more commonly analyzed spherical-shaped GNPs, which display LSPR peaks typically located at *ca.* 520 nm in nanostructures with diameters in the range between 5 nm and 10 nm. However, the position of the LSPR peak in this typology of GNPs can only be displaced in a minimal way, observing slight variations lower than 60 nm when the size of the nanostructures was increased up to 80–100 nm [41]. Furthermore, GNSs exhibit high C_{ext} values, which comprises the sum of absorption (C_{abs}) and scattering (C_{sca}) cross-sections. This fact provides the GNSs with different properties that are essential to their potential applications. Firstly, GNSs can generate heat through the adsorption of incident photons and their conversion into lattice vibrations (phonons). This process occurs on a picosecond timescale, and the collective release of heat by GNSs is sufficient to increase the temperature of the surrounding medium up to several tenths of Celsius degrees [42]. Based on this phenomenon, GNSs have been preclinically explored as potential nanotools for the treatment of different human diseases, particularly for heat-mediated therapy of harmful tumors, leading to the development of the so-called plasmonic photothermal therapy (PTT) (Fig. 4C–i). Secondly, the elastic scattering of light in all directions upon the irradiation of GNSs can be exploited for bioimaging applications. Scattering of light, along with absorption, refraction, and reflection, constitutes the four possible mechanisms of interaction between matter and light, contributing to the attenuation of incident light intensity as it passes through a NP suspension [43]. For gold-based nanostructures, and more specifically in the case of GNSs, light scattering, followed by absorption, is the most prominent interaction mechanism among those mentioned. Due to these remarkable light scattering properties, GNSs can be utilized to "stain" abnormal tissues and cells for visualization in optical imaging devices (Fig. 4C–ii). This approach offers advantages over fluorescence-based imaging techniques, primarily due to the negligible photobleaching (see below) and the superior particle extinction coefficients. The proportion between absorbed and scattered light when GNSs are irradiated is highly dependent on the size, thickness, and/or surface topography of the nanostructures. Thus, it was found that in small GNSs with global diameters of a few tens of nm, absorption phenomenon dominates over scattering, while for larger nanostructures (more than 100 nm) the contribution of scattering is the most relevant [21]. In a similar way, in terms of nanoshell thickness, it has been demonstrated that extinction phenomena are mainly determined by absorption and scattering for thin (less than 5 nm) and thick (more than 25 nm) GNSs, respectively [37]. Between both extremes, there exists an optimal window of overall size and shell thickness at which the GNSs display large scattering and absorption efficiencies, thus being highly suitable nanotools both for bioimaging and PTT applications.

GNSs also exhibit another unique property, namely their enhanced LSPR-mediated photoluminescence [44], distinct from those observed in conventional fluorophores. This photoluminescence arises from the radiative recombination of electron-hole pairs at selected symmetry points in the Brillouin zone [45]. Photoluminescence phenomenon with small quantum efficiencies (*ca.* 10^{-10}) had been reported for smooth gold films [46], but these quantum efficiencies can be increased by a factor of a million in the case of gold nanorods and GNSs [47]. These photoluminescence properties of GNSs (Fig. 4C-**iii**), in combination with their photostability, minimal susceptibility to photobleaching, and high biocompatibility, common properties of most gold-based nanostructures [37], make them suitable candidates for bioimaging applications [48,49].

In addition, GNSs can be used as *nanoantennas*, efficiently focusing incident electromagnetic radiation into the near-field region close to their surface. This results in intense electromagnetic near-field enhancements, as demonstrated for silver nanoshells and GNSs [22,50]. In this regard, near-field interactions between fluorophores and nanoshells surfaces can either drive quenching or enhancement of fluorescence, occurring at the excitation, emission, or both stages. These metal-fluorophore interactions arise from: i) alteration of the electromagnetic field, and ii) the photonic mode density near the fluorophores. At short metal-fluorophore distances, below 5 nm, damping of molecular oscillators by processes such as electron tunneling and image interactions between the metal and the fluorophore typically leads to strong quenching of molecular fluorescence [51]. However, for larger metal-fluorophore distances (5–10 nm), an increase in fluorescence intensity can be explained by a combination of enhanced absorption of the fluorophore by the metal surface field and an enhanced radiative decay rate of the fluorophore [52,53]. Both processes can increase the quantum yield of the fluorophore. Additionally, when located near the nanoantenna surface, the emission of fluorophores can be further enhanced by coupling their fluorescence emission to the far-field through scattering [51]. For example, fluorescence of the Food and Drug Administration (FDA)-approved NIR fluorophore indocyanine green was enhanced 8-fold by placing it near to GNSs surfaces, enabling enhanced fluorescence imaging both *in vitro* and *in vivo* [52,54]. On the other hand, heterogeneous bimetallic nanoshells composed by gold and silver displaying two LSPR peaks have shown greater fluorescent enhancements with large Stoke shifts as compared to monometallic shells displaying a single LSPR peak [55]. Surface-enhanced Raman scattering (SERS) is a vibrational spectroscopic technique that increase the intensity of Raman scattering by molecules adsorbed on the surface of

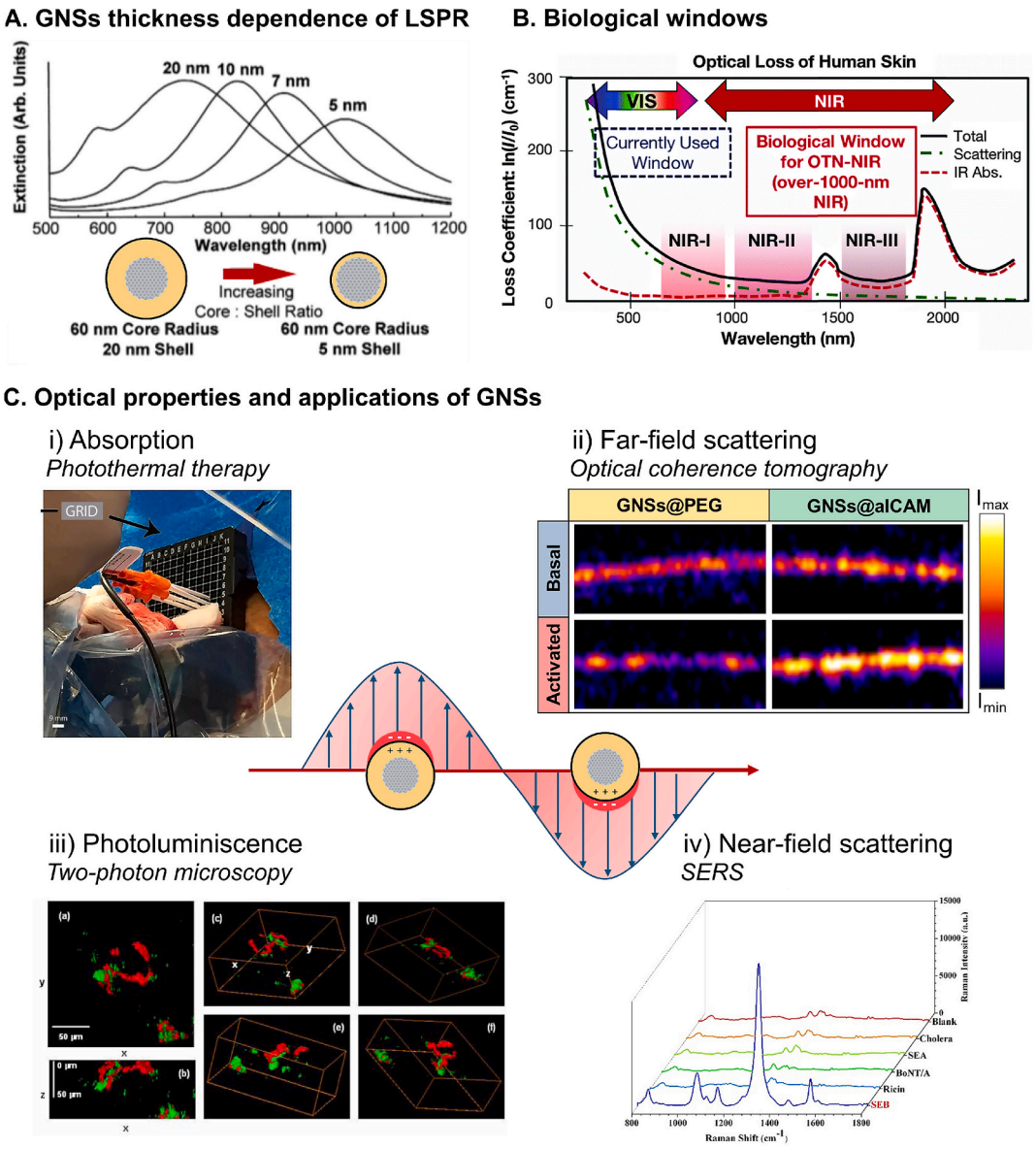

Fig. 4. **A.** Calculated extinction spectra of silica-core GNSs with constant 60 nm core radius and decreasing thickness (Reproduced with permission [38] Copyright 1998, Elsevier). **B.** Wavelength range of the "biological windows" of the electromagnetic spectrum and absorption spectra of human tissue components (Reproduced with permission [40] Copyright 2016, Royal Society of Chemistry). **C.** Most relevant optical properties of GNSs and examples of their respective applications: i) Photo absorption and their subsequent conversion to metal lattice phonons has been employed in clinical photothermal therapy of prostatic cancer (Reproduced with permission [69] Copyright 2019, National Academy of Sciences). ii) Backscattered photons enhance the contrast in optical imaging techniques (Reproduced with permission [70] Copyright 2022, Elsevier, CC BY 4.0 DEED). iii) GNSs are efficient two-photon imaging probes that favor *in vivo* imaging by avoiding the auto-fluorescence of biological specimens (Reproduced with permission [49] Copyright 2008, Optical Society of America). iv) Hot-electrons are generated at tips and gaps normally found in branched/spiky GNSs or porous hollow GNSs, being this phenomenon exploited for sensing applications (Reproduced with permission [71] Copyright 2022, Elsevier).

metallic NPs, being the obtained effect highly dependent on the optical properties of the designed nanostructures. This enhancement factor depends on the electromagnetic field enhancement associated with plasmon excitation in metal NPs and on chemical enhancement associated with the target molecule's ability to transfer electrons to/from the NPs, both in ground or excited states, often during the process of forming a molecule-metal bond [6]. The enhancement factor can reach the single molecule detection limit [56], allowing the study of surface dynamics such as molecular conformational fluctuations and interactions with ligands. The size, morphology, porosity, and/or composition of NPs, among other characteristics, are key factors that dictate their optical properties and, consequently, their performance in this field. Although SERS can be achieved at the surface of single NPs, the enhancement factor can be remarkably higher in the gaps between two nanostructures or in complex NPs with surface roughness or spikes, such as star-shaped, branched, or porous GNSs [57]. The design of GNSs with this type of complex morphologies leads to the generation of highly localized regions known as *hot spots* where the electromagnetic field is extremely strong. In this way, nanoporous and branched GNSs represent highly promising materials for enhancing the Raman scattering of targeting molecules owing to their nanopore- or nanospike-induced large surface area and high density of *hot spots* within a robust structure [58–60]. This phenomenon, together with their intrinsic large C_{ext} values (*ca.* 6 orders of magnitude larger than traditional fluorescent probes) [37,61], has been exploited for the design of advanced nanoplatforms based on GNSs with potential applications in *in vitro* and *in vivo* biosensing and Raman

imaging-based diagnosis (Fig. 4C–iv) [62–67].

3. Synthesis of GNSs

Over the past few decades, different synthetic approaches have extensively explored the preparation of GNSs with diverse characteristics in terms of structure, dimensions, morphology, and/or composition, among others. (Fig. 5 and Table 1) [72–74]. Pioneering theoretical and simulation works proposed that metal-based core-shell nanostructures might exhibit controllable plasmon resonances across the visible and infrared regions of the electromagnetic spectrum [75]. Experimentally, the seminal study devoted to the synthesis of core-shell nanostructures using different core templates and shell coating materials date back to 1993 [76], while the first attempt to produce metal-based nanoshells

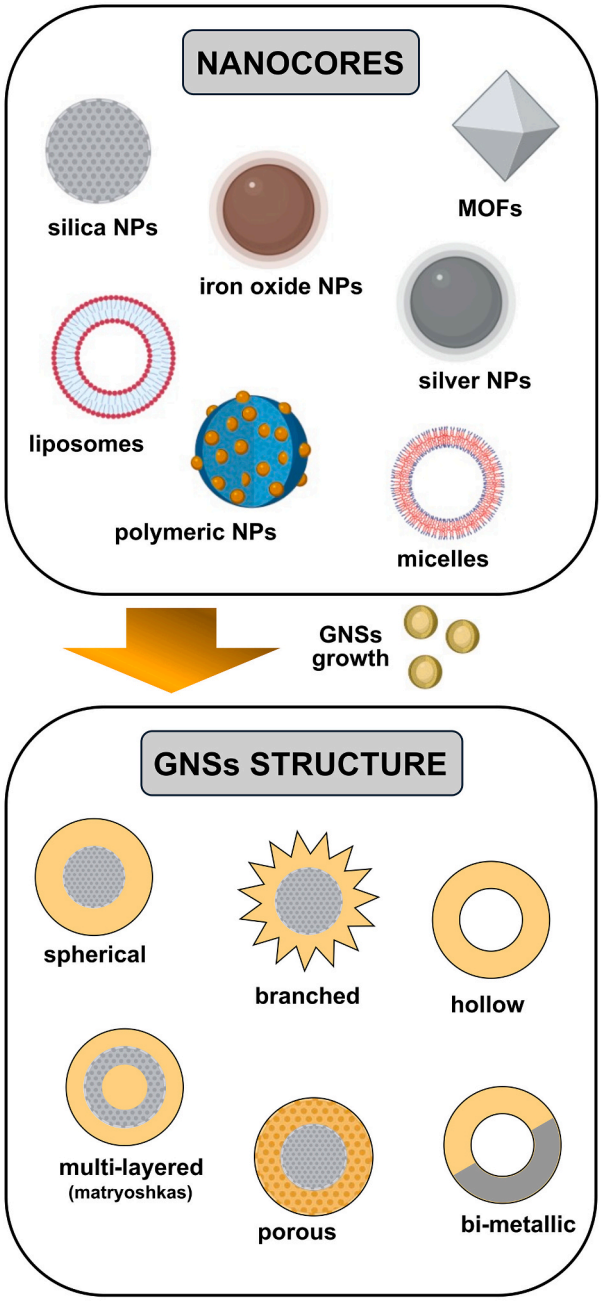

Fig. 5. Schematic illustration of the different types of nanocores most typically used as templates alongside the principal structures/morphologies of synthesized GNSs.

Table 1
Main advantages and disadvantages of the most common synthetic methods for the synthesis of GNSs and key characteristics of the typically obtained nanostructures.

Synthetic method	Advantages	Disadvantages	Key characteristics
Seeded growth	High control over core-shell size and morphology, suitable for applications requiring precise optical properties. Versatile for creating multifunctional structures. Potential scalability for mass production.	The process is more complex, involving multiple steps and incurring higher costs. It requires meticulous control of reaction conditions to ensure reproducibility, and it offers a narrower range of attainable sizes.	Can produce smooth or rough surfaces ranging in size from 60 to 200 nm. With cores made of various materials and shapes, along with spiky or branched surfaces, they are rendered multifunctional.
In situ growth	Simpler and faster process with fewer steps and reactants, making it suitable for large-scale production. Can be easily adapted to continuous production using microfluidics. Economical with good reproducibility.	Less control over the final morphology and uniformity. Limited to simpler core-shell structures, less suitable for complex multifunctional or texturized surfaces. Difficult to produce hollow structures.	Produces smooth, solid core-shell structures with uniform coverage. Sizes range from 6 to 150 nm. Generally, low PDI, but may lack complex features like porosity or roughness.
Galvanic replacement	Efficient formation of hollow nanoshells with tunable porosity and morphology. Can produce bimetallic structures with unique properties. Ideal for creating nanoshells for drug delivery or catalysis.	Requires precise control over the reaction to avoid structural collapse. Not as simple as *in situ* growth and may involve more expensive precursor materials. More difficult to scale up due to the complexity of maintaining uniformity.	Results in hollow, porous nanoshells with tunable sizes from 20 to 150 nm. Structures can be rough or branched. Suitable for creating bimetallic compositions and multifunctional applications, including drug-loaded carriers, and ultra-sensitive biosensors.

was reported one year later. In this last work, Au_2S cores were coated with GNSs of various thicknesses, thus allowing a tunable LSPR in the range of 520–900 nm [77]. However, the developed synthetic method lacked high control over the characteristics of the obtained nanostructures, which displayed large polydispersity degrees both in core and shell dimensions. Moreover, large amounts of bare gold spheres were also formed as by-products. Interestingly, the use of silica NPs as core templates led to the first successful synthesis of highly monodisperse and size-controllable GNSs by Oldenburg et al. [38]. In this approach, monodisperse silica cores were synthesized using the classical Stöber method [78], following by the electrostatic attachment of small negatively charged GNPs (called *gold seeds*) onto their aminated surfaces. Thereafter, the gold layer was grown by mixing the seed-covered silica NPs with a growth solution containing Au^{1+}. This was followed by the addition of a weak or mild reducing agent to induce the deposition of Au^0 onto the gold seeds, that eventually grew until generate continuous gold layers around core templates. Nowadays, the standardized synthesis methods for silica-core GNSs are generally based on this *seeded-growth* method (Fig. 6A). Next, we are going to briefly describe the influence of the selected synthetic approach, the precursor materials, the conditions/parameters during the preparation process, and/or the post-processing of the samples, among other factors, over the characteristics of the obtained GNSs, highlighting in each case the most relevant seminal studies that delved into these analyses (Table 2).

3.1. Batch vs. flow reactors

In the most typical and traditional approaches, GNSs are synthesized in stirred batch reactors by controlling the type, concentrations, and ratios between reagents, the pH, or the temperature, among many other factors. However, the use of continuous flow reactors has been increasingly explored in recent years [79–82]. Among the most remarkable advantages of continuous reaction procedures to synthesize nanostructured materials are the reduction of synthetic times, or the easier scalability of the synthetic processes to obtain larger amounts of NPs with high monodispersity degrees [83]. In the specific case of GNSs, a representative example of their controlled synthesis onto silica cores using a flow reactor was reported by Watanabe et al. [84]. More specifically, they used a central collision type microreactor consisting of two inlet flows that then are separated into seven channels each one before the final convergence of the fourteen streams into a mixing point, thus achieving a quick and homogeneous mixing of two inlet fluids. By altering the properties of the used silica templates, and the type and concentration of reducing agent and growth solution, this procedure can be exploited to obtain GNSs with controlled characteristics. In another interesting approach, a flow reactor was used for the continuous synthesis of magnetoplasmonic GNSs [85]. For that, seed-decorated silica-coated magnetic NPs were synthesized in a Y-shaped flow device that allowed a controlled mixing of the used reagents, followed by the growth of gold shells also inside a continuous flow reactor. This flow-based method enabled subtle control on the dimensions of the GNSs grown surrounding the magnetic cores, yielding thickness ranging from 140 to 400 nm, thus offering high tunability of the optical properties of the obtained nanostructures.

3.2. Materials used as core templates: hard, soft, and hollow GNSs

Different materials have been evaluated to replace the traditional silica NPs as core templates during shell formation, thus modifying the physicochemical properties and functionalities of the finally obtained nanostructures. Depending on their nature and mechanical properties, these core templates can be either hard or soft. Among hard templates, iron oxide NPs [86–89], quantum dots [90], or nanosized metal organic frameworks [91], have been among the most widely evaluated alternatives to silica nanocores. Of particular interest are the magnetoplasmonic nanostructures, in which GNSs are grown surrounding magnetic cores, since they allow the combination of multiple capabilities such as photothermia, magnetic hyperthermia, or contrast for bioimaging in a single nanoplatform [92].

Besides the preparation procedure using a flow reactor described in detail in previous section, magnetic cores coated with GNSs displaying dimensions below 10–20 nm, which are required for specific biomedical applications, can be obtained through other synthetic strategies. For example, in a simple and highly reproducible methodology, hydrophobic iron oxide NPs obtained through thermal decomposition can be incubated at high temperatures in the presence of gold acetate and reducing agents. This process promoted the thermal desorption of the original capping agents of the magnetic cores and the gold acetate reduction and subsequent formation of GNSs onto their surfaces. The addition of surfactants into the solution allowed to control the dimensions of the grown GNSs even at very low thickness values below 3 nm [88].

On the other hand, soft self-assembled nanostructures like micelles and liposomes can be used as soft templates to fabricate GNSs [93–96]. In a representative example of this approach, spiky GNSs have been synthesized using poly(acrylic acid)-*co*-poly(styrene) block copolymer micelles as core material [97]. This type of nanostructures allows the easy encapsulation of drugs, bioactive molecules, and/or imaging contrast agents, which constitutes a remarkable design advantage for the preparation of GNSs for biomedical purposes. Moreover, the obtained GNSs can be also classified as hollow or non-hollow, depending on whether the core template is removed or not. Thus, in the case of hollow GNSs the coating material is deposited on a template that afterwards can be degraded through different mechanisms such as chemical etching, dissolution with selective solvents (*e.g.* hydrofluoric acid for silica cores), or galvanic replacement of metallic NPs. These hollow GNSs display specific optical properties stemming from their double surface and also allow the encapsulation of large amounts of different compounds/bioactive molecules, which make them highly suitable for several applications that will be addressed in following sections.

3.3. Role of ligands in the synthesis of GNSs

Besides the typology of core templates, the linker used to attach the gold seeds to them also plays a key role in the successful synthesis and the physicochemical properties of the obtained GNSs. In this sense, Westcott et al. modified silica nanocores with different linkers, observing that the amino and thiol groups present in 3-(aminopropyl) triethoxysilane and 3-(mercaptopropyl)triethoxysilane, respectively, facilitated the attachment of gold seeds, while other silane-based linkers bearing $–CH_3$ and PPH_2 groups failed to generate gold coverage [98]. The essence of these electrostatic amino-citrate and Au-S bonding interactions later inspired the use of other ligands for the synthesis of GNSs. For example, cysteamine was proposed as linker to attach gold seeds to the surface of doxorubicin-loaded poly(lactic-*co*-glycolic acid) (PLGA) NPs. The PLGA reacted with the cysteamine's amine groups through a carbodiimine/sulfo-NHS assisted reaction, leading to thiol-functionalized nanostructures capable to easily attach the gold seeds by Au-S bonds [99]. Positively charged polymers, polyaminoacids, or polysaccharides such as chitosan [31], among others, have been evaluated as potential ligands to attach gold seeds to polymeric templates.

3.4. Effect of pH, precursors ratio and reducing agent

In addition to the characteristics of core templates and used surface ligands, the physicochemical properties of the synthesized GNSs are also dictated by many other factors with strong influence over the growth process of the nanostructures. Thus, since gold shells growth mechanism is governed by the redox potential between the reducing agent and Au^{+3} ions, the characteristics of the final nanostructures are highly dependent on the pH, the temperature, the type of reductant agent (*e.g.* formaldehyde, ascorbic acid, or sodium borohydride) and/or the ratios between

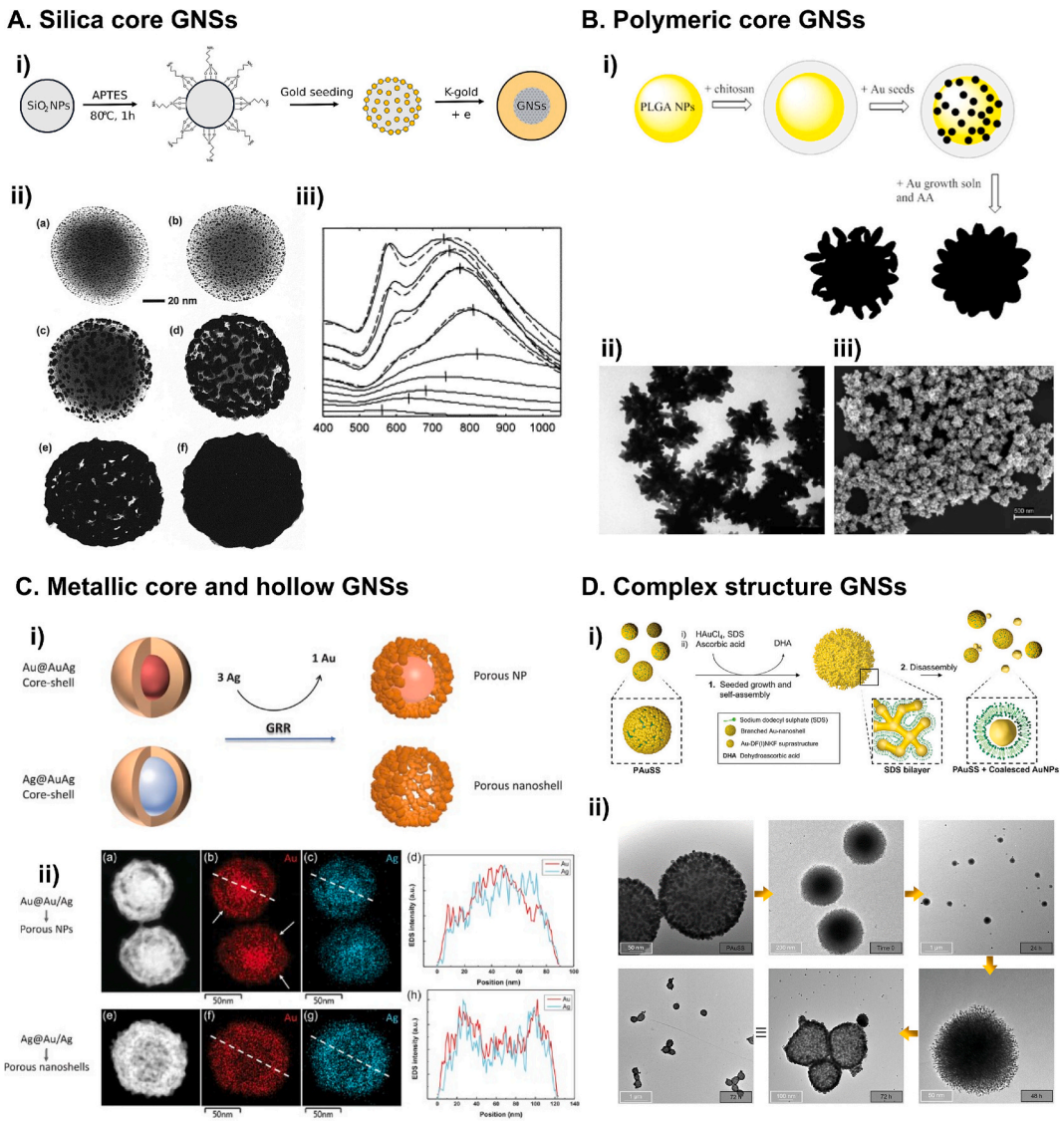

Fig. 6. A. i) Schematics of the synthetic methodology of silica-core GNSs, ii) TEM images and iii) UV–vis spectra of the nanostructures prepared by the seeded-growth method developed by Halas' group. Once seeds have coalesced, epitaxial growth of nanoshells is observed and a quadrupole resonance mode manifests as a peak at 650 nm (Reproduced with permission [38] Copyright 1998, Elsevier). **B.** i) Schematics of the synthetic method of branched GNSs obtained by seeded-growth method using low viscosity chitosan to attach gold seeds to PLGA polymeric templates. Anisotropy degree was controlled by reactants ratios. ii) TEM and iii) SEM images of the synthesized GNSs (Reproduced with permission [31] Copyright 2014, American Chemical Society). **C.** i) Schematics of the galvanic replacement reaction resulting in bimetallic porous shell with solid core (porous NPs) or hollow interior (porous nanoshells). ii) High-angle annular dark-field scanning transmission electron microscopy image of dealloyed NPs and their respective elemental mapping and composition profile of Au and Ag (Reproduced with permission [117]. Copyright 2021, Wiley-VCH GmbH). **D.** i) Schematics of growth and disassembly of the out-of-equilibrium branched GNSs. ii) TEM images at different stages of the disassembly process (Reproduced with permission [123] Copyright 2023, Wiley-VCH GmbH). (For interpretation of the references to colour in this figure legend, the reader is referred to the web version of this article.)

the different reagents involved in the synthesis.

A very complete study reported by Alonso-Cristobal et al. shed further light on the effect of various synthetic parameters in the characteristics of GNSs grown on magnetic nanocores [100]. Here, it was established that the ratio between gold precursor and core material has a stronger influence over the reaction yield than in the thickness of the grown nanoshells. Moreover, they identified a range in which the number of successfully formed GNSs was maximized, beyond which the excess of gold atoms resulted in the formation of homogeneous spherical GNPs. In the same work, it was also demonstrated that higher temperature reactions resulted in larger thickness of the obtained GNSs, also establishing that through the developed method the maximum size of magnetic cores that allow the formation of uniform and monodisperse GNSs was below 20 nm. In another interesting design approach, the effect of the ratios between PLGA cores, reducing agents and gold growth solution was evaluated, observing a variation on the topographies of the obtained branched GNSs from relatively smooth to highly branched gold surfaces similar to those observed on gold nanostars (Fig. 6B) [31]. On the other hand, the use of low-explored mild reducing agents such as carbon monoxide has also been proposed to improve the control over the growth process and the stability of GNSs [101]. However, although this strategy improved the monodispersity of the obtained nanostructures when compared with the original Oldenburg's method, it has associated important biological/toxicological concerns associated with the use of carbon monoxide. The effect of pH over the formation of GNSs was also evaluated in different works. Thus, for

Table 2
Summary and compilation of relevant references on GNSs synthesis according to the used synthetic method, precursor materials, preparation conditions, post-processing, and final morphology and structure of the obtained nanostructures.

Synthetic method	Precursor materials	Synthetic conditions	Post-synthetic processing	Morphology and structure
seeded-growth [38,97]	***Core:***	***Reaction regime:***	***Stabilizing agents:***	***Conventional:***
in situ growth [84,88,91,103–105]	silica [38,84,103]	batch	PEG [31]	non-hollow spherical
galvanic replacement [110,116,117]	iron oxide [88,100]	flow/continuous [84,85]	oleic acid/oleylamine [88]	hollow-spherical
	iron oxide/silica [85,104]			
	tellurium/selenide [118]	***Gold source:***	***Core dissolution:***	
	quantum dots [90]	K-gold solution [91,110,128]	hydrofluoric acid [115]	***Complex:***
	MOFs [91]	gold (III) solution [90]		hollow porous [117]
	polymeric NPs [31,97]	gold acetate [88]		multilayered [29]
	block copolymer micelles [97]		***Surface texturing:***	hollow rod-shaped [118]
		Additives:	cysteamine [125]	cubic [121]
	Shell:	$AgNO_3$ [97]		urchin-like [122]
	bimetallic alloy [116,117]	CTAB [97]		branched [31,123,124]
		poly(vinyl pyrrolidone) [91,105]		(Janus) half-shell [126,127]
	Seeds:	NaOH [105]		
	citrate-stabilized [31]	L-cysteine [118]		
	tetrakis-seeds [128]			
	silver seeds [97]	***Reductant:***		
		sodium borohydride [97,105,128]		
		ascorbic acid [84,97,105]		
	Seed/gold ion linkers:	formic acid/formaldehyde [91]		
	APTES, AEAPTES, APTMS [84,85,128]	carbon monoxide [101]		
	MPTES [98]	hydroxylamine [85,90]		
	cysteamine [99]	1,2-hexadecanediol [88]		
	chitosan [31]			
	PEG-lipid [90]	***Solvent during shell growth:***		
	poly(styrensulfonate) [90]	phenyl ether [88]		
	poly(L-hystidine) [90]			
	poly(ethyleneimine) [105]	***Reaction parameters:***		
	synthetic peptides [123]	effect of pH [102]		
		effect of temperature [100]		
		effect of reagent ratios [100]		

example, it was demonstrated that the redox potential of formaldehyde increased proportionally to the pH of the growth solution, enabling the obtention of complete and continuous GNSs with NIR-centered LSPRs under basic conditions [102].

3.5. *In situ formation and growth of gold seeds*

Alternative approaches to synthesize GNSs with controlled physicochemical properties rely, for example, on the *in situ* formation and subsequent growth of gold seeds over the surface of core nanotemplates, being this strategy termed as *deposition-precipitation method* [103]. Following this strategy, gold seeds were *in situ* synthesized over the surface of polymeric micelles loaded with magnetic NPs and then grown to form magnetoplasmonic GNSs [104]. In a similar way, the one-pot synthesis of GNSs based on the *in situ* formation of gold seeds over the surface of poly(styrene) nanospheres was reported [105]. The *in situ* seed growth approach was also explored in soft templates [93]. For example, copolymer micelles bearing amino blocks in their outer regions allowed the attachment of Au^{+3} to the polymeric surfaces. The *in situ* obtained hybrid particles allowed the complete growth of GNSs upon a second addition of gold precursor and reducing agent [94].

3.6. *GNSs with complex structures, morphologies, and compositions*

In view of their potential application in the biomedical field, GNSs with complex non-spherical geometries, high porosity, and/or cavities within their structure are particularly appealing, since they display special optical properties and allow the loading of larger amounts of cargo molecules/substances. More specifically, hollow, porous, and/or spiky plasmonic nanostructures are particularly useful for theragnosis and biosensing due to their larger specific surface area and higher density of hot spots compared to their counterparts with homogeneous structure. The lower amount of gold or the reduced synthetic cost of this type of nanomaterials are also key advantages to be consider [106].

The aforementioned hollow GNSs can be synthesized, for example, through a galvanic replacement reaction based on the reduction of gold on sacrificial metallic core templates such as silver or cobalt NPs through a redox process [106–109]. The large standard reduction potential of the $AuCl_4^-/Au^0$ redox pair (0.99 V) in comparison with those of Ag^+/Ag (0.80 V) [106], and Co^{+2}/Co (−0.28 V) [109], promotes the fast oxidation of silver or cobalt NPs by $AuCl_4^-$, thus forming Au^0 hollow nanostructures. This galvanic replacement strategy was exploited by Duran-Meza et al., who used silver NPs as templates to obtain hollow GNSs with small sizes ranging from *ca.* 17 to 25 nm [110]. However, it is worth mentioning this synthetic procedure can lead to the presence of residual cobalt or silver inside the hollow gold nanostructures, or even become alloyed [111], thus potentially altering the properties and decreasing the stability and/or the biocompatibility of the designed GNSs in their final *in vivo* application [112–114]. To address this concern, the synthesis of GNSs through the controlled erosion or clearance of highly biocompatible silica dielectric cores has been also proposed. In this case, hydrofluoric acid can be used for the degradation of silica templates, being possible to obtain hollow GNSs or even control the porosity of the cores by varying concentration or time exposure of the nanostructures to this reagent [115].

Interestingly, the aforementioned use of silver NPs as core templates can also be exploited for the controlled formation of nanoshells composed by alloys of gold and silver. Choi et al., for instance, synthesized hollow silver/gold bimetallic nanoshells by using silver NPs with sizes ranging from 20 to 100 nm as templates [116]. Alloyed-shell nanostructures with different compositions were prepared by varying the amounts of silver seeds and gold precursor growth solution at a fixed molar ratio. In another interesting recent work, the galvanic replacement strategy using silver cores was used to design silver/gold bimetallic nanoshells with high porosity and hollow structure, being potential nanotools for SERS or drug delivery applications (Fig. 6C) [117]. This type of bimetallic nanoshells can also be synthesized surrounding silica NPs through the simultaneous or successive reduction of

gold and silver precursor solutions onto the surface of the dielectric cores [55].

In addition to their thickness, structure, porosity, and/or composition, the morphology of nanoshells is another key parameter that strongly influence their physicochemical properties. Although the synthetic and/or post-processing procedures required to obtain GNSs with non-spherical shape are typically more complex and delicate processes, many different works have explored the preparation of this type of nanostructures. In an innovative and complex approach, Ayala-Orozco et al. reported the synthesis of the so-called *gold nanomatryoshkas*. These consist on multi-layered GNSs composed of a gold nanocore surrounded by a first layer of dielectric silica, which is covered by a second layer of gold [29]. The silica layers were grown using the standard Stöber method [78], while the external gold layers were obtained through the attachment of negatively charged gold seeds and their subsequently overgrowing onto the positively amine-functionalized silica layer. The careful control over thicknesses of the different layers allows the precise tuning of the hybridized plasmon resonance modes in the designed *nanomatryoshkas*. In another unconventional design strategy, rod-shaped GNSs with hollow structure and controlled aspect ratio were synthesized, thus allowing the tuning of the LSPR peak within NIR-II window. In this case, the templates used to grow the GNSs around were tellurium nanorods dopped with selenide, subsequently exposed to chloroauric acid to undergo a replacement reaction in the presence of *L*-cysteine as shape-modulating agent [118]. The obtained hollow GNSs with rod-like morphology showed enhanced properties for chemo-photothermal therapy and multimodal imaging. The design of rod-shaped GNSs with non-hollow structure have been also proposed, being a representative example the so-called gold nanorices, in which the metallic nanoshells surround hematite cores with spindle-like morphology [119,120]. In this approach, the dielectric cores served as template to adsorb GNPs, which is a simple and fast strategy to prepare GNSs with different characteristics. Thus, through variations in the size of the iron oxide templates and in the thickness of the grown nanoshells, variations in the optical response towards incoming light were observed. In a similar way, GNSs with cubic or urchin-like morphologies have also been synthesized in recent works [121,122].

On the other hand, GNSs displaying highly rough surfaces or branched morphologies, characterized by distinct elements or narrow spaces that promote the attraction of analytes or payloads, have also been widely explored due to their high potential in applications such as SERS. An interesting approach to design this type of nanostructures was recently reported by Marchetti et al., who synthesized *templated out-of-equilibrium* self-assembled branched GNSs [123]. Here, a mixture of synthetic peptides coupled with GNPs were self-assembled into spherical templates named *peptide-gold-superstructures* that then gave rise to multilayers of interconnected NP-branches network (Fig. 6D). After 72 h, the branched GNSs returned to their initial state, revealing the metastable nature of these peculiar nanostructures. Regarding the roughness of the GNSs, it can be controlled by establishing the adequate synthetic conditions [31,124], but also through the post-fabrication treatment of the obtained GNSs. For example, the site-selective chemical etching of GNSs by exposing them to cysteamine was demonstrated as an effective strategy to increase the surface roughness of the metal nanoshells upon their synthesis [125]. Interestingly, the synthesis of half-GNSs has also been explored. In a representative example of this complex procedure, PLGA NPs were spun-coated onto a silicon substrate and then used as core templates for the grown of GNSs through the electron beam evaporation of gold precursor solution onto their surfaces [126,127]. Depending on the evaporation conditions, the thickness of the gold layer in the obtained Janus half-shelled nanostructures can be controlled.

In summary, the synthetic strategies developed during the last decades allow the preparation of GNSs with highly controlled characteristics in terms of size, morphology, structure, or the material of core template, among others. The careful design of GNSs allows the precise tuning of their physicochemical properties, thus potentially leading to the optimization of their performance in the intended application. The following sections provide an overview of the most relevant works that have explored the biological evaluation and further biomedical application of GNSs as diagnostic and/or therapeutic nanotools.

4. Bio-interactions of GNSs

For an efficient *in vivo* (bio)activity of GNSs, the designed nanostructures must display the adequate photophysical properties to optimize their performance as (bio)sensing, (bio)imaging, and/or therapeutic nanotools. However, in addition to this, the first and most important property of any type of NPs in view of their potential biomedical application is their capability to be accumulated at the desired target site while minimizing concentrations in surrounding healthy tissues. In this section, we will discuss the main processes and mechanisms that underlie the interaction of GNSs with biological barriers and the immune system, as well as the different strategies proposed to enhance their targeting to the desired sites (Fig. 7).

4.1. Biodistribution and toxicity of GNSs

The *in vivo* biological transport and time-dependent distribution of gold-based nanostructures in tumors, blood, tissues, or major organs have been widely addressed by many pharmacokinetic studies [129–134]. In general, GNPs larger than 10 nm tend to accumulate in the liver and spleen, while smaller particles undergo rapid renal clearance with minimal accumulation in other organs [135,136]. In a similar way, a recently reported study evaluated the biodistribution of anti-HER-2 and not-targeted silica-magnetite-core GNSs with 130 nm in diameter in a mice model. The injected hybrid nanostructures were almost completely cleared from the bloodstream after 72 h, observing their time-dependent accumulation in the liver and the spleen, with no visceral damages detected in either of these two tissues or in the bone marrow or kidneys (Fig. 9A) [137]. In another interesting work, the biodistribution of GNSs in *in vivo* cancer models was evaluated through neutron activation analysis techniques [138]. In this way, it was observed that GNSs were much more accumulated in the tumor than in blood, lungs, brain or kidneys upon 24 h of their intravenous administration. However, the accumulation of gold in the liver and the spleen was 20–25 times higher than that observed in the tumor, representing this latter only 1 % of the administered dose of GNSs.

To the best of our knowledge, comprehensive studies evaluating the long-term toxicity of GNSs over periods of several years have not been reported yet. However, the previously described works, as well as others that also evaluated the biological behavior of GNSs at short and mid-term periods [131,133,139–141], clearly showed that they are not

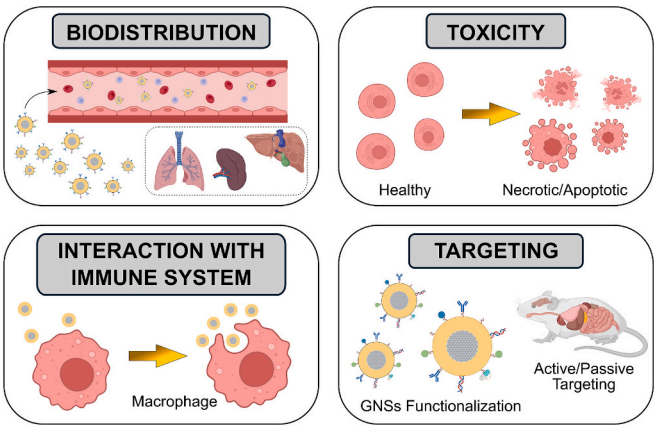

Fig. 7. Schematic illustration of the main processes and mechanisms that underlie the interaction between GNSs and biological systems: biodistribution, toxicity, interaction with immune system, and active/passive targeting.

cytotoxic and do not pose short–term health risks at typical therapeutic doses. Here, it is worth mentioning the study conducted by Gad et al., where the biodistribution and toxicity of 155 nm silica-core GNSs, commercially traded as AuroShell®, were carefully evaluated for periods up to 400 days. The performed trials included the evaluation of cytotoxicity, pyrogenicity (in rabbits), hemolysis *in vitro*, *in vivo* micronucleus formation in mice, intracutaneous reactivity in rabbits, sensitization in guinea pigs, and acute systemic toxicity in mice, among others, with no evidences of cell/tissue toxicity [142].

4.2. Interaction of GNSs with the immune system

The immune system constitutes the first defense mechanism of living organisms against foreign materials. Specialized cells and molecules detect and eliminate strange and 'non-self' proteins, particles, microorganisms, or small molecules that represent a potential threat to the host tissue/organ. When nanostructured materials are injected into the bloodstream, which is the most typical administration route of NPs for biomedical purposes, they rapidly interact with serum proteins forming highly complex biocoronas surrounding their surfaces that plays a crucial role in the stability, degradation degree, biodistribution, and interaction of nanomaterials with biological entities [143–145].

In particular, blood serum opsonins are extracellular proteins that bind to the surface of NPs very quickly upon their injection, marking them for the subsequent recognition by mononuclear phagocytes, such as macrophages. This phenomenon causes the early clearance of most of the injected NPs before they reach the target organ or tissue. More specifically, nanostructures displaying sizes between *ca.* 50 and 200 nm, such as the most commonly synthesized GNSs here discussed, are typically internalized by macrophages through phagocytosis processes mediated by the scavenger receptor-A and pinocytosis [146]. As a consequence of this, the GNSs internalized/removed by macrophages are accumulated in liver, spleen, and/or bone marrow tissues after short times upon injection, as previously discussed. In this sense, ultrastructural analyses of liver and spleen tissues carried out 72 h after the injection of GNSs in mice confirmed the presence of almost intact gold-based nanostructures in both and their predominant accumulation within the macrophages [137].

However, not only macrophages are involved in the recognition and processing of NPs [147,148]. Other cells of the innate and the adaptative immune system also play a key role in the defensive response of the body to the presence of strange nanomaterials. In this regard, several works have established that GNPs injected in the bloodstream can also be internalized by dendritic cells [149,150], natural killer cells [151], and T cells [152]. In general, the observed toxic effects of gold-based nanostructures over the cells of the immune system are not significant, being their functions minimally altered due to the presence of this typology of inorganic nanomaterials. However, it is important to note that the interactions of GNSs with the wide range of cells of the immune system could lead to stimulation or suppression phenomena, which might alter the normal immune response and induce dangerous side effects [150,153]. In this sense, there are two different situations in which the presence of GNSs might alter the immune response. The first one occurs when the sole injection of GNSs into the bloodstream induces an inflammatory response, while in the second scenario this inflammation is associated with the light irradiation typically used to stimulate the GNSs, which is required for many of their applications that will be discussed below.

Although there are only a few specific works devoted to the careful analysis of the immunogenicity of GNSs, both possible scenarios have been preliminarily studied. For instance, the effect of surface coating on the capability of GNSs to induce an inflammatory response by activating the NALP-3 inflammasome followed by the release of the pro-inflammatory cytokine IL-1β by macrophages was recently evaluated [154]. NALP-3 inflammasome activation and IL-1β secretion were associated with the generation of reactive oxygen species by GNSs and, interestingly, the functionalization of the nanostructures with poly (ethylene glycol) (PEG) had a highly beneficial effect by considerably decreasing the secretion of IL-1β and the influx of neutrophils. In the second scenario, the application of light stimuli to exploit the properties of the injected GNSs for the intended biomedical application can induce necrotic cell death and the subsequent release of different danger-associated molecular patterns (DAMPs), (*e.g.* DNA, RNA, heat shock proteins, uric acid) which induce an immunogenic response. The stimulation of different toll-like receptors such as TLR2 and TLR4 by these patterns released upon light stimulation of GNSs can induce the production of pro-inflammatory pro-IL-1β and pro-IL-18, which regulate a cascade of immune response phenomena generated in response to the caused cellular damages [155,156]. In this regard, Nguyen et al. evaluated *in vitro* the capability of light-irradiated GNSs to produce enough levels of molecular patterns to activate the inflammasome and secretion of IL-1β, as well as to activate immature dendritic cells, being observed a weak immunogenic response of the designed GNSs under the tested conditions [157].

4.3. Targeting of GNSs

As previously mentioned, the immune response of the body limits the effective targeting of the GNSs injected in the bloodstream, with only a reduced percentage of doses reaching the desired tissue/organ. However, in most cases the use of gold-based nanostructures in the biomedical field is related with cancer diagnosis and/or therapy applications, and the characteristics of tumors are more favorable than those of healthy tissues for the efficient targeting and accumulation of nanostructured materials. Thus, the abnormal physiology and biochemical behavior of tumors enable the passive accumulation of NPs, proteins, and supramolecular aggregates within their highly vascular structures [158]. More specifically, solid tumors typically exhibit three important features that facilitate the internalization and retention of NPs within them despite the internal pressure gradient generated due to deficient drainage: i) enhanced angiogenesis with increased vascular permeability, ii) deficient vascular architecture (fenestrations) to supply the expanding tumor masses, and iii) impaired lymphatic drainage. These physiological features have traditionally been acknowledged as responsible for the so-called passive targeting of nanodrugs to solid tumors. Semantically, this passiveness attributed to the natural accumulation of NPs within solid tumors leads to the perception of energy-independent processes, exclusively driven by the size of the injected elements and the free endothelial gaps. However, recent studies have demonstrated that the accumulation of nanomaterials in tumors is highly dictated by dynamic energy-dependent transcellular transport mechanisms [159].

In addition to the passive accumulation phenomenon derived from their physicochemical properties and the characteristics of tumors, the targeting of GNSs towards the desired site of action can be significantly improved through the conjugation of the adequate ligands to the surface of the nanostructures, a process known as active targeting. Thus, the functionalization of GNSs with targeting molecules (*e.g.* antibodies, aptamers, peptides) that exhibit high specificity degrees to surface markers overexpressed in cancer cells has been widely evaluated to increase the targeting efficiency of the designed nanostructures [160–163]. These active targeting mechanisms allow to enhance the accumulation of GNSs in solid tumors, thus also improving their performance on the intended biomedical application. One of the first works that explored the active targeting strategy with GNSs was based on the conjugation of the nanostructures with anti-HER2 (human epidermal growth factor receptor 2) monoclonal antibodies for the subsequent photothermal ablation of the tumor where the GNSs were accumulated [164]. In a similar active targeting strategy, streptavidin-functionalized GNSs were conjugated with biotinylated anti-HER2 antibodies, being observed an increased cellular uptake and cytotoxicity against HER2-overexpressing SKBR breast cancer cells compared to the HER2-

negative MDA-MB-231 triple-negative breast cancer cells [52].

After these pioneering works, the active targeting of GNSs using different groups of antibodies has been widely evaluated for biomedical purposes. For instance, the covalent conjugation of hollow GNSs with anti-EGFR (epidermal growth factor receptor) antibodies was demonstrated as an efficient strategy to enhance the targeted killing of human squamous carcinoma A431 cells *in vitro* [165]. Moreover, the reduced size of the GNSs obtained by a galvanic replacement method in this work constitutes an advantageous feature for their *in vivo* application, due to the already discussed easier biological clearance of low-size NPs [166]. On the other hand, a recent work has evaluated the active targeting of silica-core GNSs functionalized with thiolated chitosan, paclitaxel and anti-EGFR antibodies. The nanostructures were efficiently internalized by MDA-MB-231 breast cancer cells both *in vitro* and *in vivo* through a fast receptor-mediated endocytosis process [167]. The conjugation of GNSs with anti-CD47 antibodies was also analyzed, being these nanostructures designed to specifically target cells with CD47 receptors, a membrane protein that is overexpressed in, for instance, ovarian cancer cells [168]. The specific targeting efficiency of these GNSs was tested *in vitro* using ID8 mouse ovarian cancer cells, which do not express human CD47, and also CD47-rich TOV21G human ovarian cancer cells. Moreover, the targeting capability of the gold-based nanomaterials was further evaluated *in vivo* using a xenograft TOV21G-luc human ovarian cancer model, being observed a superior accumulation and photothermal therapeutic effect of the CD47-targeted nanoconstructs.

Besides the typical use of different antibodies, other typologies of molecules have been also proposed for the active targeting of GNSs. For example, PLGA-core GNSs was conjugated with folic acid [169], whose alpha receptors (FRα) are overexpressed in different types of solid tumors, including ovarian, lung and breast cancers [170]. As expected, the cellular uptakes of folic acid-conjugated GNSs were significantly higher than those observed for unmodified GNSs. In a very interesting design approach, the same authors demonstrated that the combination of ligand-based active targeting with magnetically induced targeting through the incorporation of iron oxide NPs into the polymeric core of GNSs enhanced their cellular uptake and internalization more than two-fold.

Between macromolecular antibodies and low-size molecules, we can find other ligands with high potential as targeting agents such as the so-called cell-penetrating peptides (CPPs). Also known as protein transduction domains or membrane translocating sequences, CPPs are short peptides, typically consisting of 5 to 30 amino acids, with the capability to penetrate cell membranes while transporting different cargoes, including proteins, nucleic acids, drugs, or NPs, among others [171]. In a representative example of active targeting of GNSs using CPPs, the designed hollow gold-based nanostructures were electrostatically decorated with "pH low insertion peptides" [172]. These attached peptides served as a targeting ligand due to their affinity to low pH tumor microenvironments, thereby conferring cell-penetrating capability to the GNSs. The use of CPPs was also proposed to enhance the active targeting of magnetoplasmonic GNSs with iron oxide-based nanocores, being demonstrated that the used ligands can be selectively degraded by matrix metalloproteinases, which are predominantly present in several types of solid tumors [173].

Nevertheless, and although the above discussed strategies based on the decoration of GNSs with different specific ligands remarkably increased their active targeting capability in *in vitro* studies, the provided specificity can be not enough when they are injected into living organisms. This loss of targeting functionality *in vivo* is attributed to the extremely high and still not fully understood complexity of biological systems, in which cross-reactions of different nature, the formation of complex protein coronas surrounding the GNSs, and/or the activation of the aforementioned immune mechanisms play a key role. Additionally, the presence of various biological barriers such as the liver, kidneys, blood-brain barrier, blood-ocular barrier, or skin also diminish the targeting capability of ligand-decorated GNSs [133,135]. All these phenomena involved in the normal function of living organisms can lead to a decrease on the percentage of the designed GNSs that finally reach the intended site of action and to their subsequent undesired fast degradation and clearance from bloodstream [174].

More specifically, the essential roles of liver-resident macrophages (Kupffer cells) and splenic macrophages in removing NPs from circulation before their accumulation in tumor xenografts were demonstrated through an innovative experimental procedure [175]. Briefly, Kupffer cells were depleted from mice by using dichloromethylene diphosphonic acid liposomes (clodronate liposomes), being observed that after this procedure the blood half-life of 100 nm GNPs increased from 0.64 to 8 h. Additionally, the accumulation of GNPs in the liver was also evaluated, observing a reduction to less than 10 % of the injected dose upon the depletion of the macrophages, while the gold nanostructures in the tumor increased from 0.03 to 0.50 %. To prevent the rapid clearance of GNSs from bloodstream in living organisms, the chemical functionalization of their external surface with polymers such as PEG [130], dextran [132], poly(vinyl alcohol), alginate and chitosan [176] has been also primarily evaluated.

Finally, it is important to highlight that, even in the case of achieving an efficient targeting of GNSs in the surface of the tumor, the subsequent diffusion of the NPs within the cancerous growth is typically inefficient. This is due to the highly complex physiology of tumors, which are composed of extracellular matrix, cancer cells, immune cells, and other stromal cells such as fibroblasts and pericytes. Additionally, tumors are stratified into a necrotic, hypoxic core and viable external layers, which hinder the facile diffusion of nanoparticulated systems to the innermost regions, leading to resistance and tumor relapse [177]. Despite the efforts of the scientific community during the last decades to enhance the diffusion of NPs within the structure of solid tumors [178], performed studies consistently report limited accumulations of nanostructured materials inside tumoral tissue. In this regard, a comprehensive meta-analysis quantified this phenomenon, being revealed that only a mere 0.7 % of the administered doses of NPs are finally accumulated in solid tumors [179]. Furthermore, experimental findings indicate an even lower percentage of NPs reaching tumor cells (0.0014 %) [180]. Current research is trying to address this problematic by developing more efficient strategies, such as those based on the leverage of immune cells with natural tumor-chemotaxis that we will discuss in following sections.

5. Biomedical applications of GNSs

Despite the aforementioned limitations of nanoparticulated systems to reach tumor growths and penetrate within them when injected in living organisms, gold-based nanostructures, and more specifically the GNSs here discussed, have been widely evaluated for different biomedical applications (Fig. 8). This interest for the biomedical evaluation of GNSs arises from their outstanding optical and physicochemical properties, which we have discussed in detail in Section 2. Basically, when GNSs are irradiated with light they experienced coherent collective oscillations of their valence electrons, which lead to the scattering of the incident light and to energy absorption and the subsequent release of heat. The size of GNSs is a critical feature that dictates the predominance of one or another of these phenomena: smaller nanostructures are better NIR-light absorbers, while by increasing particle size their scattering cross section is enhanced. Interestingly, and although it is also highly dependent on their other physicochemical characteristics, in general GNSs with *ca.* 100 nm in diameter display both resonant absorption and scattering properties, making them the most commonly evaluated for biomedical applications. Hence, this capability of GNSs to absorb NIR light results in a strong and highly localized photothermal heating upon laser illumination, which can be exploited, for example, to induce cancer cell death and tumor remission [69]. On the other hand, the light scattering properties of GNSs can be utilized for contrast enhancement in bioimaging. The plasmon-based optical properties of GNSs also enable the efficient release of bioactive compounds (*e.g.* drugs, genes), thus

providing light-triggerable delivery nanosystems on demand [95,181,182]. In this section, we are going to thoroughly review these and other biomedical applications of GNSs, highlighting the current advantages and limitations of each one and describing some of the most relevant works in the field.

5.1. Photothermal therapy

5.1.1. Photothermal effect

The irradiation of GNSs using NIR light with frequencies close to that of surface plasmon leads to an intense photon absorption phenomenon, producing a hot electron gas that results in rapid non-equilibrium heating. This initial heating is followed by energy exchange between the electrons and the lattice through electron-phonon collisions until thermal equilibrium is reached. Subsequently, this energy is released by phonon-phonon exchange to the molecules of the surrounding medium, leading to the cooling of the nanostructures and the concomitant heating of the medium, being this the basis of the so-called PTT [188]. The temperature increase will depend on the number of photons collected by the nanostructures, dictated by their concentration and physicochemical characteristics, but also on the time, intensity and type of light irradiation [189]. Thus, both continuous and pulsed lasers have been proposed in combination with GNSs for PTT applications [190]. The photothermal response of GNSs when exposed to continuous wave laser irradiation typically results in sustained and moderate temperature increases in the surrounding environment, being this the most used approach for PTT purposes. However, controlled pulsed irradiations can be exploited to generate higher energy densities in the vicinity of GNSs. Although more typically evaluated for other applications such as transfection or photoacoustic imaging [191], the irradiation of GNSs with short-pulsed laser has been also proposed for PTT applications [190,192]. Thus, the use of pulse widths in the femtosecond regime enables very high-localized temperature increases on the surface of GNSs. This type of lasers produces free electrons *via* nonlinear absorption interactions, thus differing from continuous wave or long-pulsed lasers, which depend on the linear absorption of photons (one photon at a time) that can lead to greater heat accumulation and increased collateral damage [193,194].

The local temperature increases reached upon the light irradiation of GNSs can be exploited for therapeutic purposes by inducing the heat-mediated death of the surrounding cancer cells. The main mechanism proposed to explain PTT-mediated cell death (thermal ablation) is the denaturation of cytoplasmatic membrane and functional proteins, essential to sustain cellular integrity and viability. Moreover, the rapid formation and subsequent explosion of steam nanobubbles may also play an important role in causing tumor cell damages [42]. Interestingly, it has been observed that mild hyperthermia can be used as complement to chemo- and radio-therapies, since cancerous cells are more sensitive to these treatments above 43 °C [195,196].

It is worth mentioning that gold-based nanostructures, including GNSs, exhibit high thermal stability, not being observed noticeable alterations on their structures when exposed to light irradiations typically used for PTT. For example, the excellent thermal stability of hollow GNSs was established by applying continuous and cyclic irradiation

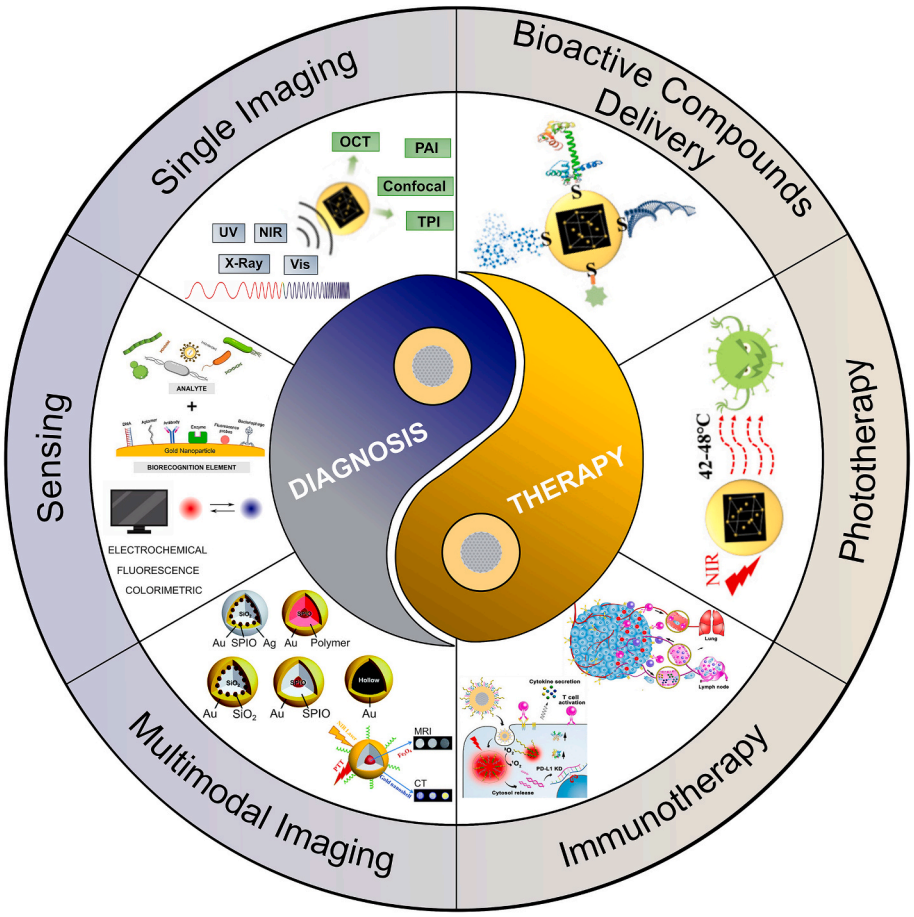

Fig. 8. Schematic illustration of the main biomedical applications of GNSs for diagnostic (single imaging, multimodal imaging, sensing) and therapeutic purposes (transport and delivery of bioactive compounds, phototherapy, immunotherapy). Adapted with permission from Ref. [183]. Copyright 2020, MDPI, CC BY 4.0; Ref. [184]. Copyright 2022, Elsevier B.V.; Ref. [185]. Copyright 2018, Elsevier B.V.; Ref. [186]. Copyright 2017, Royal Society of Chemistry, CCBY 3.0 DEED; Ref. [187]. Copyright 2014, Royal Society of Chemistry.

using a 808 nm laser, being hypothesized that their performance as PTT agents can be maintained without the need of multiple dosages [197]. However, when gold nanostructures are exposed to extremely high light intensities, higher than those typically required for PTT strategies, the generated heat can induce the melting or reshaping of the GNPs and irreversibly changing their optical properties [198,199].

5.1.2. Photothermal cancer therapy

After the pioneering works by Halas' group analyzing the photothermal potential of GNSs [164], several reports have explored the potential of PTT provided by GNSs of different sizes and shapes for cancer treatment, from which interesting information can be collected [200]. The role of morphology and structure of gold-based nanostructures over their performance as photothermal agents has been extensively studied. In a representative work focused on the analysis of this influence, rod-shaped GNPs, silica-core GNSs and hollow GNSs were evaluated under light irradiation using a 808 nm laser at 30 $W{\cdot}cm^{-2}$ for 7 min [201]. Interestingly, the dose required to reach the desired photothermal effect on A549 (lung), HeLa (cervix) and TCC (bladder) cancer cells was lower when using silica-core GNSs, following by hollow nanostructures and nanorods, being inferred that the nanoshell-like structures here reviewed are those with higher photothermal capabilities. In a similar comparative study, GNSs have demonstrated the capability to produce larger temperature increases than gold nanorods when both are used at equal concentrations [202].

In this way, it was established that GNSs with the most simplistic design, consisting of dual core-shell nanostructures or hollow nanocapsules, showed enhanced photothermal efficacy in comparison with the more typically used gold nanorods. Moreover, other additional advantages of GNSs over gold nanorods is their higher biocompatibility, since the synthesis of these later nanostructures usually involves the use of potentially cytotoxic surfactants [203,204]. Interestingly, it is possible to further increase the performance of gold-based nanosystems for PTT applications by designing GNSs with highly complex structures consisting of more than two layers. For example, the innovative gold nanomatrioskhas that we already described in previous sections have been evaluated for the PTT-mediated treatment of triple negative breast cancer xenografts on female athymic nude mice [29]. These multilayered nanostructures, which consist of gold nanocores coated with thin silica layers, and finally surrounded by external GNSs with 90 nm in diameter, were compared with conventional 150 nm silica-core GNSs in terms of cell uptake and PTT efficiency. After the intravenous injection and NIR irradiation of both nanosystems, 83 % of tumor-bearing mice treated with gold nanomatryoshkas appeared healthy after 60 days, while only 33 % of mice treated with conventional GNSs survived during the same period. According to the authors, the smaller size and larger absorption cross section of the designed complex NPs make them more effective therapy in the evaluated application. Other additional remarkable features of this study were the use of large tumors, that better mimic advanced cancers typically diagnosed and treated in clinical practice, on the elucidation of the size effect (keeping the LSPR peak constant) on the *in vivo* intra-tumoral accumulation of GNSs (Fig. 9B).

The specific and triggered photothermal cell-killing effect of GNSs has been demonstrated several times in different cancer cells and tissues, using both *in vitro* and *in vivo* models, thus confirming the high potential of GNSs as photothermal therapeutic agents. The types of cancerous tumors that have been successfully ablated in mice models by using GNSs include cervix [172], colon [95,164,205,206], human squamous cell carcinoma [127,165,207], melanoma [208–211], brain [212,213], liver [214], breast [215–217], ovarian [168], pancreas [218], or lung [219,220], among others.

Alternatively to systemic or intra-tumoral administration of nanotherapeutics, a new dosage form was proposed by Redolfi-Riva et al., who developed GNSs/polysaccharide composite nanofilms for controlled laser-assisted tissue ablation [221]. The authors created stable, flexible, and ultrathin free-standing polymeric film platforms through a layer-by-layer assembly of biocompatible and mucoadhesive chitosan and sodium alginate, incorporating the GNSs. Basic laser-induced heating functionality was demonstrated through *in vitro* hybrid nanofilm-mediated thermal ablation of human neuroblastoma cancer cells, confirming irreversible damage to cell membranes and nuclei. Application of the standing hybrid films onto tissue surfaces and subsequent *ex vivo* analysis also demonstrated localized vaporization and carbonization of animal muscular tissue. Thermal distribution in the tissue reached a steady state in a few seconds, ensuring an excellent control of local photothermally induced heating and providing more safety and predictability with respect to traditional laser surgery. These nanocomposites are expected to enhance particle manipulation and density control in plasmonic-mediated photothermal ablation and hyperthermia. Moreover, the bio-adhesive properties of the nanofilms allow stable adhesion to the external surface of organs or mucosal tissues affected by tumoral masses/cells.

Finally, another crucial and typically overlooked factor that can hinder successful heat generation using GNSs in PTT procedures is the efficient light delivery to the nanostructures. This is an especially critical point in the case of GNSs targeting deep tumors because light penetration into living organisms is limited when it is irradiated from an external source. This fact can increase the likelihood of tumor recurrence and the development of photothermal resistance by cancer cells upon a light irradiation that reaches the region of interest with very diminished intensity. Hopefully, various types of devices and strategies have been developed for effective light delivery, ranging from the use of optical fibers to the implantation of light devices, resulting in better outcomes compared to conventional light sources for deeper tissues. This last approach give rise to the still under development technique of interstitial PTT, in which an intra-tumoral implanted light generation device is used to efficiently stimulate the injected photosensitive agents that reached the cancer growth [222]. This strategy has the potential to enhance the efficacy of the photothermal-mediated treatment of any type of tumor, but it results especially appealing for in deep-seated tumors or for those with very large dimensions (thicker than 10 mm). For a more exhaustive description of the interstitial PTT technique and its advantages respect the more traditional superficial PTT, we refer readers to a recent systematic comparative preclinical study in which both procedures are evaluated [223].

5.1.3. Photothermal therapy for other diseases

Although most works that evaluated the application of PTT using gold nanostructures were focused on cancer, the photothermal capability of GNSs has also been leveraged for the therapeutic treatment of other biomedical disorders/conditions. For example, Paithankar et al. conducted a pilot human clinical study for the treatment of acne ailment in which the designed GNSs were accumulated inside the follicles with the help of low-frequency ultrasound to facilitate their penetration [224]. Afterwards, the skin was illuminated with a NIR laser to induce local thermolysis of sebaceous glands, not being observed any remarkable damage in the surrounding skin tissue (Fig. 9C). The treatment of rheumatoid arthritis has also been studied by using PLGA-core GNSs loaded with the anti-rheumatic drug methotrexate. The nanoplatform was administered to collagen-induced arthritic mice, being accumulated in the inflamed paws of the rodents and inducing a healing process mediated by the accelerated diffusion and release of the drug [225].

In another interesting approach, the unique photo-responsiveness of GNSs has been exploited to inhibit the growth and proliferation of Gram-positive and Gram-negative bacteria through the local generation of heat [226]. To increase their antibiotic effect, streptomycin was attached to the surface of oligochitosan-coated GNSs, which were functionalized with anti-bacterial antibodies to target *Lysteria Monocytogenes*. The antibacterial efficacy of the nanoplatform was evaluated in mouse models with infected wounds, being established that the combination of the antibiotic drug and PTT surpassed either of the individual treatments (Fig. 9D) [227]. In a similar way, bimetallic silver/

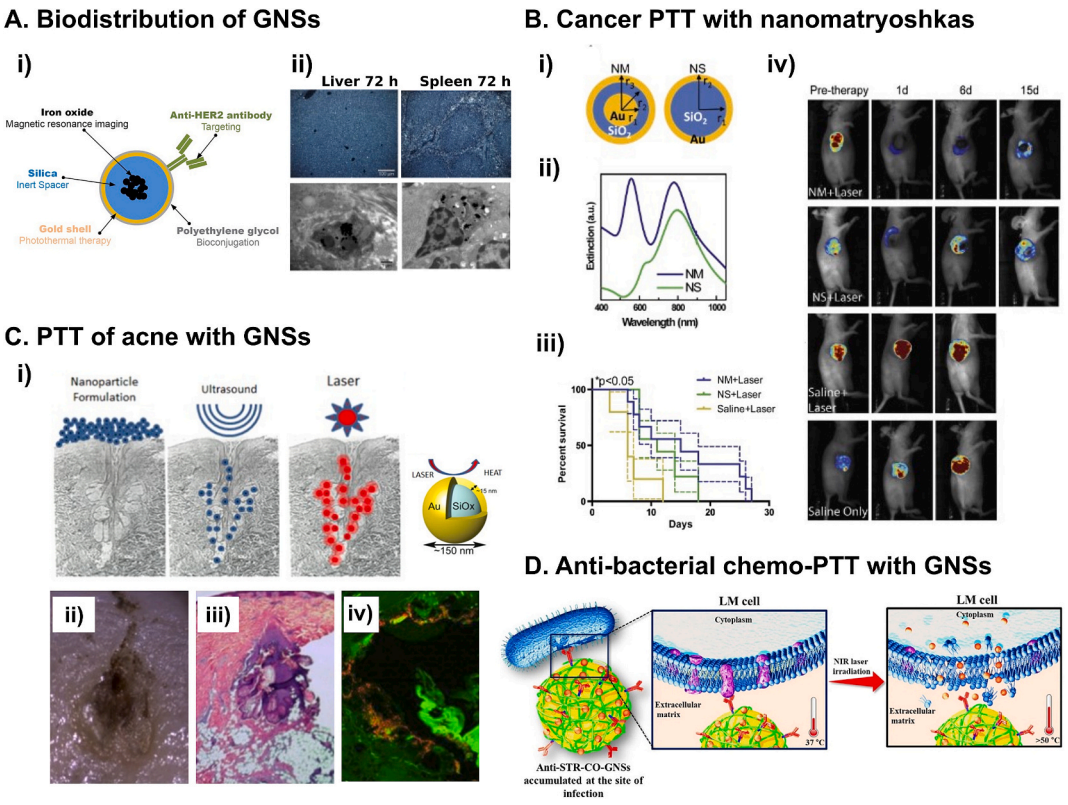

Fig. 9. A. i) Schematics and TEM image of the multifunctional anti-HER2 targeted GNSs. ii) Dark field images of tissue sections acquired from the liver and spleen after injection of anti-HER2 GNSs and TEM images of anti-HER2 GNSs internalized in liver and spleen cells (Adapted with permission [137] Copyright 2019, Springer Nature). **B.** i) Schematic representation and ii) LSPR associated spectrum of gold nanomatryoshkas (NM) and typical silica-core GNSs (NS). iii) Kaplan-Meier plots of tumor-bearing mice treated with saline physiological solution, gold NM or NS. All tumors were irradiated 5 min with a laser of wavelength at 808 nm and power of 3 $W{\cdot}cm^{-2}$. iv) The efficacy of PTT utilizing NM and NS in tumor response was assessed through bioluminescence imaging, wherein tumor cells were transfected with the luciferase gene. In both instances, residual cancer cells were detected post-treatment, leading to tumor recurrence during the experiment's duration (Adapted with permission [29] Copyright 2014, Elsevier). **C.** i) Schematics of GNSs and their ultrasound-aided incorporation in the sebaceous follicle for further NIR-laser photothermal treatment. ii) Thermally damaged sebaceous gland, iii) H&E staining demonstrating localized damage to a sebaceous gland, and iv) imaging of GNSs (orange) by TPPL imaging (Reproduced with permission [224] Copyright 2015, Elsevier B.V.). **D.** Schematic representation of the killing process on Listeria monocytogenes by antibody-conjugated and streptomycin-coated GNSs with laser irradiation (Reproduced with permission [227] Copyright 2023, Elsevier, CC BY NC ND). (For interpretation of the references to colour in this figure legend, the reader is referred to the web version of this article.)

gold hollow nanoshells have been evaluated for the elimination and inhibition of colony expansion of multidrug-resistant bacterial strains, as well as for the wound healing in mouse models with infected open wounds. Through the developed strategy, PTT synergized with the release of silver ions, showing an enhanced anti-microbial activity [228].

In a representative example of GNSs-mediated PTT for other diseases unrelated to cancer, gold nanostructures functionalized with carboxylate-terminated organosulfur ligands were attached to model catheter surfaces, after which they showed highly effective to cause the thermal-induced death of the adhered bacteria [229]. Thus, it was demonstrated that the photothermal properties of GNSs can also exploited to prevent or combat the typical formation of pathogenic biofilms on implant/catheter surfaces.

5.2. *Immunotherapy*

Immunotherapy is a type of treatment based on helping the immune system of the patient to fight against cancer, infections, or other diseases [230,231]. In the specific case of cancer immunotherapy, it is a research field that has gained major attention in recent years due to its outstanding results in the treatment of certain types of tumors, such as melanoma [232]. One prominent modality of immunotherapy is based on the genetic modification of immune cells to induce the production of proteins called chimeric antigen receptors (CARs) (*e.g.* CAR-T cells, CAR-Natural Killer cells), thus enhancing their ability to recognize and destroy cancer cells [233]. Another immunotherapy strategy exploits the properties of immune checkpoint inhibitors, a family of receptors found on immune cells that play an essential role on their function and allow the dynamic control of the immune balance. The primary ligand associated with one of the most relevant checkpoint inhibitors, the so-called PD-L1, is particularly interesting, since it is expressed on tumor cells and tumor-infiltrating myeloid cells. Different types of nano-structured materials, included GNSs, have been explored for cancer immunotherapy applications. In a representative recent example, GNSs with hollow architecture were loaded with the anticancer drug doxo-rubicin and functionalized with antibodies targeted to the immune checkpoint PD-L1 to target melanoma cells [211]. The cellular uptake of the designed GNSs was assessed in two different melanoma cell lines, CLONE-M and B16F10, that exhibit low and high expression levels of PD-L1, respectively. The performed flow cytometry assays revealed a remarkable enhanced cellular uptake of gold nanostructures by B16F70 cells, thus demonstrating the capability of the nanoplatform to target melanoma cells with high PD-L1 expression levels. Furthermore, doxorubicin-loaded GNSs were also evaluated *in vivo* with promising chemo-phototherapy effect against B16F10 tumors in C57BL/6 male mice (Fig. 10A).

On the other hand, adoptive cellular immunotherapies have inspired the development of new strategies to overcome the already discussed problematic of the typical low accumulation of injected NPs in solid

tumors [179]. In this sense, it is worth mentioning a recently published work that analyzed the key role of tumor-associated macrophages (TAMs) in the transport of NPs to the most inaccessible regions of tumors [234]. By using intravital confocal microscopy video-imaging, it was observed the gathering of these macrophages gather around the site where GNPs were extravasated, following by their phagocytosis and the subsequent migration and transport of GNPs in various directions, thus being confirmed that they are able of transport NPs from their extravasation point into the tumor stroma.

In the specific case of the GNSs here reviewed, this type of nanostructures has been loaded into specialized cells of the innate or adaptive immune system to exploit their chemokine-driven (chemotaxis) mobilization to tumors and their capability to infiltrate within them. Thus, for example, the internalization of GNSs by murine monocytes and macrophages without toxic effects and the subsequent infiltration of the GNSs-loaded cells (referred to as cellular Trojan horses) into tumor spheroids has been successfully evaluated through microscopy techniques (Fig. 10B) [147]. The macrophage-based vectorization of GNSs has been also evaluated to target and infiltrate the nanostructures within tumors located at barely accessible physiological niches, such as the case of human glioma spheroids [235]. Interestingly, in addition to macrophages, other types of cells of the immune system such as activated T cells have also been also proposed as tumor targeting transporters of GNPs [152,236]. Most recent strategies have already combined the use of immune cells as living transporters of GNSs with the subsequent exploitation of the photothermal properties of the nanostructures once accumulated within the tumor. In a representative example of this approach, 150 nm silica-core GNSs were loaded within rat alveolar macrophages through a simple co-incubation process [237]. The temperature increase generated upon the light irradiation of GNSs-macrophages hybrid bio-nanotherapeutics revealed a promising antitumoral efficacy *in vitro* against FaDu-macrophage spheroids, as well as a biocompatible profile when evaluated *in vivo* in Sprague Dawley rats. In a different approach inspired by previous studies that used red blood cell membranes as camouflaged coatings for theragnostic NPs, Xuan et al. proposed the use of macrophage cellular membranes to hide GNSs (Fig. 10C) [238]. This strategy aims to improve the transport and accumulation of the gold nanoparticulated systems within tumors by

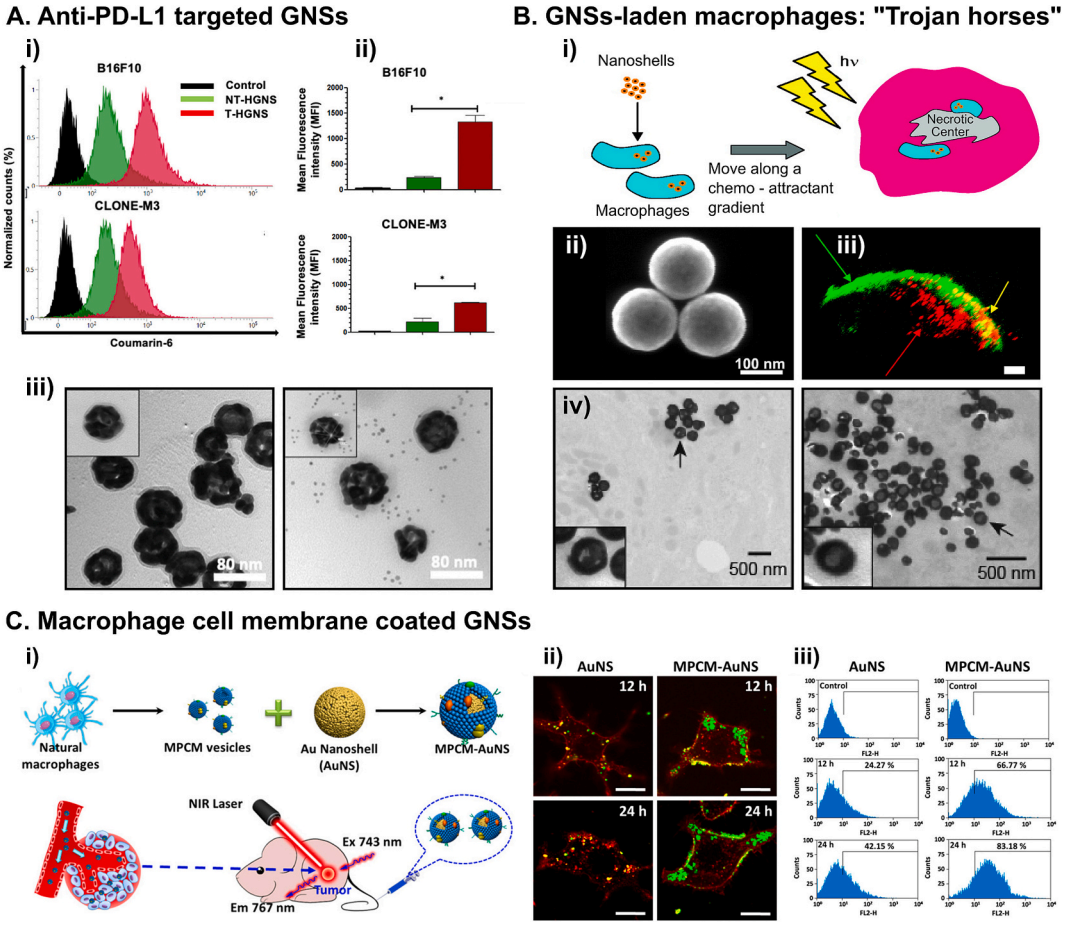

Fig. 10. A. Flow cytometry analysis for intracellular uptake of hollow GNSs after the treatment with coumarin-6 loaded non-targeted-hollow GNSs (NT-HGNS) and targeted-hollow GNSs (T-HGNS) on B16F10 and CLONE-M3 melanoma cell lines at 24 h time point and ii) their respective quantitative analysis. iii) Immuno-TEM images of NT-HGNS (left) and T-HGNS (right). Anti-PD-L1 antibodies were labeled with 5 nm gold labeled anti-rat IgG (Reproduced with permission [211] Copyright 2020, Elsevier). **B.** i) Schematic of "Trojan Horse" therapeutic GNSs delivery into the hypoxic region of tumor. ii) SEM image of GNSs with well-defined spherical morphology. iii) 3D reconstruction of two-photon image of a T47D-cell tumor spheroid treated with GNSs-laden macrophages and laser irradiation. Live cells were stained with CellTracker (green), dead cells were stained with propidium iodide (red). Green arow signals unirradiated cells; red arrow, GNSs-laden macrophages infiltrated in the necrotic center of the spheroid; and yellow arrow/cells, T47D cells which have been thermally damaged due to their location next to macrophages. Scale bar is 50 μm. iv) TEM micrograph of a GNSs-laden macrophage (left) and a GNSs-laden monocyte (right) with GNSs dispersed in intracellular vacuoles. (Adapted with permission [147] Copyright 2007, American Chemical Society). **C.** i) Schematics of the preparation of macrophage cell membrane-camouflaged GNSs for *in vivo* photothermal cancer therapy. ii) Confocal microscopy images and iii) flow cytometry histograms displaying the enhanced recognition of macrophage cell membrane-camouflaged GNSs by 4 T1 triple negative breast cancer cells at 12 h and 24 h (Reproduced with permission [238] Copyright 2016, American Chemical Society). (For interpretation of the references to colour in this figure legend, the reader is referred to the web version of this article.)

leveraging the homotypic recognition capacity of the extracted cellular membranes.

5.3. GNSs as nanocarriers for bioactive compounds

The controlled transport and release of bioactive compounds using nanoparticulated carriers is one of the most attractive and challenging potential applications of nanotechnology in the field of biomedicine. The cargoes attached or incorporated into the nanocarriers can range from drugs and other therapeutic biomolecules to photosensitizers, among many others, being their on-demand release controlled through local or external activation mechanisms. The local stimuli-triggered releases of carried cargoes depend on subtle changes in microenvironmental conditions (*e.g.* pH, temperature, redox environment, surrounding solute concentrations), which destabilize the cargo-nanocarrier complex due to bonds rupture, swelling/de-swelling, and/or oxidative and enzymatic degradation of the containing nanostructures. On the other hand, external stimuli-triggered cargoes release mainly relies on the application of exogenous physical energy sources (*e.g.* light, magnetic fields, pressure gradients) that eventually cause the aforementioned phenomena and the subsequent destabilization of the nanocarrier complex.

The intrinsic properties of GNSs, such as their sensitivity to light stimuli or their reservoir-like geometry, as well as the simple functionalization of their surface, make this type of metallic nanostructures highly suitable for incorporating various bioactive molecules within their cavity/core or onto their surface. In this section, we will briefly review the use of GNSs for the transport and delivery of biologically active cargos, while protecting them and inhibiting their non-specific spreading to off-target tissues and cells.

5.3.1. Delivery of nucleic acids

The recent development and successful application of messenger RNA (mRNA)-NPs vaccines has revealed the enormous potential of nucleic acid-based treatments to completely change the current pharmacological and biomedical landscapes [239]. Among the different nanostructured materials evaluated for the transport and delivery of nucleic acids, the use of GNSs constitutes one of the most interesting and promising approaches. Interestingly, it was observed that different release mechanisms of the cargoes can be induced depending not only on the physicochemical characteristics of the GNSs, but also on the nature of the activating laser. For example, double-stranded DNA separates when illuminated with continuous wave-laser illumination. This phenomenon can be exploited for the controlled release of single-stranded DNA, while the complementary strands remain attached to the nanocarrier surfaces through, for example, gold-thiol bonding in the case of GNSs [240]. However, when double-stranded DNA is illuminated with pulsed NIR laser, it can result in either the dehybridization of the molecule or the breaking of the gold-thiol bond between DNA and the gold-based nanocarrier, the latter giving rise to the release of the entire double-stranded DNA [241,242]. It has been hypothesized that there may be two different mechanisms behind the observed effect of illumination on nucleic acids bound to gold nanostructures. First, the photothermal properties of GNPs can cause temperature increases upon light irradiation, giving rise to the melting of DNA molecules. On the other hand, hot-electron transfer from plasmon decay may be the cause of DNA denaturation or gold-thiol bonds breaking.

In a very representative work in the field of nucleic acids delivery using GNSs from Halas´ group, it was experimentally demonstrated that DNA release upon continuous wave laser illumination is consequence of the light-induced temperature increases. Remarkably, these authors confirmed that the heat generated using this laser arises from collective heating effects and not by hot-electron injection, as previously stated, causing the dehybridization of DNA molecules and the subsequent release of single-stranded DNA. However, when the GNSs loaded with double-stranded DNA were illuminated using a pulsed femtosecond NIR laser, the DNA release was found to occur through a hot-electron transfer process which breaks gold-thiol bonds, releasing the double-stranded DNA molecules without observing any bulk temperature increase (Fig. 11A) [243].

Interestingly, the same research group also achieved an efficient light-induced release of single-strand antisense oligonucleotides and small interfering RNA (siRNA) electrostatically bound to poly(lysine)-coated GNSs through a slightly different approach. In this case, NIR irradiation was used to modulate the interaction between the cationic polyelectrolyte attached to the GNSs and the loaded cargos, thus being possible to control either their thermally- or non-thermally-induced release [244].

5.3.2. Delivery of small drugs

The potential of GNSs for the transport and delivery of low molecular weight pharmacological compounds have been widely analyzed both *in vitro* and *in vivo*. Typically, the particular architecture of GNSs, with an inner cavity/core with controlled dimensions and physicochemical properties, has been exploited for drugs encapsulation, while the already detailed photo-responsiveness of these nanosystems were used for the subsequent release of the cargoes [245]. In one of the most typical approaches, GNSs are used for the transport and controlled release of the anticancer drug doxorubicin. In a representative example of this strategy, hollow GNSs with 40 nm in diameter were synthesized through a galvanic replacement reaction, and doxorubicin was loaded both in the inner and outer surfaces of the nanostructures through hydrogen bonding [246]. Confocal microscopy images demonstrated the successful internalization of drug-nanocarrier complexes within the cytoplasm of MDA-MB-231 cancer cells *in vitro*. In the absence of NIR illumination, the red fluorescence of doxorubicin and the scattering signal of the GNSs were observed only in the cytoplasm, but not in the nuclei of cancer cells. However, when NIR irradiation was applied the drug was observed inside the cell nuclei, indicating that the doxorubicin loaded in the GNSs was light-triggered released. GNSs have been also evaluated as nanocarriers for the targeted release of other medications such as nitric oxide, a pleiotropic bioregulatory molecule known to inhibit cell proliferation and induce cell death at appropriately high concentrations. For example, Levy et al. functionalized the external surface of GNSs with hollow architecture using a thiol-functionalized derivative of cupferron, reaching a controlled spatio-temporal release of nitric oxide upon pulsed NIR laser irradiation [247]. The encapsulation of drugs within the dielectric core of GNSs constitutes a particularly interesting alternative to their attachment to the external metallic surfaces of the nanostructures. In this scenario, the design of GNSs with highly porous structure are required to allow the release of the encapsulated drugs. On the other hand, the mobility of drug molecules within the core can be enhanced through light-induced heat generation, thus facilitating their release. In the specific case of GNSs with polymeric core, the temperature increases upon NIR illumination also enables the fluidization, or even the melting, of the polymeric chains, thereby promoting even more the diffusion of drugs from the cores. This mechanism was demonstrated by inducing the intracellular release of a model drug, Nile Red, from PLGA-core GNSs, exploiting the photothermal properties of the designed porous metallic nanoshells [169]. Thus, it was observed that NIR light illumination promoted the delivery of the drug encapsulated within the polymeric cores inside the cells, while in the absence of irradiation no release of the probe was detected.

In the previously discussed approaches, low temperature increases are enough to promote or enhance the release of drugs loaded into GNSs. However, when illumination conditions and the properties of GNSs allow larger heat generation, the gold-drug tandem can be exploited for combined dual therapies involving hyperthermia and the pharmacological effect of drugs. For this reason, different drugs have been loaded in the external surface or in the core of GNSs to then determine the potential of the designed systems as dual therapeutic nanotools. In a representative work evaluating this strategy, silica-core GNSs were

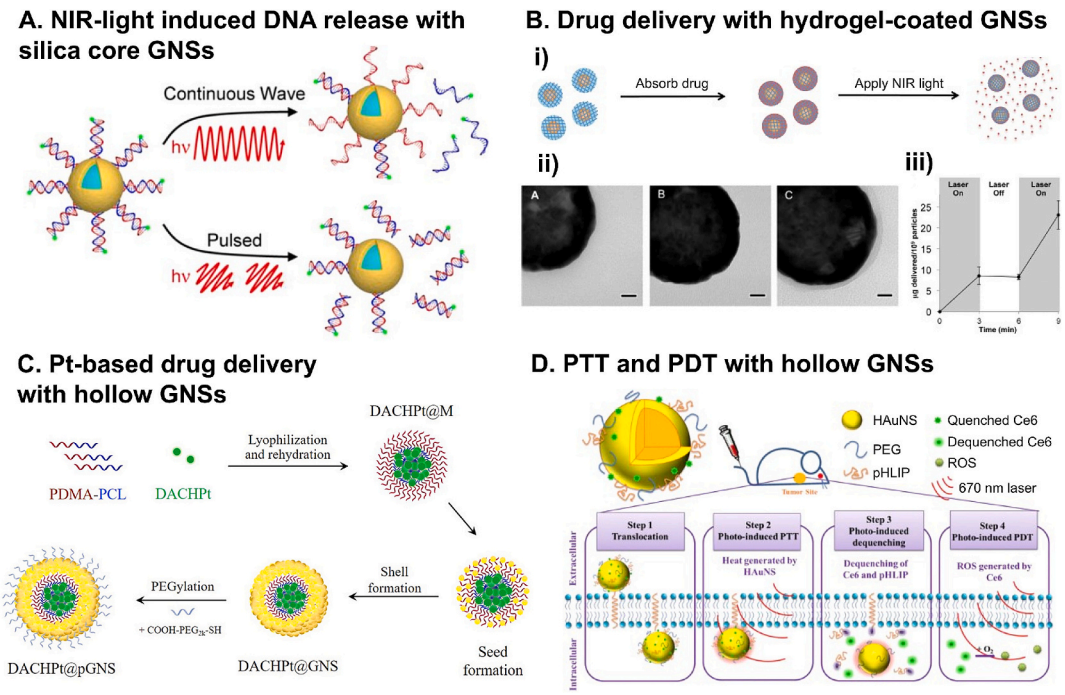

Fig. 11. **A.** NIR-light-induced DNA release under continuous wave irradiation induce dehybridization and release of fluorescently tagged single-stranded DNA, while pulsed irradiation derives in Au-S bond breakage and release of double-stranded DNA (Reproduced with permission [243] Copyright 2017, American Chemical Society). **B.** i) Schematics illustrating PNIPAM-coated GNSs soaked in doxorubicin solution and laser-triggered release of the drug. ii) TEM images of bare, initiator functionalized, and hydrogel-coated GNSs. **iii)** The release of doxorubicin encapsulated within hydrogel-coated GNSs is accelerated with NIR laser activation, while minimal release is observed during periods without light stimulus (Reproduced with permission [206] Copyright 2015, American Chemical Society). **C.** Fabrication of GNSs with polymeric micellar template cores loaded with platinum-based drug (Reproduced with permission [95] Copyright 2020, American Chemical Society). **D.** Schematic illustration of hollow GNSs-pH low insertion peptide-Ce6-driven PTT therapy. The process of cellular uptake and bimodal therapy activation is depicted in four stages: 1) in the low pH tumoral microenvironment the pH-responsive peptide spontaneously acquires an helical formation that facilitates the cellular entrance; 2) PTT is actuated by 670 nm laser; 3) The generated heat triggers the release of the photosensitizer Ce6 and the peptide; 4) Reactive oxygen metabolites are generated by light-activation of Ce6 upon irradiation with 670 nm laser (Reproduced with permission [172] Copyright 2015, Elsevier).

modified by growing a layer of poly(*N*-isopropyl-acrylamide-*co*-acrylamide) (PNIPAM) hydrogel loaded with antineoplastic doxorubicin surrounding them [206]. These drug-loaded polymeric layers showed a temperature dependent transition from a swollen configuration under physiological conditions to a collapsed state at elevated temperatures, which allowed a burst release of the drug controlled by NIR laser illumination. The efficiency of the nanosystem was tested in murine colon carcinoma cells, revealing an increased cell death when NIR irradiation was exploited for both heat generation by GNSs and drug release (Fig. 11B).

In addition to doxorubicin, other bioactive molecules such as actinomycin D or platinum-based compounds (*e.g.* cisplatin, carboplatin, oxaliplatin) have also demonstrated an enhanced anticancer effect when administered concurrently with local or loco-regional hyperthermia [248]. Interestingly, it is worth mentioning that this phenomenon is not observed with other anticancer agents such as taxanes (*e.g.* paclitaxel, docetaxel) [249]. The combination of chemotherapy and PTT using GNSs modified with the aforementioned platinum-based compounds was evaluated against colorectal cancer in a recently published work [95]. More specifically, the authors designed GNSs with polymeric micellar cores in which dichloro(1,2-diaminocyclohexane) platinum (II), the active metabolite of the third-generation platinum-based drug oxaliplatin, was encapsulated (Fig. 11C). The *in vitro* results of this study demonstrated that the combined effect of PTT and chemotherapy exerted an additive/synergistic cytotoxic effect over HT29 and LS174T human colorectal cancer cell lines. Interestingly, the synergistic effect was notably more pronounced in LS174T cells, which indicates that the effect of the combined simultaneous therapy differs between cancer cells depending on their different susceptibility to each treatment modality. Furthermore, the *in vivo* assays conducted in a murine subcutaneous xenograft model demonstrated a more powerful antitumor effect of combined therapy when compared to the administration of free drug or PTT alone.

As discussed in the previous section, gold-based nanostructures can be exploited for the transport and release of different typologies of nucleic acids. However, the attachment of these biomolecules to gold surfaces through chemisorption or physisorption processes can also be used as an intermediate step for the subsequent loading of small-sized drugs. In this way, nucleic acids, such as siRNA or thiolated DNA, and other proteins have been proposed as anchoring moieties for different drugs in the surface of GNSs. For example, docetaxel (a chemotherapeutic compound) and lapatinib (a targeted inhibitor of the ATP binding site of the HER2 tyrosine kinase domain) were loaded into silica-core GNSs modified with DNA molecules or human serum albumin [250]. In the first case, a dodecamer DNA sequence with high affinity to taxol was utilized to attach the docetaxel, whereas for lapatinib, which features a pyrimidinamine group analogous to adenine, a thymine-rich sequence was employed. Conversely, human serum albumin formed a protein corona surrounding GNSs with multiple binding regions that allow the entrapping of both drugs. The therapeutic efficacy of the designed nanoplatforms was assessed in two breast cancer cell lines, MDA-MB-231 (triple-negative breast cancer) and SKBR3 (overexpressing HER2), as well as in the macrophage cell line RAW256.2, being demonstrated their capability to achieve precise drug releases within narrow time windows, thus distinguishing them from conventional chemotherapy. In another interesting approach, Villar-Alvarez et al. recently reported the development of multifunctional branched GNSs decorated with siRNA molecules designed to inhibit the expression of HER3 (human epidermal growth factor receptor 3) in breast cancer cells and mice models [251]. In more detail, the nanoplatform was

comprised of doxorubicin-loaded GNSs decorated with the photosensitizer indocyanine green, a siRNA against HER3, and the HER2-specific antibody trastuzumab. The performed *in vitro* experiments showcased a successful HER3 silencing induced by the released siRNA, an inhibition of HER2 oncoproteins by trastuzumab, and a remarkable reduction in the p-AKT pathway, a protein linked to cell survival and proliferation, that enhancing the chemotherapeutic effect of doxorubicin. On the other hand, *in vivo* studies in mouse models bearing breast tumors showed a substantial and gradual reduction in tumor volume upon the administration of the nanoplatform followed by NIR light irradiation, thus demonstrating the potential of the developed strategy against HER2+ breast cancer.

5.4. Alternative therapeutic outcomes of GNSs

In addition to the already discussed use of gold nanostructures for photothermal therapy of cancer and other diseases, immunotherapy, and/or the controlled transport and release of nucleic acids and small drugs, these nanomaterials have also been proposed for alternative therapeutic strategies. For example, there is compelling evidence demonstrating that radiotherapy is highly potentiated by the presence of gold-based NPs. Radiation therapy is a type of cancer treatment based on the application of high-energy ionizing beams (*e.g.* X-rays, proton radiation), being its efficacy enhanced when GNPs are incorporated in the tumoral zone and act as radiosensitizers due to the high atomic number of gold. This phenomenon is based on the increased absorption of ionizing radiation by gold nanostructures, leading to the production of secondary electrons that provoke DNA damage and generate reactive oxygen species (ROS), thereby amplifying the cytotoxic effect over tumor cells [252].

Moreover, it has been observed that the efficacy of radiotherapy and hyperthermia is enhanced when both treatments are combined. This synergistic effect is attributed to the inhibitory impact of heat on the repair mechanisms of double-strand breaks caused by radiation, as well as to the reoxygenation of tumor microenvironment [253]. In this context, Diagaradjane et al. demonstrated the feasibility of modulating the *in vivo* tumor response to radiotherapy through hyperthermia generated by GNSs [254]. This enhanced sensibility to the applied radiation beams was attributed to the increase in tumor perfusion induced by the generated heat, which reduces the fraction of radiation-resistant hypoxic cells, followed by the induction of tumor-specific localized vascular damage and extensive associated necrosis. In another illustrative work exploring this dual therapeutic strategy, the synergy between the photothermal properties of GNSs and radiotherapy was evaluated in two different breast cancer models [255]. Firstly, in a genetically engineered breast cancer murine model rich in cancer stem cells, which have been associated to high resistances to chemo- and radiotherapy and metastatic invasiveness [256]. On the other hand, in a triple negative breast cancer human xenograft tumor model, a subtype of cancer characterized by the absence of estrogen, progesterone and HER2 receptors that is considered one of the most aggressive forms of this disease, often associated with poorer overall patient prognosis [257]. When the tumors were exposed exclusively to ionizing radiation, it was observed either a null or a slight increase on the size of the cancer growths, but with a relative increase in the ratio of stem-like to normal cells in the residual tumor. However, tumors that were radiosensitized through the accumulation of GNSs and the subsequent light-induced hyperthermia, followed by the same dose of ionizing radiation, exhibited large reductions in tumor size without increases in the proportion of stem-like cells in the residual tumor. These observations suggest that the sequential application of GNSs-targeted hyperthermia and radiotherapy could significantly enhance the current treatments of radioresistant tumors, such as triple negative breast cancer.

A different type of therapy using GNSs that has been widely proposed is the so-called photodynamic therapy (PDT). This is based on the light excitation of photoactive molecules known as photosensitizers to generate cytotoxic reactive oxygen species, mainly singlet oxygen ($^1O_2$), through energy transfer to molecular oxygen [258]. PDT has been evaluated to treat different diseases, but its application in cancer therapy is the most commonly analyzed [259,260]. The intrinsic properties of GNSs-based nanoplatforms can be exploited to use them simultaneously as both PDT and PTT agents under adequate light irradiation conditions. In a representative example of this approach, different GNSs with hollow architecture were proposed for the treatment of melanoma tumors through combinatorial PTT and PDT by exciting them with low doses of NIR light [210]. Hollow GNSs with spherical, cubic, and rod-like morphology were evaluated, being established the better efficiency of the first ones in converting incident photons into heat. However, GNSs with rod morphology were those that showed the highest singlet oxygen production yield.

Although the intrinsic properties of GNSs allow their use as PDT nanotools, their performance in PTT-PDT dual therapies can be remarkably enhanced by modifying them with molecular photosensitizers. In an interesting work exploring this strategy, a human serum albumin-indocyanine green complex was adsorbed onto the surface of GNSs with branched structure [261]. The incorporation of the photosensitizer in the formulation of the nanoplatform increased its cytostatic effect on HeLa and MDA-MB-231 cancer cell lines when both PTT and PDT were applied simultaneously under suitable irradiation conditions. In another work, the photosensitizer methylene blue was loaded within hollow GNSs, resulting in their increased uptake in breast cancer and melanoma cell lines and leading to higher ROS production and increased cell death upon light irradiation [262]. In a similar way, Yu et al. proposed the decoration of hollow GNSs with the PDT photosensitizer chlorin e6 (Ce6) and a pH low insertion peptide to target the nanostructures towards acidic tumor microenvironments [172]. The applied light irradiation induced the generation of heat due to the photothermal properties of the GNSs and also the generation of ROS by the chlorin e6. In this study, the non-specific generation of ROS by Ce6 and its consequent unwanted cytotoxic side effects on healthy cells were mitigated by the proximity of the dye probe to the GNSs. Specifically, only NIR-light activation triggered the detachment of Ce6 from the GNSs (Fig. 11D).

5.5. Imaging and diagnosis with GNSs

The detection of diseases in their earliest stages is an essential factor to increase the effectiveness of therapeutic treatments. In the case of cancer, and although it is highly dependent on the type of tumor and affected organ/tissue, early detection is correlated with large increases on the survival rates. Unfortunately, nowadays more than 50 % of cancers are only detected at advanced stages [263]. Since many cancers originate from a reduced number of malignant epithelial cells, the ability to detect them early with maximum precision would represent a significant step towards reducing cancer mortality. In this point, the intrinsic properties of nanoparticulated systems of different nature have been exploited to develop and/or enhance the performance of sophisticated diagnostic techniques. In the specific case of the GNSs here reviewed, their large extinction coefficients and superior photo-stability establish them as highly potential nanotools to be used as contrast agents. In this section, we are going to discuss the application of GNSs in different medical bioimaging techniques, namely in optical coherence tomography (OCT) [70,205,209,264–266], two-photon imaging (TPI) [48,49,209], optical imaging [65,209,267,268], computed tomography (CT) [91,269], and photoacoustic imaging (PAI) [91,269–272].

5.5.1. Optical coherence tomography

OCT is a bioimaging technique that broadly relies on measuring the backscattered light from tissues or organs to create high-resolution cross-sectional images [273]. The optical properties of gold-based nanostructures targeted to the desired region of interest can be exploited to enhance the contrast of the obtained OCT images, being the selective accumulation/binding of the metallic nanosystems at diseased

cells, organs, and/or tissues a key requirement to reach this effect. The *in vitro* performance of GNSs as OCT contrast agents was evaluated in a pioneering way in a HER2 overexpressing breast adenocarcinoma cell line [267]. On the other hand, a representative *in vivo* application of this strategy was proposed by Gobin et al., who injected PEG-capped GNSs in BALB/c mice bearing subcutaneous murine colon carcinoma tumors 20 h before acquire OCT images [205]. The large resonant scattering cross sections of the GNSs and their ability to accumulate at the tumor site resulted in a remarkable contrast increase in OCT images, with 56 % higher integrated scattering intensity in tumoral tissue than in healthy tissue. In contrast, control mice injected with PBS showed only a 16 % contrast difference between both tissue types.

The use of GNSs as contrast agents in OCT images has not been only evaluated for cancer diagnosis, but also for other highly prevalent diseases. For example, atherosclerosis is an inflammatory process that causes gradual thickening of artery walls, thus reducing blood flow and limiting oxygen and nutrients delivery to the body [274]. Cardiovascular OCT is the bioimaging technique with the highest spatial resolution to detect the formed plaques (in the order of 10 μm), and its use at the molecular level might help to detect specific biomarkers of the early stage of development of this disease (*e.g.* intercellular adhesion molecule 1 (ICAM-1)). In a recently reported work, silica-core GNSs functionalized with cLABL peptides were evaluated for the detection of early stages of atherosclerosis using OCT [70]. The metallic nanostructures were carefully designed (silica core diameter of 200 nm and gold shell thickness of 15 nm) to have extinction spectra displaying a maximum in backscattering at *ca.* 1320 nm, which was the working OCT wavelength. On the other hand, the peptide attached to the surface of the nanostructures specifically binds to the aforementioned ICAM-1 protein overexpressed in the early stages of atherosclerosis, thus providing the GNSs with the desired targeting capability. The nanoplatform was evaluated in human microvascular endothelial cells, which overexpressed ICAM-1 when inflamed, both in conventional static 2D cell cultures and also in dynamic adhesion experiments. Interestingly, higher adhesion degrees of the GNSs were observed in dynamic studies, but in both scenarios the incorporation of peptide-modified GNSs resulted in significant enhancements in the contrast of OCT images, thus confirming their potential as molecular contrast agent for early atherosclerosis detection (Fig. 12A).

5.5.2. Photoacoustic imaging

PAI is a bioimaging technique that combines the contrast capability of optical imaging with the larger penetration of ultrasounds, thus allowing the obtaining of precise images of deep tissues/organs. In addition, PAI provides valuable information about the morphological damage, functional metabolism, and the physiological and pathological characteristics of tissues, and can also be exploited to perform a continuous monitoring of the desired region of interest [275].

When exposed to light irradiations at LSPR wavelengths, gold-based nanomaterials can efficiently convert the absorbed energy into acoustic signals through the so-called photoacoustic effect. This phenomenon makes GNPs a highly suitable contrast agents to improve the visibility of tissues in photoacoustic images [276]. More specifically, the possibility to easily tune the absorption peak of GNSs by adjusting their size and shape allows their precise to match the desired imaging wavelengths, increasing their versatility in PAI applications.

In this regard, the original method developed by Halas et al. to synthesize silica-core GNSs typically results in particle diameters above 100 nm, which exhibit better scattering efficiency than absorption properties. Likewise, the lowest-size commercially available silica-core GNSs have 101 nm in diameter. However, for certain bioimaging applications, such as PAI, smaller GNSs in which the absorption phenomenon dominates are the most suitable. Mie theory simulations predict that GNSs with an overall diameter of *ca.* 60 nm (50 nm core diameter and 5 nm shell thickness) display the higher absorption efficiency and volumetric absorption [272]. Based on this hypothesis, Manuel et al. have recently reported a reliable synthetic method to design GNSs with 48 nm core diameter and 7 nm gold shell thickness [272]. These sub-100 nm absorption-dominant GNSs have been evaluated as potential contrast agents in photoacoustic images, being established their better performance at different depths (from 3 to 6 cm) and at lower laser fluences when compared to commercial GNSs and also to scattering-dominant GNSs prepared through the developed method (Fig. 12B). The capability of the designed nanostructures to enhance PAI contrast even at low light intensity is relevant because of the current design trends of photosensitive systems, prioritizing those that require light irradiation sources with low operating fluences, less bulky, and more affordable, such as light-emitting diodes.

Considering these theoretical hypothesis and design guidelines, different types of GNSs have been synthesized and then evaluated to enhance the contrast of photoacoustic images in the diagnosis of different diseases. Besides their widely evaluated application in the detection or identification of cancer tumors [91,167,269,277,278], GNSs-contrasted PAI has found a very interesting application field in the early diagnosis of cardiovascular diseases. For example, GNSs with hollow structure and *ca.* 40 nm in diameter displaying a LSPR peak centered at 800 nm have been proposed as PAI contrast agents to visualize the mouse brain vasculature *in vivo* [270]. A considerable contrast enhancement of brain blood vessels was observed upon GNSs injection in comparison to control experiments carried out with saline solutions. On the other hand, the enhancement of the contrast of photoacoustic images mediated by GNSs has been also evaluated in the diagnosis of cerebral ischemia/reperfusion injury (CISI). The early diagnosis of this disease and the identification of the responsible lesion is here an especially critical factor, being PAI is a highly suitable detection technique due to its rapid and non-invasive acquisition/processing of high-resolution images in comparison with CT or magnetic resonance imaging (MRI). In a representative recent example of this strategy, Yu et al. synthesized silver/gold bimetallic nanoshells with hollow architecture and 80 nm in diameter. The designed nanostructures were conjugated with the antibody anti-tropomyosin 4, an overexpressed marker of CISI, demonstrating a high performance as contrast agents for the diagnosis and location of CISI in a murine model using through PAI [275].

5.5.3. Confocal and two-photon imaging

The use of confocal microscopy for the visualization of thick/deep biological tissues presents important challenges that hinder the obtaining of high-resolution images with the adequate contrast. In brief, this technique is based in the light excitation of fluorophores throughout the sample, including regions outside of the focal plane. These background signals from out-of-focus planes, as well as the attenuation of excitation and emission signals, especially relevant when trying to observe deep tissues, limits the potential of confocal microscopy for bioimaging applications. Some of these issues can be partially addressed by leveraging the nonlinear optical properties of different contrast agents, including gold-based nanostructures and, particularly, GNSs. The potential of GNSs to enhance the contrast of confocal images of deep living tissues was recently demonstrated by, for example, Nishida et al. [268]. In the performed experiments, the authors designed GNSs that reached a saturation scattering intensity when exposed to 780 nm NIR light. Afterwards, the nanostructures were encapsulated at a depth of 400 μm within biomimetic phantoms that resemble the physicochemical properties of muscles tissues, being demonstrated their capability to improve the contrast and spatial resolution of the obtained confocal images (Fig. 12C).

On the other hand, TPI has emerged as a more powerful tool than confocal microscopy for the early non-invasive detection of cancer cells. It is based in the excitation of fluorophores with two NIR photons and the subsequent emission of a high-energy single visible photon [49]. Although the absorption is much lower when compared to confocal imaging, which often leads to the use of high and potentially dangerous light intensities, TPI allowed the visualization of thick tissues, with

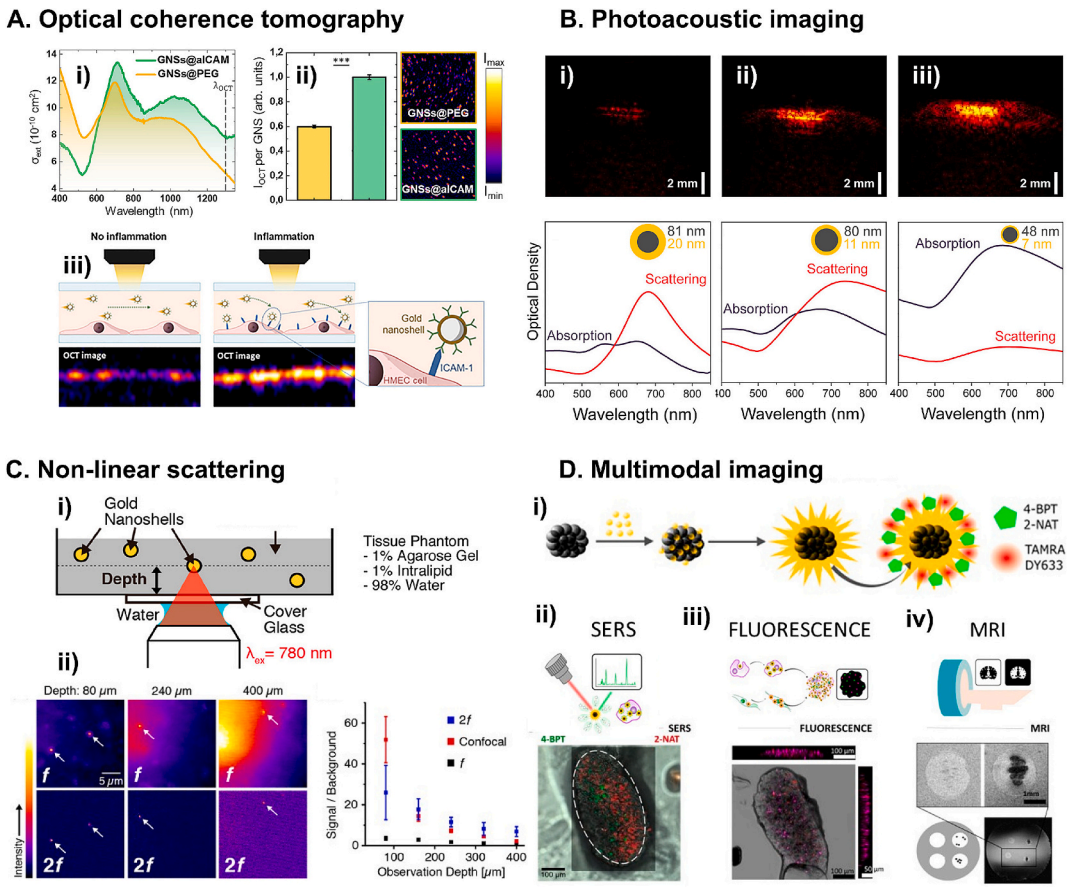

Fig. 12. **A.** i) Extinction spectra, and ii) OCT intensity per nanoparticle signal (left) and comparative OCT cross-sectional images (right) of GNSs functionalized with aICAM and PEG. ii) GNSs functionalized with cLABL peptides provides them with aICAM-1 targeting capabilities, permitting the detection of inflammation in arteries, even in dynamic conditions (Reproduced with permission [70] Copyright 2022, Elsevier, CC BY 4.0 DEED). **B.** PAI images and absorption and scattering spectra for i) commercial GNSs, ii) scattering-dominant GNSs, and iii) sub-100 nm absorption-dominant GNSs. Dimensions of GNSs are shown in the insets (Reproduced with permission [272] Copyright 2023, American Chemical Society, CC BY 4.0 DEED). **C.** i) Schematic of the sample condition for the observation of GNSs in a tissue phantom. ii) Scattering images of GNSs obtained by SAX microscopy at different depths: 80 μm (first column), 240 μm (second column), and 400 μm (third column). The images were reconstructed by analyzing the scattering signal at both the fundamental frequency (shown in the first row) and the second-harmonic frequency (shown in the second row). White arrows in each image highlight the locations of GNSs. The relationship between the signal-to-background ratio and observation depth varies across different image reconstruction methods. In the case of images reconstructed using linear signals (black), those obtained through a 1.3 Airy confocal pinhole (red) show a distinct pattern. Additionally, images reconstructed using second-order nonlinear signals (blue) exhibit their own characteristic relationship between signal-to-background ratio and observation depth (Reproduced with permission [268] Copyright 2020, American Chemical Society). **D.** i) Schematic of the synthetic process of hybrid magnetoplasmonic nanoprobes comprised the adsorption of small gold NPs onto premade iron oxide cores, followed by the controlled growth of spiky GNSs. Evaluation of magnetoplasmonic iron oxide-GNSs for multimodal imaging. ii) SERS map of a transversal cut (area 360 × 560 μm^2, 50 μm in thickness) of a fixed and embedded spheroid, the presence of biphenyl-4-thiol and 2-naphthalenethiol positive pixels is observed consistently across the xy plane. iii) Orthogonal projection obtained through confocal fluorescence imaging of a transverse section across a fixed and embedded spheroid. iv) MRI images from spheroids embedded in an agarose phantom, with (right) and without (left) iron oxide-GNS (Reproduced with permission [293] Copyright 2022, American Chemical Society). (For interpretation of the references to colour in this figure legend, the reader is referred to the web version of this article.)

penetration depths up to 1 mm. Moreover, in TPI the laser excites fluorophores only at the focal plane, thus remarkably increasing the resolution of the obtained images. In a similar way than confocal imaging, the accumulation of fluorescent contrast agents in the target zone can be exploited to the monitoring of several biomolecular signatures highly related with cancer diseases [279]. In this way, to harness the full potential of TPI, scientists delve into the exploration of both traditional and engineered organic fluorophores, alongside novel luminescent contrast agents like quantum dots and metallic nanostructures [280]. Although fluorescent semiconductor quantum dots display extremely large two-photon action cross-sections, the most typical formulations of this type of nanostructures include heavy metals that are cytotoxic, thus hindering their *in vivo* clinical application. In this point, GNPs emerge as excellent candidates to be used as contrast agents in TPI, since they combine their widely demonstrated high biocompatibility with resistance to photobleaching and, despite lower than quantum dots, much larger two-photon action cross-sections than organic fluorophores [281].

Although GNPs with the most typical spherical morphology and gold nanorods have been more widely proposed for TPI applications, the GNSs here reviewed have been also evaluated as potential contrast agents in this bioimaging technique. In this regard, it is worth mentioning the comparative study performed by Gao et al., in which the single particle scattering and the two-photon photoluminescence properties of spherical, rod-like, cubic, triangular, and branched GNPs were carefully analyzed [282]. Interestingly, branched nanostructures showed the largest two-photon absorption cross-sections, in the order of $4{\cdot}10^6$ GM (Goeppert-Mayer units), remarkably higher than those showed by the other GNPs ($83–4.2{\cdot}10^4$ GM) and organic dyes (1–100 GM). Based on this evidence, it is reasonable to expect that spiky and

branched GNSs will display enhanced properties; but a direct comparison to elucidate this point has not been performed yet. Although still scarce, several works have already exploited the optical properties of GNSs to increase the contrast of TPI images. In a representative example of this approach, 800 nm-resonant GNSs were evaluated *in vivo* in a mice model. Under adequate light conditions, it was possible the imaging of single GNSs flowing in mice blood vessels, thus, allowing the reconstruction of vessel structures from time series by utilizing a reconstruction algorithm [48].

5.5.4. Multimodal imaging

Multimodal imaging, also known as multiplexed imaging, involves the simultaneous production of signals for two or more different imaging techniques. In this way, multimodal imaging has the potential to overcome the limitations of independent techniques by combining them with others imaging strategies. For example, an anatomic imaging technique such as MRI allow the acquisition of images at deep tissue level and initial recognition of suspicious lesions, whilst optical imaging is useful to more accurately diagnose at the molecular level. Thus, the combination of the strengths of both techniques in the acquisition of a single image allows a better characterization of the analyzed tissue or organ.

The intrinsic properties of different typologies of GNSs have been widely exploited to enhance the contrast and resolution of multimodal images [91,209,269,275,283]. Depending on the composition of the cores surrounded by the metallic nanoshells and/or the coating or surface chemistry of the designed nanostructures, they have been proposed as multimodal agents in different combination of imaging techniques. However, the most commonly explored approach by far is the design of magnetoplasmonic NPs composed by magnetically responsive cores and surrounding GNSs, thus displaying the adequate properties for their use as MRI-optical multimodal nanotools. The interest of gold nanostructures as contrast agents in optical imaging has already been discussed in previous sections, while the potential of magnetic nanomaterials as contrast agents for MRI arise from their capability to change transversal and relaxation times of water protons that compose the tissues [284–286]. For example, Brennan et al. reported two different works in which GNSs with different thickness were grown surround magnetite nanocores [92,287]. The influence of the ratio between core and shell dimensions over different properties of the nanostructures was carefully analyzed, thus establishing the key role of this design parameter in the magnetic hyperthermia efficiency and photothermal activity. Regarding the potential use of the synthesized magnetoplasmonic NPs as potential multimodal imaging nanotools, it was established that thicker shells increased the optical contrasting capability of the nanosystems. However, it was also shown that the magnetic properties of the particles and their MRI contrast capability decreased with the shell thickness due to the magnetic shielding effect of the grown gold layer.

In a slightly different and more complex design strategy, polymeric cores were surrounded by heterogeneous multi-layer nanoshells with both iron and gold in their formulation [225]. In this way, the capability of the synthesized NPs to improve the contrast and resolution of multimodal MRI-optical images is exclusively derived from the composition of the metallic nanoshells, being the polymeric cores exploited for the encapsulation of drugs. Interestingly, magnetic nanomaterials have shown much larger efficacy as T_2 (transversal relaxation) than as T_1 contrast agents (longitudinal relaxation) in MRI applications (for a detailed description of these complex phenomena, we refer the readers to recent review articles focused on the topic) [286,288,289]. In this way, the use of alternative materials with higher T_1 contrast capability, such as gadolinium or europium, has been proposed for the design of nanostructures with potential application as contrast agents in T_1-weighted MRI and also in multimodal imaging. For example, a recent wok proposed the incorporation of gadolinium oxide NPs in the structure of mesoporous silica cores before the growth of GNSs with different thickness surrounding them [290]. Thus, the synthesized nanostructures displayed contrast capabilities for optical imaging and MRI, derived from the presence of gold and gadolinium, respectively, together with photothermal properties for their use in PTT. More specifically, the performed MRI experiments showed longitudinal relaxivity values 3-fold larger than typical T_1 contrast agents while maintaining transversal relaxation properties. To assess the clinical viability of the designed GNSs, multimodal imaging experiments were conducted in agarose phantoms, being observed remarkable enhancements in the contrast and resolution of the obtained images using low GNSs doses within the therapeutical range.

In a more complex approach, GNSs can include in their formulation both gadolinium and magnetic materials, thus comprising a T_1-T_2 dual modal MRI contrast agent in combination with the contrast capability of gold for optical or X-Ray/CT imaging. In a representative example, magnetite NPs doped with europium and gadolinium were synthesized through a thermal decomposition method and then used as core templates to grow GNSs surrounding them [291]. The developed strategy allowed the design of multimodal imaging nanotools with enhanced contrast capabilities for T_1-T_2 dual MRI and X-Ray/CT imaging, being all these functionalities combined in a single sub-10 nm nanoplatform, which opens a wide range of potential clinical applications.

Providing GNSs with MRI contrast capability through the incorporation of the aforementioned materials/elements in their formulation has not been the only strategy explored for the design of multimodal imaging nanotools. Although less frequently, GNSs-based nanoplatforms with potential application in other types of multimodal imaging different from optical-MRI have also been proposed. For example, an interesting recent work evaluated the design of hybrid diamond-core GNSs, seeking to exploit both the spectroscopical and optical properties of each part of their dual structure for multimodal imaging applications [292]. As expected, the synthesized core-shell NPs displayed intense and narrow Raman and fluorescence peaks derived from the composition of the core. The high potential of the nanosystem as multimodal imaging contrast agent was established in A549 cell line and zebrafish embryos by means of Raman imaging, two-photon excited fluorescence, and high-resolution X-Ray imaging.

GNSs can be also provided with Raman imaging capability through their modification with the so-called reporter molecules (*i.e.* molecules with a high Raman cross section with defined vibrational peaks). Recently, De La Encarnación et al. developed hybrid NPs composed by magnetite nanocores and a spiky gold layers for simultaneous bioimaging and sensing [293]. The designed nanostructures were evaluated in various biological models such as 2D cell cultures, 3D spheroid models, or *ex situ* brain tissue, being established their high biocompatibility and their excellent performance as multimodal imaging nanotools (Fig. 12D).

5.6. GNS-based sensors

The precise detection of analytes in complex samples, either chemical species or biological agents (biosensing), requires a transductor which transforms a non-measurable signal into a quantifiable one. In last decades, the field of nanotechnology has devoted many efforts to the design of sophisticated biosensing nanotools with different nature and physicochemical properties [294]. Among the wide range of different nanomaterials explored so far, GNPs represent one of the most promising options for the successful development of analytical methods for biosensing [295]. In particular, the interfacial properties of GNPs have a great influence in the position of the LSPR peak, because they alter the boundary conditions for the polarizability of the metal [188]. In this way, the plasmonic response of gold-based nanostructures can be affected by many different external stimuli/phenomena, such as changes in the local environment composition or adsorption of molecules on the particle surface, thus opening many doors for their use as biosensing agents in different applications.

Interestingly, the GNSs here reviewed exhibit higher optical

sensitivity than other typologies of gold nanostructures to some specific changes in the surrounding environment. For example, Sun et al. demonstrated that hollow GNSs are much more sensitive to changes in the refractive index of the surrounding media than spherical-shaped GNPs. More specifically, a 10 % variation on the refractive index of the medium resulted in a 59 nm shift of the LSPR of GNSs, being this displacement much lower in the case of spherical GNPs [296]. On the other hand, GNSs can generate strong electromagnetic fields on their surfaces, thus amplifying many orders of magnitude (*ca.* 10^{12}–10^{15}) the SERS signals through strong electromagnetic near-field enhancement. This phenomenon has motivated the evaluation of GNSs for the detection of ultra-low concentrated analytes, potentially reaching even single molecule detection [60]. Therefore, in this section we are going to briefly review the most relevant developed sensing devices/methods based on GNSs, separating them in LSPR-based (absorption and far-field scattering) and Raman-based sensors (near-field scattering).

5.6.1. LSPR-based sensors

In general, the scattering and absorption spectra of GNPs undergo a red shift when the dielectric constant of the surrounding medium increases. This variation on the optical properties of GNPs occurs in response to changes in the chemical composition of the medium and/or to the attachment of biological analytes to their external surfaces, in some cases previously functionalized with recognition molecules such as antibodies or aptamers [297]. In this way, different typologies of gold-based nanostructures have been proposed as potential tools for quantify changes in the properties of the dispersion medium and for the detection of analytes, due to their capability to reduce the number of GNPs-molecule interactions required to generate a detectable signal. More specifically, and as previously commented, GNSs have demonstrated enhanced capability as sensing devices than other GNPs with different architectures [298].

For example, a very recent work reported by Sun et al. proposed the use of hollow GNSs to measure changes in the refractive index of the dispersion medium [30]. The study was focused on measure the so-called refractive index sensitivity (RIS) and the figure of merit (FoM), defined as the band shift of GNSs per refractive index unit and the ratio of RIS to the full wavelength at half-maximum, respectively. The synthesized GNSs displayed maximum RIS and FoM values of 349 nm per refractive index unit and 1.82, respectively, much higher than those determined for spherical-shaped GNPs immobilized in glass substrates also measured, thus indicating the high performance of the designed nanostructures as LSPR-based sensors. Interestingly, the authors attributed the higher sensing efficiency of the evaluated GNSs to their hollow architecture. More specifically, the increased contact area with the surrounding media derived from the double interface and the amplified plasmonic effect originated from the interaction between external and internal surfaces are key factors that enhance the sensing performance of hollow nanostructures (Fig. 13A).

In a seminal evaluation of their potential as biosensing nanotools, GNSs were utilized for simple whole blood immunoassays due to their easy functionalization with antibodies [299]. For this purpose, GNSs were functionalized with rabbit anti-IgG antibodies, being achieved a detection limit 4.4 $ng{\cdot}mL^{-1}$ of rabbit IgG in blood based on the shift of LSPR peaks. Another example of LSPR shift-based sensing was carried out by using bimetallic gold/silver hollow nanoshells electrostatically decorated with enzyme glucose oxidase [300]. It was established that the control over the enzymatic reaction of glucose oxidase can be used to finely tune the optical response of the nanostructures, which was further exploited as a new method for glucose sensing. The developed strategy was based on the selective H_2O_2-mediated dissolution of silver from the preformed bimetallic, nanoshells which is originated from the enzymatic oxidation of surface-confined glucose in the presence of oxygen. This dissolution process gradually shifted the LSPR of the resultant porous nanoshells, thus reflecting concentration change of glucose in the reaction system. The detection limit of the developed sensing nanoplatforms reached *ca.* 4.5 mM of glucose in serum samples, which is lower than the concentrations detected by commercial blood glucose monitors (5.4 mM).

5.6.2. Raman-based sensors

As already discussed, GNPs have been widely explored for the development of (bio)sensing nanotools based on the shifts induced in their LSPR by different mechanisms/phenomena. However, probably the most powerful sensing application of gold-based nanostructures is derived from their capability to enhance the inelastic scattering (or Raman scattering) by certain molecules adsorbed on their surface. In this way, GNPs have found application in SERS, a surface-sensitive technique used for the sensing of molecules in trace amounts within the fields of chemical and biochemical analytics. The potential of GNPs in SERS applications is based on the existence of highly localized regions known as hot-spots in their surfaces in which the generated electromagnetic fields are exceptionally high. This phenomenon is especially relevant in the corners, gaps, cavities and/or spikes of metallic NPs with irregular morphologies and geometries, being the GNSs here reviewed, in many cases with hollow architectures, porous structures or spiky shapes, a particularly appealing SERS nanotools [58–60].

In this way, GNSs have been evaluated as SERS sensing agents for the detection and quantification of different chemical analytes [128,216,301]. A representative application of GNSs-SERS sensing technology for the quantification of chemical analytes was reported by Heck et al., who analyzed the room-temperature glycerol oxidation in aqueous media by using GNSs as both SERS- and catalytically-active probes [302]. Carbon monoxide was established as probe molecule, being observed that hydroxyl moieties adsorbed onto the surface of GNSs during the reaction decreased their surface charge, which can lead to enhanced O_2 adsorption and may help to explain the activity of many gold-based catalysts. In a different approach, GNSs-based SERS sensors have also been applied for the quantification of toxic chemical analytes such as Hg^{+2} ions in water media [303]. The designed nanoplatform consisted of multilayered constructs formed by a magnetite core, an intermediate silica shell, and a final layer of gold (Fig. 13B). Since Hg^{+2} ions do not have Raman scattering cross section, 4-mercaptopyridine was introduced as molecular probe for the successful detection of toxic analytes, because pyridine rings can effectively capture the mercury ions thus leading to measurable changes in the SERS spectra of the molecule. The designed system showed a negligible interference with other metallic ions and also an excellent recyclability over multiple washing cycles.

On the other hand, the detection of biological analytes by exploiting the SERS biosensing capability of GNSs-based nanoplatforms, these even act as diagnostic agents, has also been widely explored. This approach usually involves the attachment onto the surface of GNSs of Raman reporter molecules, such as p-mercaptoaniline and 4-mercapto-benzoic acid and targeting ligands with strong affinity to receptors overexpressed in diseased cells/tissues. After reaching the target site, the generation of strong Raman signals derived from the presence of reporter molecules indicates an elevated population of receptor-overexpressing tumoral cells or tissues. In this way, the detection of biological analytes, such as histone acetyltransferase p300 [304], and beta-amyloid [305], has been performed exploiting GNSs-SERS technology. This type of nanostructures has been also used to determine redox potentials inside hypoxic cells associated with cellular processes such as apoptosis, signaling, and differentiation through SERS techniques. These redox potentials are indicative of the progression of various diseases, including cardiovascular disorders, neurodegenerative diseases, or different types of cancer [306].

For example, a microfluidic approach incorporating magneto-plasmonic GNSs as multiplexed SERS nanotags was recently proposed for the early diagnosis of cancer metastasis through the immobilization and detection of circulating tumor cells (Fig. 13C) [307]. The synthesized anisotropic GNSs were functionalized with different antibodies,

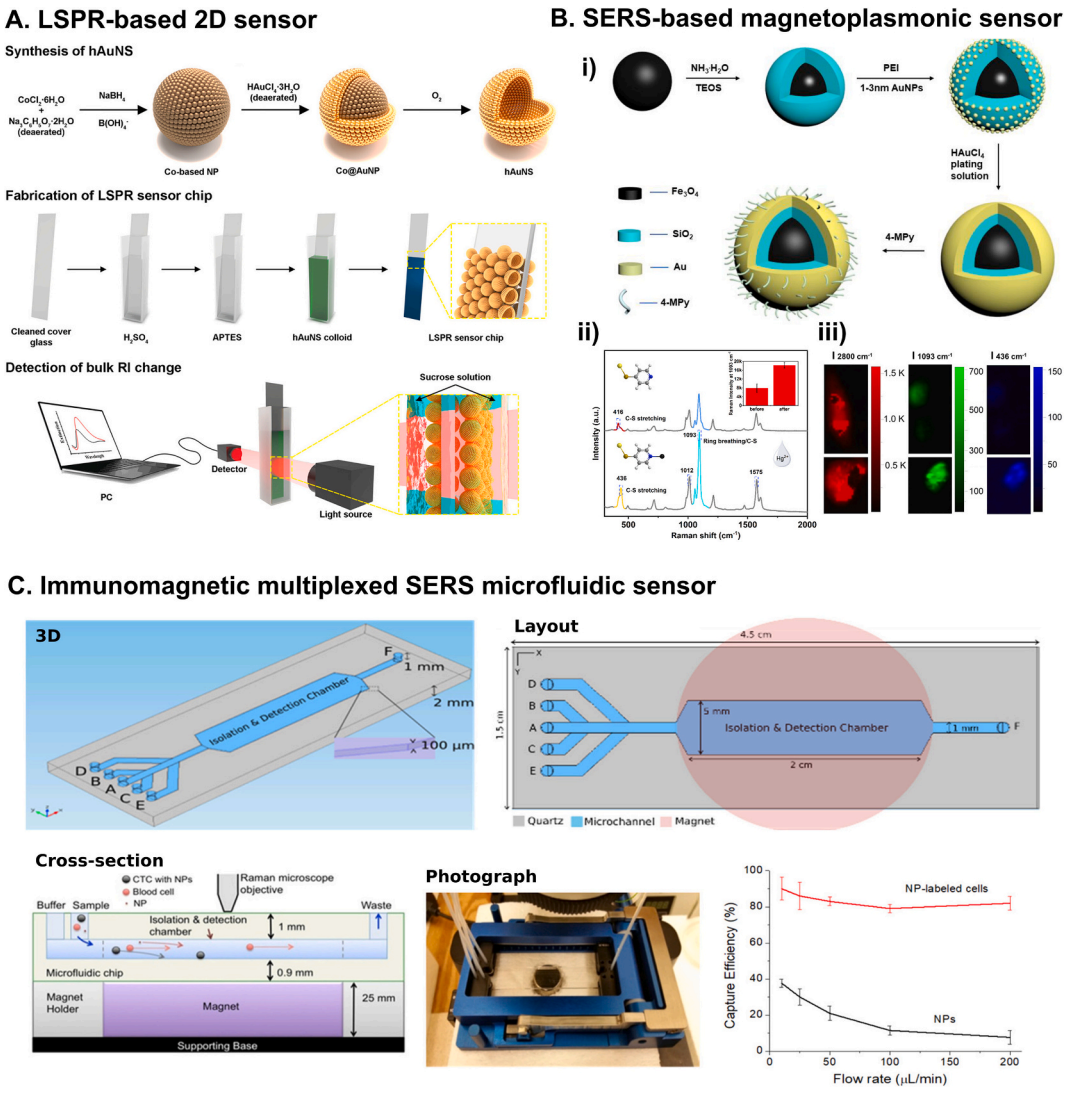

Fig. 13. A. Schematics of the bottom-up strategy for preparing substrate-based LSPR sensors. Hollow GNSs synthesized through a galvanic replacement reaction using Co_2B nanoparticles as sacrificial templates are immobilized onto functionalized glass slides to create a basic LSPR sensor chip. The refractive index sensitivity of the sensor chip is determined by measuring the shift in the plasmon band using a spectrophotometer (Reproduced with permission [30] Copyright 2024, American Chemical Society). **B.** i) Synthesis of magnetoplasmonic-SERS encoded nanosensors for quantification of Hg^{+2} in aqueous environments. ii) Change in the Raman-spectrum of the nanosensors after addition of 10 ppm of Hg^{+2}. The inserted image corresponds to the Raman intensity of 4-Mpy at 1093 cm^{-1}. iii) SERS image of single cell endocytosed NPs before (up) and after (down) incubation with Hg^{2+} for 1 h. Raman mappings at 2800 cm^{-1} (red channel), 1093 cm^{-1} (green channel), and 436 cm^{-1} (blue channel) are shown. (Reproduced with permission [303] Copyright 2023, MDPI, CC BY 4.0 DEED). **C.** Design of an immunomagnetic microfluidic sensor for the detection of circulating tumoral cells. 3D view, layout, cross-sectional view (not to scale), and photograph of the microfluidic system for both on-chip magnetic isolation and optical detection of cells. The graph with the capture efficiencies of SK-BR-3 cells labeled with a cocktail of anti-EpCAM and anti-HER2 IO–Au NPCs (red curve) and free IO–Au NPCs (black curve) is also shown (Reproduced with permission [307] Copyright 2020, American Chemical Society). (For interpretation of the references to colour in this figure legend, the reader is referred to the web version of this article.)

anti-EpCAM, anti-HER2, anti-CD44 or anti-IGF1R, to target specific populations of cancerous cells, after which different SERS probe molecules were added *via* nonspecific adsorption. The biosensing capabilities of the developed nanosystem was evaluated in healthy blood samples with added breast cancer cells. For that, dispersions of antibodies-modified GNSs in the biological medium loaded with cancer cells were circulated through the designed microfluidic device, where they were magnetically separated by applying external magnetic fields prior to SERS analysis. The performed strategy showed a cell capture efficiency higher than 85 %, while cell retention in the absence of GNSs was below 20 %. This confirms the potential of the designed system for the detection of low concentration cells in human blood, with the added ability to discriminate between different cancerous cellular populations through ELISA assays.

By adopting similar strategy to the previously discussed one for the chemical detection of harmful elements in water, GNSs-SERS sensing can be also exploited for the identification of biotoxins, potentially even within living organisms. In a representative recent example of this approach, silica-core GNSs were evaluated for the detection of three different toxins (ricin, staphylococcal enterotoxin B and botulinum neurotoxin type A) using SERS technology [71]. The designed gold-based nanostructures were modified with 5,5-dithiobis-(2-nitrobenzoic acid) as SERS reporter molecule and also leveraging the free thiol groups as anchoring points to bind toxin detection antibodies. The developed biosensors showed ultra-low detection limits below 0.1 $ng{\cdot}mL^{-1}$ for the three evaluated biotoxins, and also a high selectivity, since when not using the correct antigen-antibody combination the Raman signals decreased to background noise range. In addition, when compared with biosensors based on spherical-shaped GNPs with homogeneous structure, results showed a 100-fold decrease in the

detection limit of the biotoxins, thus confirming the suitability of GNSs for this application.

In a recently reported very interesting design strategy, Bock et al. synthesized silica-core GNSs in which the outer layers were not homogeneous structures, but they were formed by individual GNPs with different sizes [308]. They hypothesized that by controlling the gap between the GNPs that formed the nanoshells, the creation of plasmonic hot spots with different intensities was possible, leading to an optimization of the SERS signal intensity. Interestingly, the nanostructures with the narrower gaps between the GNPs displayed the largest SERS enhancing factor. Afterwards, the designed GNSs were labeled with 14 different Raman reporter molecules and evaluated as multiplex sensing agents in a mice model, being possible the separated identification of each Raman reporter into the same mouse even at low particle concentrations.

Interestingly, the SERS sensing capability of GNSs can be combined with other properties/applications of this type of nanostructures that we have discussed before. For example, a recent study evaluated the use of GNSs for the SERS identification and the subsequent photothermal-mediated inactivation of the pathogen *S. aureus* [309]. For that, aptamer-conjugated magnetite-core GNSs were incubated with the bacteria and magnetically separated prior to the performing of SERS experiments, being established a detection limit of 25 colony-forming unit per milliliter. Afterwards, the photothermal properties of GNSs were exploited to inactivate *S. aureus* in contaminated milk samples, observing a 97 % higher sterilization rate compared to control samples.

5.7. GNSs as theragnostic agents

Theragnosis is a concept that emerged in the early years of this century coined by the bio-nanotechnology community, and it refers to the biomedical application of biomaterials that, either by their intrinsic properties or through their controlled modification, can simultaneously detect a target and exert a therapeutic effect on it. In this way, drug-loaded polymeric NPs modified with pH-sensitive compounds, magnetic nanosystems with heat generation and MRI contrast capability, or fluorescent quantum dots have been proposed as potential theragnostic nanotools for the detection and subsequent therapy of different diseases, in most cases cancer [310]. Despite these examples, the typology of nanomaterials that have been most commonly evaluated for theragnostic applications are undoubtedly GNPs [311–313]. As we discussed in detail in previous sections, the intrinsic light absorption and scattering properties of gold-based nanostructures allow their implementation in many different diagnostic and therapeutic procedures.

However, in addition to the bio-interaction concerns described in section 4, one of the main factors that hinders the use of GNPs as theragnostic nanotools is derived from the light intensities required for each application, which are typically much lower for imaging purposes than for the leveraging of photothermal effect. This problem can be partially mitigated through the controlled aggregation of the GNPs, thus being possible to shift the position of LSPR peak to NIR wavelengths and exploit the nanoaggregates as simultaneous imaging and photothermic agents [314]. The precise design of gold-based nanostructures with the adequate structural characteristics also allows enhancing their capability as theragnostic agents. In this point, the GNSs here reviewed emerge as a particularly appealing option, since by tuning the physicochemical properties of both parts of their dual structure, the balance between scattering and absorption can be adjusted over a wide range, thus achieving the adequate optical behavior for the desired application. This enables appropriately designed GNSs to scatter NIR radiation for bioimaging or biosensing purposes while absorbing NIR radiation for efficient heat generation, thus selectively destroying targeted tumor cells. Moreover, as we already detailed, GNSs can also be formulated incorporating materials with different imaging contrast capabilities or can be loaded with drugs and nucleic acids, among many other design options, thus opening a wide range of potential theragnostic modalities where they can find application.

Although this review article was structured by individually discussing the different specific applications of GNSs, many of the referenced works have validated the use of these nanosystems as theragnostic tools. In general, we focused on the main application of GNSs evaluated in performed research, but in some cases the experiments carried out in a single work were described separately in both the therapy and diagnosis sections. In this way, the following table is intended to serve as a summary of the previous application sections of GNSs, listing those nanostructures that have been evaluated as both diagnostic and therapeutic agents during the last ten years, and the most relevant information related with their design, physicochemical properties and theragnostic performance (Table 3).

6. Concluding remarks and outlook: translation of GNSs to clinic

Gold-based nanostructures have been confirmed as promising nanomaterials for biomedical purposes, both for diagnosis and/or therapy applications. By carefully controlling the physicochemical features of the designed GNPs, their optical response can be finely tuned, thus providing them with the adequate properties for the intended specific application. Among the wide range of gold-based NPs with different structures, dimensions, morphologies, and/or compositions proposed so far, GNSs constitute an especially interesting option for many biomedical applications. The complex dual core-shell architecture of this kind of nanostructures allows a wider modification range of their properties than in the case of GNPs with homogeneous structure. In this way, besides through the aforementioned basic design parameters such as size or morphology, the properties of GNSs can also be controlled by modifying the core material, being possible the design of nanosystems with multiple functionalities. Moreover, these core parts can also be removed after growing GNSs surrounding them, thus obtaining metallic nanoshells with hollow architectures that have attracted strong interest for different biomedical uses. This control over the physicochemical properties of GNSs can be achieved by carefully establishing key synthetic parameters such as the ratio between precursors, pH, selected ligands, or the typology of nanocores, among many others, as well as through the adequate post-synthetic processing of the obtained nanosystems.

Due to these outstanding and highly tunable properties, GNSs have found application in many areas within the biomedical field. As example, the intrinsic properties of gold nanomaterials have been exploited in the evaluation of GNSs as potential contrast agents in bioimaging and biosensing techniques. Remarkably, the particular structure of GNSs gives them a higher potential for these applications in comparison with other types of GNPs. For instance, magnetoplasmonic NPs formed by magnetic nanocores surrounded by GNSs have demonstrated an impressive performance for MRI-optical multimodal bioimaging; while hollow GNSs showed enhanced biosensing capability due the increased contact area with the surrounding media and the amplified plasmonic effect derived from their double interfaces.

In a similar way, the inherent properties of nanostructured gold materials underlie certain therapeutic applications of GNSs, such as their proposed use as photothermal nanotools. Nevertheless, the singular structural attributes of GNSs enable once more a superior performance compared to alternative GNPs in this specific application, owing to the previously mentioned heightened plasmonic effect. Moreover, these nanostructures are also a highly appealing option for other therapeutic uses. Thus, for example, hollow GNSs stand out as powerful tools for the transport and delivery of drugs/bioactive molecules because of the high encapsulation degrees facilitated by their structures featuring internal cavities. Interestingly, the highly adjustable optical properties of GNSs have further enhanced their potential application as theragnostic agents; that is, the integration in a single nanostructure of both simultaneous diagnostic and therapeutic functionalities. By carefully controlling the features of the designed GNSs, their LSPR can be

Table 3
Summary of GNSs used as theragnostic agents in different biological models.

Core	Shell	Coating	Size (nm)	LSPR peak (nm)	Cell line (cancer) or model	Therapy	Diagnostics	Outcomes	Refs.
Gold	Concentric SiO_2/Au shells	PEG	Core = 42 SiO_2 Shell = 10 Au Shell = 13 D_H = 137	560 783	MDA-MB-231LM2 (breast)	*In vivo*: PTT @ 808 nm, 3 W·cm^{-2}, 5 min	*In vitro*: dark field microscopy	Nanomatryoshkas showed greater tumor penetration and antitumor effect against triple negative breast cancer as compared to typical silica-core GNSs.	[29]
PLGA, Doxorubicin, Magnetite NPs	Branched, porous	PEG-folic acid	Core = 124 Shell = 32 D_H = 188	800	HeLa (cervix)	*In vitro*: ChT, PTT @ 808 nm, 2.5 W·cm^{-2}, 5 min	*In vitro*: reflectance CLSM, MRI	Ligand and magnetically targeted GNSs displayed enhanced T_2-MRI contrast. The combined chemo-photothermal therapy showed a synergistic anti-cancer effect.	[169]
Silica	Spherical	PEG-Gd	Core = 120 Shell = 16 D_H = 231	800	HepG2 (liver), B16-F10 (melanoma)	*In vitro*: PTT @ 808 nm, 35 W·cm^{-2}, 3 min	*In vitro*: MRI, X-ray, OCT, CLSM and TPI. *In vivo*: MRI, X-ray. *Ex vivo*: OCT	GNSs were functionalized with PEG and chelated Gd. The system featured multimodal *in vitro* and *in vivo* imaging and anti-melanoma NIR-PTT *in vitro*.	[209]
PLGA, Doxorubicin, Magnetite NPs	Branched, porous	HSA-folic acid-indocyanine green	Core = 100 Shell = 17.5 D_H = 135	770	MDA-MB-231 (breast)	*In vitro*: ChT, PTT and PDT @ 808 nm, 2 W·cm^{-2}, 3 × 5 min	*In vitro* and *in vivo*: fluorescence imaging	HSA/FA/ICG coating and Dox-load enabled simultaneous PTT, PDT and chemotherapy, with synergistic cytotoxic effect.	[261]
Hollow	Au-Ag	Dextran-doxorubicin conjugate	Core = 50 Shell = 5	900	HeLa (cervix)	*In vitro* ChT, PTT @ 808 nm, 7 W·cm^{-2}, 5 min.	*In vitro*: fluorescence microscopy	IC50 of Dox-hollow GNSs was 315.4 nM, 3.2-fold lower than that of free Dox (~1 μM).	[315]
Hollow	Nanocage[a], spheroid shell[b] and rod-like shell[c]	Lipofectamine 2000 (phospholipid bilayer), lipid folate.	Core[a] = 200 Core[b] = 80 Core[c] = 120 × 30; Shell ~6 nm.	Nanocages: > 1100; spheroid shell: 850; rod-like shell: 670	HeLa (cervix), B16F0 (melanoma)	*In vitro* and *in vivo*: PDT and PTT @ 980 nm, 0.15 W·cm^{-2}, 10 min; @ 808 nm, 0.15 W·cm^{-2}, 13 min	*In vitro* and *in vivo*: NIR-excited imaging	All hollow nanostructures exerted PTT and PDT upon ultra-low dose NIR light excitation and can emit plasmonic luminescence to act as fluorescence cellular markers.	[210]
Silica	Spherical	PEG-anti-CD47	Core = 130 Shell = 13	750	ID8, TOV21, SKOV-3 (ovary)	*In vivo*: intraperitoneal PTT @ 808 nm, 3.2 W·cm^{-2}, 5 min	*In vitro*: optical microscopy	Repeated PTT using intraperitoneally administered antiCD47-GNSs led to a significant inhibition of tumor growth as compared to control groups.	[168]
Silica	Spherical	PNIPAM soaked in Dox	Core = 120 Shell = 15 D_H = 337.4	785	CT-26.WT (colon)	*In vitro* ChT, PTT @ 808 nm, 4 W·cm^{-2}, 3 min.	*In vitro*: fluorescence microscopy	The release of Dox was controlled by the irradiation with NIR laser.	[206]
PLGA, methotrexate	Au/Fe/Au half-shell	PEG, RGD peptide	Core = 105 Au/Fe/Au half Shell = 10/5/10 D_H = 135	800	Collagen-induced arthritic (CIA) mice	*In vivo*: NIR- triggered anti-rheumatic therapy, @ 808, 1.3 W·cm^{-2}, 10 min	*In vivo*: T_2-MRI, NIR absorbance imaging	*In vivo* imaging confirmed the accumulation of half-GNSs in the inflamed paws of CIA mice. NIR light increased the local temperature and triggered the release of MTX, requiring just 0.05 % of the MTX dosage.	[225]
Hollow	Spherical	PEG-pHLIP-Ce6	Core = 28 Shell = 10	650	HeLa (cervix)	*In vitro* and *in vivo*: PDT and PTT, @ 808 and 670 nm, 2 W·cm^{-2}, 5 min	*In vivo*: real-time thermal imaging, intravital and *ex vivo* fluorescence imaging	PTT and PDT was simultaneously activated by single NIR laser and provided mutual feedback to promote their therapeutic effect.	[172]
Silica, magnetite	Spherical	PEG-cell penetrating peptide	Core = 125 Shell = 23.5 D_H = 216	800	MCF-7 (breast)	*In vitro* and *in vivo*: PTT @ 808 nm, 1.2–1.9 W·cm^{-2}, 10 min	*In vivo*: X-ray CT imaging and MRI	The system showed excellent photothermal efficiency and high CT and MRI contrast, both *in vitro* and *in vivo*.	[173]
Mesoporous silica, Cy7, dextran-FITC	Spherical	Macrophage cell membrane	Core = 80 Shell = 12 D_H = 100	810	4 T1 (breast)	*In vitro* and *in vivo* PTT @ 808 nm, 1 W·cm^{-2}, 5 min	*In vitro* and *in vivo*: fluorescence imaging	Macrophage cell membrane coated GNSs exhibited good biocompatibility, reduced opsonization, long-circulating time and enhanced tumor accumulation.	[238]
Silica	Spherical	dsDNA + docetaxel[a]; HSA + lapatinib[b]	D_H = 155.4[a] D_H = 178.9[b]	774[a]; 786[b]	MDA-MB-231, SKBR3 (breast)	*In vitro*: ChT, PTT CW @ 1.5 W and pulsed @ 160 fs, 25 mW, 2 min	*In vitro*: dark field, bright field, and reflectance microscopy	A greater cytotoxicity was observed with CW compared to pulsed-laser-induced release of DTX and lapatinib from a DNA and protein hosts, respectively	[250]

(*continued on next page*)

Table 3 (*continued*)

Core	Shell	Coating	Size (nm)	LSPR peak (nm)	Cell line (cancer) or model	Therapy	Diagnostics	Outcomes	Refs.
Hollow, gemcitabine	Spherical	PEGylated thermosensitive lipids, bortezomib, FITC	Core = 58.6 Shell = 2.4 D_H = 84.6	839	MIA PaCa-2, PANC-1 (pancreatic)	*In vitro*: ChT, PTT @ 808 nm, 1 W·cm^{-2}, 5 min	*In vitro*: CLSM	The lipidic coating enhanced intracellular entry of GNS. Light-triggered treatment with drug-loaded GNSs increased the percentage pre-apoptotic and apoptotic cells.	[218]
Silica	Spherical	Thiol-chitosan, paclitaxel, anti-EGFR	Core = 120 Shell = 9 D_H = 135.98	779	MDA-MB-231 (breast)	*In vitro* and *in vivo*: ChT, anti-EGFR, and PTT @ 808 nm, 1.2 W·cm^{-2}, 300 s	*In vivo*: NIR reflection mode fluorescence imaging, PAI	Anti-EGFR targeted GNSs exhibited enhanced tumor cellular uptake through a receptor mediated endocytosis process. *In vivo* therapy with laser irradiation showed a 97.43 % tumor inhibition rate.	[167]
Magnetite/silica	Spherical	PEG-anti-HER2	Core = 130 Shell = 10 D_H = 148	630	BT474, BT474R (TZB resistant), MDA-MB-213 (breast)	*In vivo*: anti-HER2, PTT @ 808 nm, pulsed laser 120 fs, 1 mJ/pulse, 1 kHz, 5 min	*In vitro* and *in vivo*: dark field microscopy and T_2-MRI	A preferential accumulation of anti-HER2 HGNS in tumor xenografts was observed at 72 h; after pulsed laser radiation, significant inhibition of proliferation and significant apoptosis of tumor cells is observed.	[137]
Silica	Spherical	PEG	Core = 60 Shell = 15 nm	805	FaDu (head and neck)	*In vitro*: PTT @ 810 nm, 14 W·cm^{-2}, 10 min	*In vitro*: phase contrast microscopy and holographic analysis	Macrophage-GNSs PTT was evaluated in 3D cancer/macrophage hybrid spheroids. Macrophages-GNSs had a good toxicology profile.	[237]
Platinum drug-polymeric micelle	Spherical	PEG	Core = 88.4 Shell = 19.5 D_H = 183.0–298.6	620	HCT116, HT29, LS174T (colorectal)	*In vitro* and *in vivo* ChT, PTT @ 808 nm, 1 W·cm^{-2}, 10 min	*In vitro*: dark field microscopy	Combined Ch-T and PTT resulted in stronger cytotoxicity and tumor suppression than free drug or PTT alone with no adverse side effects observed.	[95]
Hollow, DTTC	Au-Ag	–	D_H = 49.5		Multi-drug resistant *E. Colli* and *S. aureus*, infected open wounds	*In vitro* and *in vivo*: ionic Ag, PTT @ 808 nm, 1 W·cm^{-2}, 10 min	*In vivo*: SERS imaging	The PTT synergized with the release of silver ions, showing an enhanced anti-microbial activity	[228]
Hollow, Doxorubicin	Spherical	PEG-anti-PD-L1	Core = 58.29 Shell = 4.89 D_H = 90.3	735	B16F10, CLONE -M3 (melanoma)	*In vitro* and *in vivo*: ChT, anti-PD-L1, PTT @ 808 nm, 2 W·cm^{-2}, 2 × 3 min.	*In vivo*: fluorescence imaging	Cells treated with anti-PD-L1-HGNS-DOX and NIR irradiation dramatically reduced cell viability, increased ROS, and showed a higher apoptotic effect.	[211]
Hollow	Porous	PEG, maytansine and TZB	D_H = 113	750	SKBR3, MCF-7 (breast)	*In vivo*: ChT, anti-HER2, and PTT @ 808 nm, 3 W·cm^{-2}, 5 min	*In vivo*: PAI, CT imaging, and photothermal imaging	The combined therapy increased HSP70 levels and inhibited the pro-tumor M2 macrophage phenotype. The synergistic effect of ChT/PTT efficiently inhibited tumor growth.	[269]
PLGA/ Doxorubicin	Branched, porous	HSA–ICG–TZB complex; siRNA	Core = 96 Shell = 10.5 D_H = 106.5	730	SKBR3 (breast)	*In vitro* and *in vivo*: ChT, anti-HER3 siRNA, anti-HER2, PDT and PTT @ 808 nm, 0.5 and 2 W·cm^{-2}, 3 min, 5 min	*In vivo*: NIR fluorescence optical imaging	The combination of TZB and specific siRNA suppressed HER2 and HER3 protein expressions and p-AKT signaling. An enhanced anti-tumor effect without major affectation to healthy tissues was observed.	[251]
Nanoscale metal organic framework	Octahedron	PEG	D_H core = 216 D_H = 278	1300	MCF-10 A, 4 T1 (breast)	*In vitro*: PTT @1064 nm, 1.5 W·cm^{-2}, 3 min. *In vivo*: PTT @ 1064 nm, 1 W·cm^{-2}, 10 min	*In vitro* and *in vivo*: PAI, CT	Octahedron-shaped GNSs exhibited a LSPR in the NIR-II window, performing as theranostic agents with PTT, PAI and CT contrast properties.	[91]
PLGA, paclitaxel	Half shell	PEG, cycloRGDfk peptide	Core = 72 Half Shell = 10	> 1000	HeLa (cervix), MDA-MB-231 (breast)	*In vitro*: ChT, PTT @ 808 nm, 0.5 W·cm^{-2}, 10 min	*In vitro*: fluorescence microscopy	RGD peptide efficiently targeted the half-GNSs to integrins overexpressed in cervix and breast cancer cells. The combined treatment had a synergistic cytotoxic effect.	[316]

(*continued on next page*)

Table 3 (*continued*)

Core	Shell	Coating	Size (nm)	LSPR peak (nm)	Cell line (cancer) or model	Therapy	Diagnostics	Outcomes	Refs.
Cisplatin-HSA-PEI NPs	Spherical	–	Core = 136.1 Shell = 19.5 D_H = 181.8	660	A549 (lung)	*In vitro* and *in vivo*: ChT, PTT @ 808 nm, 1.5 W·cm^{-2}, 10 min	*In vitro*: dark-field microscopy	Combined ChT/PTT showed good tumor growth suppression with a 60 % tumor clearance rate without noticeable adverse effects in the main organs.	[220]
Silica	Spherical	Oligochitosan, streptomycin, anti-bacterial antibodies	Core = 120 Shell = 10 D_H = 137.56	790	*Listeria Monocytogenes*, infected open wounds	*In vitro* and *in vivo*: Ch-T and PTT @ 808 nm, 0.8 W·cm^{-2}, 5 min	*In vivo*: real-time fluorescence imaging	An increased accumulation in the infected tissue and a synergy between streptomycin and PTT was observed.	[227]

D_H: hydrodynamic diameter; ChT: chemotherapy; CW: continuous wavelength; TZB: trastuzumab; pHLIP: DTTC: 3,3′-diethylthiatricarbocyanine iodide.

precisely tuned, thus aligning the light intensities required for their use as bioimaging and photothermal agents, which are usually quite different in other types of GNPs.

Despite all the highlighted benefits of GNSs when compared to alternative gold-based NPs and their promising performance in the assessed applications, there are still many challenges related to the implementation of these nanosystems in the biomedical field. Hence, although gold nanomaterials are more biocompatible that other types of inorganic NPs, in many cases elevated doses are required to reach the desired effect in cell cultures or living organisms, potentially leading to cytotoxicity problems. Moreover, the control over their biodistribution, their effective targeting, and their interaction with the immune system, that we have discussed in detail above, remains a formidable challenge not only for GNSs, but also for practically any type of nanoplatform upon its injection in living organisms.

Another key point to consider is that the potential harmful effects, the precise biological pathways, and the ultimate clearance mechanisms of GNSs are largely dependent on minor fluctuations on their physicochemical properties. In this way, ideally it would be necessary that each work in this field performed exhaustive *in vivo* trials of the formulated NPs. However, there are a couple of basic rules that each *in vivo* experiments must adhere to, thus enabling a genuine comparison between the biological performance of different GNSs and the establishment of fundamental design principles. Firstly, the biological validation of the designed nanostructured systems must be carried out in the long term, since trace amounts of GNSs can remain in the organisms and the knowledge about their potential adverse effect is essential, but still low-explored. Conversely, following their thorough and prolonged *in vivo* assessment in standard small animal models, it becomes crucial to conduct preclinical studies involving larger mammals to elucidate the feasibility of GNSs-based procedures in humans. In this regard, it is worth mentioning the comprehensive study conducted by Schwartz et al., in which the thermal ablation of brain tumors using silica-core GNSs was performed in an orthotropic canine model [212]. For this purpose, canine transmissible venereal tumors were inoculated in the parietal lob of immunosuppressed hound dogs before the intravenous injection of GNSs, being demonstrated the capability of the strategy to ablate the brain tumors in large-size animals. However, and although *post-mortem* histopathological analysis of brain tissues showed selective accumulation of gold in the tumor, potential adverse effects of the procedure on other tissues and organs were not determined.

Despite all the aforementioned concerns related with the application of GNSs in the clinical practice, the company Nanospectra Biosciences Inc. holds the license from Rice University to the patent and the therapeutic use of a GNSs-based nanoplatform commercially known as AuroShell®, which has been categorized as a *medical device* by the FDA. The clinical safety of AuroShell® was firstly evaluated in different animal models, including dogs, being established its excellent biocompatibility and its potential for photothermal therapy purposes [142]. Afterwards, the safety of the nanoplatform-directed PTT was evaluated in different groups of patients with prostate cancer who were indicated for radical prostatectomy [317]. The dosage of AuroShell® was 7.5 mL·kg^{-1} at 2.77 × 10^{11} GNSs·mL^{-1} concentration, while an 810 nm diode laser was used for the excitation. Patients were followed for six months, being established that neither AuroShell® GNSs, nor the laser treatment and nor the prostatectomy had any significant effects on patient's chemical balance or metabolism. Next, AuroShell®-based therapy was evaluated in two open-label, multicenter, pilot study in individuals with refractory and/or recurrent head and neck tumors (NCT00848042). In such study, a total of 11 patients were treated with different doses and light intensities. A total of four patients presented minor adverse effects, although remarkably the patient subjected to the highest NP dose and laser, did not manifested any problem. Nonetheless, an objective response against the targeted tumors was not reported in the results. A second open-label, multi-center, pilot study the therapy was performed to evaluate the focal ablation of neoplastic prostate tissue

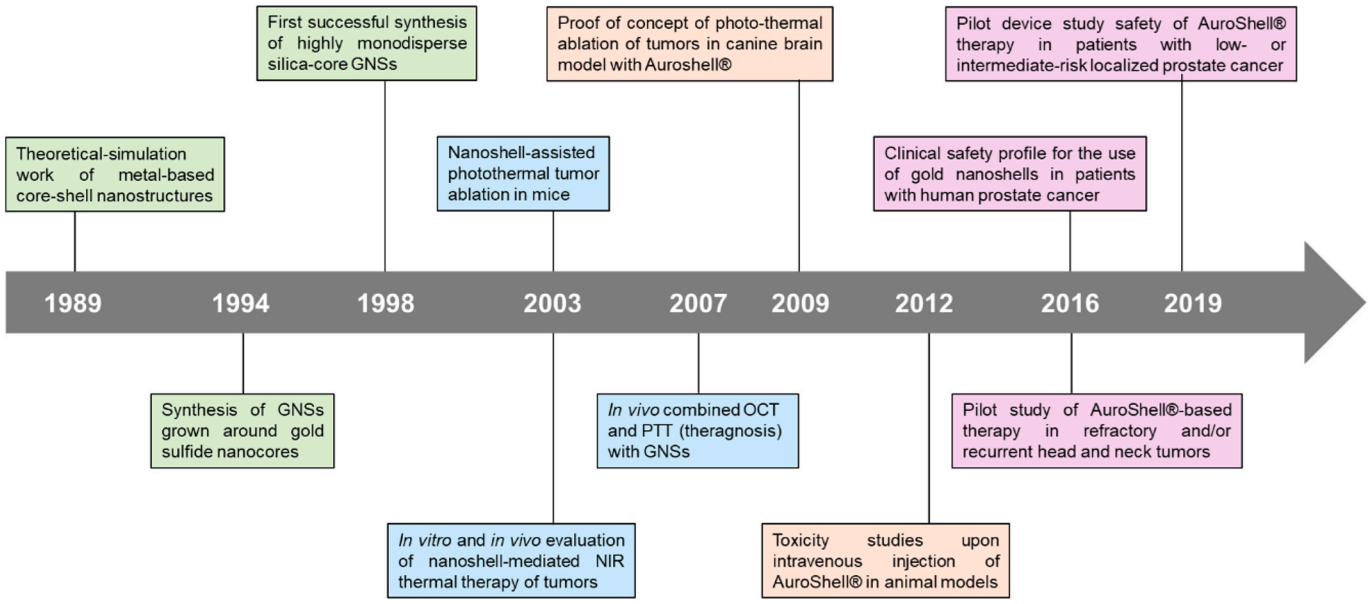

Fig. 14. Timeline diagram of the main theoretical, experimental, and preclinical stages of the development of silica-core GNSs, and the clinical translation of AuroShell®.

through the direct irradiation of AuroShell® accumulated in the tumors (the average amount of gold in the tumors was 8.28 $\mu g \cdot g^{-1}$, corresponding to $4.24 \cdot 10^8$ GNSs$\cdot mL^{-1}$) [69]. In this case, the only reported adverse event was a transient epigastric pain experienced by only one patient during GNSs infusion, who did not undergo the laser treatment. The ablation zones were negative for tumor in 62.5 % (10/16) of the patients after three months, while this percentage increase up to 87.5 % (14/16) after one year. The conversion of three biopsies from positive to negative in this timelapse could be attributed to the so-called abscopal post-ablation effect, a systemic immune response observed upon the radiation of a tissue/organ that could require up to six months.

With this exhaustive description of the validation process performed for AuroShell®, we intend to emphasize how long and complex is the translation into clinical practice of all GNSs-based nanoplatforms with promising potential in laboratory trials reviewed in this article (Fig. 14). The next generation of biomedical strategies that exploit the diagnostic and/or therapeutic properties of GNSs should definitely maintain the focus on the design of nanoplatforms with the optimal physicochemical properties, but also perform more advanced biological studies to address the feasibility of the nanosystems in a future clinical application.

If we go back to the design of GNSs, a very wide range of parameters has been already evaluated in order to optimize their performance in the desired application, as we discussed during this review article. However, there are still several areas in which the potential of complex structures with highly tunable properties such as GNSs have not yet been fully explored. For example, spiky morphologies and porous structures enhance the SERS capability of gold-based nanostructures. In this way, the design of star-shaped GNSs with high porosity and the adequate material in the core could be an interesting approach to optimize the SERS performance of this typology of nanomaterials. On the other hand, another type of gold-based nanosystems whose design could be clearly improved are the magnetoplasmonic GNSs. In most cases, the magnetic nanocores used in the formulation of these nanoplatforms are not carefully synthesized based on the intended application. Thus, commercially available magnetic NPs with weak response or the typical low-crystallinity spherical iron oxide NPs synthesized by fast and cheap methods such as co-precipitation are typically used to grown GNSs surrounding them. A precise design of these magnetic NPs in terms of size, morphology and/or doping type and degree of iron oxide could enormously improve the performance of magnetoplasmonic GNSs in, for example, MRI-optical multimodal bioimaging [286,318]. Moreover, another interesting and low-explored approach would involve the leverage of these magnetoplasmonic NPs to enhance hyperthermia treatments, capitalizing both the photothermal capabilities of GNSs and the magnetic hyperthermia potential of the cores [284,285]. Once again, the careful design of the magnetic nanocores would be a critical factor for the optimization of this strategy.

On the other hand, although gold-based nanostructures have been predominantly investigated for cancer-related applications within the biomedical field, there exist other promising areas for their utilization. This is the case of tissue engineering, where the use of nanomaterials with high electrical conductivity is a current trend for the fabrication of scaffolds that replicate the properties of highly conductive native tissues such as skeletal muscles, cardiac, or neural tissues [319,320]. Although nanomaterials with higher conductivity than GNPs, such as graphene or carbon nanotubes, are more typically used, these show lower biocompatibility degree than gold nanostructures. In this way, and since gold is also a material with quite high conductivity, GNSs grown surrounding small graphene cores could be used to reduce the amount of graphene required to provide the scaffolds with the necessary conductivity, thereby minimizing the associated toxicity risks. Interestingly, gold also displays weak piezoelectric properties, so that this GNSs-based strategy could also be leveraged to provide scaffolds with the capability to generate electrical signals in response to mechanical stimuli observed in different native tissues [321,322].

All these design approaches are just a few examples that we identified that the potential of GNSs for biomedical purposes is wide but still far from being fully exploited. We expect that this review will contribute to foster the discussion on the topic and foresee the surge of many exciting developments in this field in the near future.

Declaration of competing interest

The authors declare that they have no known competing financial interests or personal relationships that could have appeared to influence the work reported in this paper.

Data availability

No data was used for the research described in the article.

Acknowledgements

A.T. thanks CONAHCYT México Ciencia de Frontera 2019: 568483; Unión Europea NextGeneration EU: María Zambrano 2022-2023. The authors also thank Agencia Estatal de Investigación for projects PID2019-109517RB-I00 and PID2023-152062OA-I00, Xunta de Galicia for projects ED431C 2022/18 and ED481B2019/025, and Fundação para a Ciência e a Tecnologia for project 2022.05526.PTDC (Wi-Pi). European Regional Development Funds are also acknowledged. Schematics in ToC, Fig. 1, Fig. 3, Fig. 5, and Fig. 7 were created with Biorender.com.

References

[1] P.G. Jamkhande, N.W. Ghule, A.H. Bamer, M.G. Kalaskar, Metal nanoparticles synthesis: an overview on methods of preparation, advantages and disadvantages, and applications, J. Drug Del. Sci. Technol. 53 (2019) 101174. https://www.sciencedirect.com/science/article/pii/S1773224718308189.

[2] N. Sher, D.H.M. Alkhalifah, M. Ahmed, N. Mushtaq, F. Shah, F. Fozia, R.A. Khan, W.N. Hozzein, M.A.M. Aboul-Soud, Comparative study of antimicrobial activity of silver, gold, and silver/gold bimetallic Nanoparticles synthesized by green approach, Molecules 27 (2022) 7895, https://doi.org/10.3390/molecules27227895.

[3] P. Talarska, M. Boruczkowski, J. Żurawski, Current knowledge of silver and gold Nanoparticles in laboratory research-application, Toxicity, Cellular Uptake, Nanomaterials 11 (2021) 2454, https://doi.org/10.3390/nano11092454.

[4] R. Shrivastava, P. Kushwaha, Y.C. Bhutia, S.J.S. Flora, Oxidative stress following exposure to silver and gold nanoparticles in mice, Toxicol. Ind. Health 32 (2014) 1391–1404, https://doi.org/10.1177/0748233714562623.

[5] S. Barkur, J. Lukose, S. Chidangil, Probing nanoparticle–cell interaction using micro-raman spectroscopy: silver and gold nanoparticle-induced stress effects on optically trapped live red blood cells, ACS Omega 5 (2020) 1439–1447, https://doi.org/10.1021/acsomega.9b02988.

[6] E.C. Dreaden, A.M. Alkilany, X. Huang, C.J. Murphy, M.A. El-Sayed, The golden age: gold nanoparticles for biomedicine, Chem. Soc. Rev. 41 (2012) 2740–2779, https://doi.org/10.1039/C1CS15237H.

[7] K.M. Mayer, J.H. Hafner, Localized surface Plasmon resonance sensors, Chem. Rev. 111 (2011) 3828–3857, https://doi.org/10.1021/cr100313v.

[8] R. Aroca, The Interaction of Light with Nanoscopic Metal Particles and Molecules on Smooth Reflecting Surfaces, Surface-Enhanced Vibrational Spectroscopy, in, 2006, pp. 35–71, https://doi.org/10.1002/9780470035641.ch2.

[9] L.M. Liz-Marzán, Tailoring surface Plasmons through the morphology and assembly of metal Nanoparticles, Langmuir 22 (2006) 32–41, https://doi.org/10.1021/la0513353.

[10] E. Polo, M.F. Navarro Poupard, L. Guerrini, P. Taboada, B. Pelaz, R.A. Alvarez-Puebla, P. del Pino, Colloidal bioplasmonics, Nano Today 20 (2018) 58–73. http://www.sciencedirect.com/science/article/pii/S1748013217306047.

[11] N. Li, P. Zhao, D. Astruc, Anisotropic gold Nanoparticles: synthesis, properties, applications, and toxicity, Angew. Chem. Int. Ed. 53 (2014) 1756–1789, https://doi.org/10.1002/anie.201300441.

[12] N.R. Jana, L. Gearheart, C.J. Murphy, Wet chemical synthesis of high aspect ratio cylindrical gold Nanorods, J. Phys. Chem. B 105 (2001) 4065–4067, https://doi.org/10.1021/jp0107964.

[13] J. Kimling, M. Maier, B. Okenve, V. Kotaidis, H. Ballot, A. Plech, Turkevich method for gold nanoparticle synthesis revisited, J. Phys. Chem. B 110 (2006) 15700–15707, https://doi.org/10.1021/jp061667w.

[14] I. Saldan, O. Dobrovetska, L. Sus, O. Makota, O. Pereviznyk, O. Kuntyi, O. Reshetnyak, Electrochemical synthesis and properties of gold nanomaterials, J. Solid State Electrochem. 22 (2018) 637–656, https://doi.org/10.1007/s10008-017-3835-5.

[15] K. Okitsu, M. Ashokkumar, F. Grieser, Sonochemical synthesis of gold Nanoparticles: effects of ultrasound frequency, J. Phys. Chem. B 109 (2005) 20673–20675, https://doi.org/10.1021/jp0549374.

[16] J.E. Ortiz-Castillo, R.C. Gallo-Villanueva, M.J. Madou, V.H. Perez-Gonzalez, Anisotropic gold nanoparticles: a survey of recent synthetic methodologies, Coord. Chem. Rev. 425 (2020) 213489. https://www.sciencedirect.com/science/article/pii/S0010854520301375.

[17] I.B. Becerril-Castro, I. Calderon, N. Pazos-Perez, L. Guerrini, F. Schulz, N. Feliu, I. Chakraborty, V. Giannini, W.J. Parak, R.A. Alvarez-Puebla, Gold Nanostars: synthesis, optical and SERS analytical properties, Anal. & Sens. 2 (2022) e202200005, https://doi.org/10.1002/anse.202200005.

[18] L. Meng, J. Zhang, H. Li, W. Zhao, T. Zhao, Preparation and Progress in application of gold Nanorods, J. Nanomater. 2019 (2019) 4925702, https://doi.org/10.1155/2019/4925702.

[19] L. Scarabelli, A. Sánchez-Iglesias, J. Pérez-Juste, L.M. Liz-Marzán, A "tips and tricks" practical guide to the synthesis of gold Nanorods, J. Phy. Chem. Lett. 6 (2015) 4270–4279, https://doi.org/10.1021/acs.jpclett.5b02123.

[20] M. Rizwan Younis, G. He, B. Gurram, J. Lin, P. Huang, Recent advances in gold Nanorods-based Cancer Theranostics, Adv. Nano Biomed. Research 1 (2021) 2170121, https://doi.org/10.1002/anbr.202170121.

[21] X. Yang, M. Yang, B. Pang, M. Vara, Y. Xia, Gold nanomaterials at work in biomedicine, Chem. Rev. 115 (2015) 10410–10488, https://doi.org/10.1021/acs.chemrev.5b00193.

[22] R.D. Averitt, S.L. Westcott, N.J. Halas, Linear optical properties of gold nanoshells, J. Opt. Soc. Am. B 16 (1999) 1824–1832, https://doi.org/10.1364/JOSAB.16.001824.

[23] A. Umar, J. Kim, S.-M. Choi, One-pot synthesis of monodisperse single-crystalline spherical gold Nanoparticles for universal seeds, Cryst. Growth Des. 21 (2021) 4133–4140, https://doi.org/10.1021/acs.cgd.1c00412.

[24] A. Sánchez-Iglesias, K. Jenkinson, S. Bals, L.M. Liz-Marzán, Kinetic regulation of the synthesis of Pentatwinned gold Nanorods below room temperature, J. Phys. Chem. C 125 (2021) 23937–23944, https://doi.org/10.1021/acs.jpcc.1c07284.

[25] L. Scarabelli, M. Coronado-Puchau, J.J. Giner-Casares, J. Langer, L.M. Liz-Marzán, Monodisperse gold Nanotriangles: size control, large-scale self-assembly, and performance in surface-enhanced Raman scattering, ACS Nano 8 (2014) 5833–5842, https://doi.org/10.1021/nn500727w.

[26] S.E. Skrabalak, J. Chen, Y. Sun, X. Lu, L. Au, C.M. Cobley, Y. Xia, Gold Nanocages: synthesis, properties, and applications, Acc. Chem. Res. 41 (2008) 1587–1595, https://doi.org/10.1021/ar800018v.

[27] J.-E. Park, Y. Lee, J.-M. Nam, Precisely shaped, uniformly formed gold Nanocubes with ultrahigh reproducibility in single-particle scattering and surface-enhanced Raman scattering, Nano Lett. 18 (2018) 6475–6482, https://doi.org/10.1021/acs.nanolett.8b02973.

[28] S. Barbosa, A. Agrawal, L. Rodríguez-Lorenzo, I. Pastoriza-Santos, R.N.A. Alvarez-Puebla, A. Kornowski, H. Weller, L.M. Liz-Marzán, Tuning size and sensing properties in colloidal gold Nanostars, Langmuir 26 (2010) 14943–14950, https://doi.org/10.1021/la102559e.

[29] C. Ayala-Orozco, C. Urban, S. Bishnoi, A. Urban, H. Charron, T. Mitchell, M. Shea, S. Nanda, R. Schiff, N. Halas, A. Joshi, Sub-100nm gold nanomatryoshkas improve photo-thermal therapy efficacy in large and highly aggressive triple negative breast tumors, J. Control. Release 191 (2014) 90–97, https://doi.org/10.1016/j.jconrel.2014.07.038.

[30] D. Sun, F. Ben Romdhane, A. Wilson, M. Salmain, S. Boujday, Hollow gold Nanoshells for sensitive 2D Plasmonic sensors, ACS Appl. Nano Mat. 7 (2024) 5093–5102, https://doi.org/10.1021/acsanm.3c05872.

[31] A. Topete, M. Alatorre-Meda, E.M. Villar-Álvarez, A. Cambón, S. Barbosa, P. Taboada, V. Mosquera, Simple control of surface topography of gold Nanoshells by a surfactant-less seeded-growth method, ACS Appl. Mater. Interfaces 6 (2014) 11142–11157, https://doi.org/10.1021/am500989e.

[32] M. Hu, J. Chen, Z.-Y. Li, L. Au, G.V. Hartland, X. Li, M. Marquez, Y. Xia, Gold nanostructures: engineering their plasmonic properties for biomedical applications, Chem. Soc. Rev. 35 (2006) 1084–1094, https://doi.org/10.1039/B517615H.

[33] W. Chaabani, A. Chehaidar, J. Plain, Comparative theoretical study of the optical properties of silicon/gold, silica/gold Core/Shell and gold spherical Nanoparticles, Plasmonics 11 (2016) 1525–1535, https://doi.org/10.1007/s11468-016-0206-5.

[34] T.A. Erickson, J.W. Tunnell, Gold Nanoshells in Biomedical Applications, in: Nanotechnologies for the Life Sciences, Wiley-VCH Verlag GmbH & Co, KGaA, 2007, https://doi.org/10.1002/9783527610419.ntls0150.

[35] C. Oubre, P. Nordlander, Optical properties of Metallodielectric nanostructures calculated using the finite difference time domain method, J. Phys. Chem. B 108 (2004) 17740–17747, https://doi.org/10.1021/jp0473164.

[36] Y. Hu, R.C. Fleming, R.A. Drezek, Optical properties of gold-silica-gold multilayer nanoshells, Opt. Express 16 (2008) 19579–19591. https://opg.optica.org/oe/abstract.cfm?URI=oe-16-24-19579.

[37] P.K. Jain, K.S. Lee, I.H. El-Sayed, M.A. El-Sayed, Calculated absorption and scattering properties of gold Nanoparticles of different size, shape, and composition: applications in biological imaging and biomedicine, J. Phys. Chem. B 110 (2006) 7238–7248, https://doi.org/10.1021/jp057170o.

[38] S.J. Oldenburg, R.D. Averitt, S.L. Westcott, N.J. Halas, Nanoengineering of optical resonances, Chem. Phys. Lett. 288 (1998) 243–247, https://doi.org/10.1016/S0009-2614(98)00277-2.

[39] S.J. Oldenburg, J.B. Jackson, S.L. Westcott, N.J. Halas, Infrared extinction properties of gold nanoshells, Appl. Phys. Lett. 75 (1999) 2897–2899, https://doi.org/10.1063/1.125183.

[40] E. Hemmer, A. Benayas, F. Legare, F. Vetrone, Exploiting the biological windows: current perspectives on fluorescent bioprobes emitting above 1000 nm, Nanoscale Horizons 1 (2016) 168–184, https://doi.org/10.1039/C5NH00073D.

[41] N.G. Bastús, J. Comenge, V.C. Puntes, Kinetically controlled seeded growth synthesis of citrate-stabilized gold Nanoparticles of up to 200 nm: size focusing versus Ostwald ripening, Langmuir 27 (2011) 11098–11105, https://doi.org/10.1021/la201938u.

[42] X. Huang, P. Jain, I. El-Sayed, M. El-Sayed, Plasmonic photothermal therapy (PPTT) using gold nanoparticles, Lasers Med. Sci. 23 (2008) 217–228, https://doi.org/10.1007/s10103-007-0470-x.

[43] P.N. Prasad, Fundamentals of Light–Matter Interactions, in: Introduction to Biophotonics, John Wiley & Sons, Inc., 2004, pp. 92–128, https://doi.org/10.1002/0471465380.ch4.

[44] M.R. Beversluis, A. Bouhelier, L. Novotny, Continuum generation from single gold nanostructures through near-field mediated intraband transitions, Phys. Rev. B 68 (2003) 115433, https://doi.org/10.1103/PhysRevB.68.115433.

[45] G.T. Boyd, Z.H. Yu, Y.R. Shen, Photoinduced luminescence from the noble metals and its enhancement on roughened surfaces, Phys. Rev. B 33 (1986) 7923–7936, https://doi.org/10.1103/PhysRevB.33.7923.

[46] A. Mooradian, Photoluminescence of metals, Phys. Rev. Lett. 22 (1969) 185–187, https://doi.org/10.1103/PhysRevLett.22.185.
[47] M.B. Mohamed, V. Volkov, S. Link, M.A. El-Sayed, The `lightning' gold nanorods: fluorescence enhancement of over a million compared to the gold metal, Chem. Phys. Lett. 317 (2000) 517–523. https://www.sciencedirect.com/science/article/pii/S0009261499014141.
[48] G. Liang, J.V. Tegy, N. Vengadesan, Nanoshells for in vivo imaging using two-photon excitation microscopy, Nanotechnology 22 (2011) 365102, https://doi.org/10.1088/0957-4484/22/36/365102.
[49] J. Park, A. Estrada, K. Sharp, K. Sang, J.A. Schwartz, D.K. Smith, C. Coleman, J. D. Payne, B.A. Korgel, A.K. Dunn, J.W. Tunnell, Two-photon-induced photoluminescence imaging of tumors using near-infrared excited gold nanoshells, Opt. Express 16 (2008), https://doi.org/10.1364/OE.16.001590.
[50] J.B. Jackson, S.L. Westcott, L.R. Hirsch, J.L. West, N.J. Halas, Controlling the surface enhanced Raman effect via the nanoshell geometry, Appl. Phys. Lett. 82 (2003) 257–259, https://doi.org/10.1063/1.1534916.
[51] R. Bardhan, S. Lal, A. Joshi, N.J. Halas, Theranostic Nanoshells: from probe design to imaging and treatment of Cancer, Acc. Chem. Res. 44 (2011) 936–946, https://doi.org/10.1021/ar200023x.
[52] R. Bardhan, W. Chen, C. Perez-Torres, M. Bartels, R.M. Huschka, L.L. Zhao, E. Morosan, R.G. Pautler, A. Joshi, N.J. Halas, Nanoshells with targeted simultaneous enhancement of magnetic and optical imaging and Photothermal therapeutic response, Adv. Funct. Mater. 19 (2009) 3901–3909, https://doi.org/10.1002/adfm.200901235.
[53] R. Bardhan, N.K. Grady, J.R. Cole, A. Joshi, N.J. Halas, Fluorescence enhancement by Au nanostructures: Nanoshells and Nanorods, ACS Nano 3 (2009) 744–752, https://doi.org/10.1021/nn900001q.
[54] R. Bardhan, W. Chen, M. Bartels, C. Perez-Torres, M.F. Botero, R.W. McAninch, A. Contreras, R. Schiff, R.G. Pautler, N.J. Halas, A. Joshi, Tracking of multimodal therapeutic Nanocomplexes targeting breast Cancer in vivo, Nano Lett. 10 (2010) 4920–4928, https://doi.org/10.1021/nl102889y.
[55] J. Zhang, Y. Fu, F. Mahdavi, Bimetallic Nanoshells for metal-enhanced fluorescence with broad band fluorophores, J. Phys. Chem. C 116 (2012) 24224–24232, https://doi.org/10.1021/jp3057527.
[56] K. Kneipp, Y. Wang, H. Kneipp, L.T. Perelman, I. Itzkan, R.R. Dasari, M.S. Feld, Single molecule detection using surface-enhanced Raman scattering (SERS), Phys. Rev. Lett. 78 (1997) 1667–1670, https://doi.org/10.1103/PhysRevLett.78.1667.
[57] S. Jeong, M.-W. Kim, Y.-R. Jo, N.-Y. Kim, D. Kang, S.Y. Lee, S.-Y. Yim, B.-J. Kim, J. H. Kim, Hollow porous gold Nanoshells with controlled Nanojunctions for highly tunable Plasmon resonances and intense field enhancements for surface-enhanced Raman scattering, ACS Appl. Mater. Interfaces 11 (2019) 44458–44465, https://doi.org/10.1021/acsami.9b16983.
[58] H. Yuan, A.M. Fales, C.G. Khoury, J. Liu, T. Vo-Dinh, Spectral characterization and intracellular detection of surface-enhanced Raman scattering (SERS)-encoded plasmonic gold nanostars, J. Raman Spectrosc. 44 (2013) 234–239, https://doi.org/10.1002/jrs.4172.
[59] R. Alvarez-Puebla, L.M. Liz-Marzán, F.J. García de Abajo, Light concentration at the nanometer scale, J. Phy. Chem. Lett. 1 (2010) 2428–2434, https://doi.org/10.1021/jz100820m.
[60] R.A. Alvarez-Puebla, L.M. Liz-Marzán, SERS-based diagnosis and biodetection, Small 6 (2010) 604–610, https://doi.org/10.1002/smll.200901820.
[61] R. Vankayala, A. Sagadevan, P. Vijayaraghavan, C.-L. Kuo, K.C. Hwang, Metal Nanoparticles sensitize the formation of singlet oxygen, Angew. Chem. Int. Ed. 50 (2011) 10640–10644, https://doi.org/10.1002/anie.201105236.
[62] X.M. Qian, S.M. Nie, Single-molecule and single-nanoparticle SERS: from fundamental mechanisms to biomedical applications, Chem. Soc. Rev. 37 (2008) 912–920, https://doi.org/10.1039/B708839F.
[63] H. Yuan, Y. Liu, A.M. Fales, Y.L. Li, J. Liu, T. Vo-Dinh, Quantitative surface-enhanced resonant Raman scattering multiplexing of biocompatible gold Nanostars for in vitro and ex vivo detection, Anal. Chem. 85 (2012) 208–212, https://doi.org/10.1021/ac302510g.
[64] L. Rodriguez-Lorenzo, Z. Krpetic, S. Barbosa, R.A. Alvarez-Puebla, L.M. Liz-Marzan, I.A. Prior, M. Brust, Intracellular mapping with SERS-encoded gold nanostars, Integr. Biol. 3 (2011) 922–926, https://doi.org/10.1039/C1IB00029B.
[65] C. Loo, L. Hirsch, M.-H. Lee, E. Chang, J. West, N. Halas, R. Drezek, Gold nanoshell bioconjugates for molecular imaging in living cells, Opt. Lett. 30 (2005) 1012–1014. http://ol.osa.org/abstract.cfm?URI=ol-30-9-1012.
[66] X. Qian, X.-H. Peng, D.O. Ansari, Q. Yin-Goen, G.Z. Chen, D.M. Shin, L. Yang, A. N. Young, M.D. Wang, S. Nie, In vivo tumor targeting and spectroscopic detection with surface-enhanced Raman nanoparticle tags, Nat. Biotechnol. 26 (2008) 83–90, https://doi.org/10.1038/nbt1377.
[67] A.M. Fales, H. Yuan, T. Vo-Dinh, Cell-penetrating peptide enhanced intracellular Raman imaging and photodynamic therapy, Mol. Pharm. 10 (2013) 2291–2298, https://doi.org/10.1021/mp300634b.
[68] Z. Guo, G. Yu, Z. Zhang, Y. Han, G. Guan, W. Yang, M.-Y. Han, Intrinsic optical properties and emerging applications of gold nanostructures, Adv. Mater. 35 (2023) 2206700, https://doi.org/10.1002/adma.202206700.
[69] A.R. Rastinehad, H. Anastos, E. Wajswol, J.S. Winoker, J.P. Sfakianos, S. K. Doppalapudi, M.R. Carrick, C.J. Knauer, B. Taouli, S.C. Lewis, A.K. Tewari, J. A. Schwartz, S.E. Canfield, A.K. George, J.L. West, N.J. Halas, Gold nanoshell-localized photothermal ablation of prostate tumors in a clinical pilot device study, Proc. Natl. Acad. Sci. 116 (2019) 18590. http://www.pnas.org/content/116/37/18590.abstract.
[70] T. Muñoz-Ortiz, J. Hu, F. Sanz-Rodríguez, D.H. Ortgies, D. Jaque, D. Méndez-González, R. Aguilar, F. Alfonso, F. Rivero, E. Martín Rodríguez, J. García Solé, Optical detection of atherosclerosis at molecular level by optical coherence tomography: an in vitro study, nanomedicine: nanotechnology, Biol. Med. 43 (2022) 102556. https://www.sciencedirect.com/science/article/pii/S1549963422000429.
[71] X. Jia, K. Wang, X. Li, Z. Liu, Y. Liu, R. Xiao, S. Wang, Highly sensitive detection of three protein toxins via SERS-lateral flow immunoassay based on SiO2@Au nanoparticles, nanomedicine: nanotechnology, Biol. Med. 41 (2022) 102522. https://www.sciencedirect.com/science/article/pii/S1549963422000089.
[72] R. Ghosh Chaudhuri, S. Paria, Core/Shell Nanoparticles: classes, properties, synthesis mechanisms, characterization, and applications, Chem. Rev. 112 (2012) 2373–2433, https://doi.org/10.1021/cr100449n.
[73] Y. Huang, P. Huang, J. Lin, Plasmonic gold Nanovesicles for biomedical applications, Small Meth. 3 (2019) 1800394, https://doi.org/10.1002/smtd.201800394.
[74] J. Jiang, X. Cui, Y. Huang, D. Yan, B. Wang, Z. Yang, M. Chen, J. Wang, Y. Zhang, G. Liu, Advances and prospects in integrated Nano-oncology, Nano Biomed. & Engin. 16 (2024).
[75] A.E. Neeves, M.H. Birnboim, Composite structures for the enhancement of nonlinear-optical susceptibility, J. Opt. Soc. Am. B. 6 (1989) 787–796. https://opg.optica.org/josab/abstract.cfm?URI=josab-6-4-787.
[76] E. Matijevic, Preparation and properties of uniform size colloids, Chem. Mater. 5 (1993) 412–426, https://doi.org/10.1021/cm00028a004.
[77] H.S. Zhou, I. Honma, H. Komiyama, J.W. Haus, Controlled synthesis and quantum-size effect in gold-coated nanoparticles, Phys. Rev. B 50 (1994) 12052–12056, https://doi.org/10.1103/PhysRevB.50.12052.
[78] W. Stöber, A. Fink, E. Bohn, Controlled growth of monodisperse silica spheres in the micron size range, J. Colloid Interface Sci. 26 (1968) 62–69. http://www.sciencedirect.com/science/article/pii/0021979768902725.
[79] S. Damilos, I. Alissandratos, L. Panariello, A.N.P. Radhakrishnan, E. Cao, G. Wu, M.O. Besenhard, A.A. Kulkarni, C. Makatsoris, A. Gavriilidis, Continuous citrate-capped gold nanoparticle synthesis in a two-phase flow reactor, J. Flow Chem. 11 (2021) 553–567, https://doi.org/10.1007/s41981-021-00172-3.
[80] A. Herrero-Ruiz, G. Carolo, G. González-Rubio, M. Grzelczak, J.S. Niehaus, H. Weller, L.M. Liz-Marzán, Millifluidic flow reactor for reproducible seed-mediated nanoparticle synthesis, J. Phys. Chem. C 127 (2023) 19747–19758, https://doi.org/10.1021/acs.jpcc.3c03713.
[81] G. Ochoa-Vazquez, B. Kharisov, A. Arizmendi-Morquecho, A. Cario, C. Aymonier, S. Marre, I. López, Continuous segmented-flow synthesis of ag and Au Nanoparticles using a Low cost microfluidic PTFE tubing reactor, IEEE Trans Nanobioscience 21 (2022) 135–140.
[82] L. Panariello, S. Damilos, H. du Toit, G. Wu, A.N.P. Radhakrishnan, I.P. Parkin, A. Gavriilidis, Highly reproducible, high-yield flow synthesis of gold nanoparticles based on a rational reactor design exploiting the reduction of passivated Au(iii), React. Chem. Eng. 5 (2020) 663–676, https://doi.org/10.1039/C9RE00469F.
[83] J. Sui, J. Yan, D. Liu, K. Wang, G. Luo, Continuous synthesis of nanocrystals via flow chemistry technology, Small 16 (2020) 1902828, https://doi.org/10.1002/smll.201902828.
[84] S. Watanabe, Y. Asahi, H. Omura, K. Mae, M.T. Miyahara, Flow microreactor synthesis of gold nanoshells and patchy particles, Adv. Powder Technol. 27 (2016) 2335–2341. https://www.sciencedirect.com/science/article/pii/S0921883116302230.
[85] M. Mehdipour, L. Gloag, D. Hagness, J. Lian, M.S. Alam, X. Chen, R.D. Tilley, J. J. Gooding, Flow-based synthesis of gold-coated magnetic Nanoparticles for Magnetoplasmonic sensing applications, Part. Part. Syst. Charact. 39 (2022) 2200051, https://doi.org/10.1002/ppsc.202200051.
[86] Y. Jin, C. Jia, S.-W. Huang, M. O'Donnell, X. Gao, Multifunctional nanoparticles as coupled contrast agents, Nat. Commun. 1 (2010) 41, https://doi.org/10.1038/ncomms1042.
[87] C.S. Levin, C. Hofmann, T.A. Ali, A.T. Kelly, E. Morosan, P. Nordlander, K. H. Whitmire, N.J. Halas, Magnetic-plasmonic core-shell nanoparticles, ACS Nano 3 (2009) 1379–1388, https://doi.org/10.1021/nn900118a.
[88] J. WangWang, Q. Luo, M. Fan, I.S. Suzuki, M.H. Suzuki, Y. Engelhard, N. Lin, J. Q. Kim, C.-J. Wang, Zhong, monodispersed Core−Shell Fe3O4@Au Nanoparticles, J. Phys. Chem. B 109 (2005) 21593–21601, https://doi.org/10.1021/jp0543429.
[89] X. Ji, R. Shao, A.M. Elliott, R.J. Stafford, E. Esparza-Coss, J.A. Bankson, G. Liang, Z.-P. Luo, K. Park, J.T. Markert, C. Li, Bifunctional gold Nanoshells with a superparamagnetic Iron oxide−silica Core suitable for both MR imaging and Photothermal therapy, J. Phys. Chem. C 111 (2007) 6245–6251, https://doi.org/10.1021/jp0702245.
[90] Y. Jin, X. Gao, Plasmonic fluorescent quantum dots, Nat. Nanotechnol. 4 (2009) 571–576, https://doi.org/10.1038/nnano.2009.193.
[91] M. Chen, X.-T. Chen, L.-Y. Zhang, W. Meng, Y.-J. Chen, Y.-S. Zhang, Z.-C. Chen, H.-M. Wang, C.-M. Luo, X.-D. Shi, W.-H. Zhang, M.-S. Wang, J.-X. Chen, Kinetically and thermodynamically controlled one-pot growth of gold nanoshells with NIR-II absorption for multimodal imaging-guided photothermal therapy, J Nanobiotechnol. 21 (2023) 138, https://doi.org/10.1186/s12951-023-01907-1.
[92] G. Brennan, S. Bergamino, M. Pescio, S.A.M. Tofail, C. Silien, The effects of a varied gold Shell thickness on Iron oxide nanoparticle cores in magnetic manipulation, T1 and T2 MRI contrasting, and magnetic hyperthermia, Nanomaterials 10 (2020) 2424. https://www.mdpi.com/2079-4991/10/12/2424.
[93] L. Wang, Y. Yuan, S. Lin, J. Huang, J. Dai, Q. Jiang, D. Cheng, X. Shuai, Photothermo-chemotherapy of cancer employing drug leakage-free gold nanoshells, Biomaterials 78 (2016) 40–49. https://www.sciencedirect.com/science/article/pii/S0142961215009205.

[94] S.-Y. Lee, C.-L. Peng, M.-J. Shieh, Combined chemo-Photothermotherapy using gold Nanoshells on drug-loaded micellar templates for colorectal Cancer treatment, Part. Part. Syst. Charact. 35 (2018) 1800334, https://doi.org/10.1002/ppsc.201800334.
[95] S.-Y. Lee, M.-J. Shieh, Platinum(II) drug-loaded gold Nanoshells for chemo-Photothermal therapy in colorectal Cancer, ACS Appl. Mater. Interfaces 12 (2020) 4254–4264, https://doi.org/10.1021/acsami.9b18855.
[96] T. Appidi, R. P.S, S.A. Chinchulkar, A. Pradhan, H. Begum, V. Shetty, R. Srivastava, P. Ganesan, A.K. Rengan, A plasmon-enhanced fluorescent gold coated novel lipo-polymeric hybrid nanosystem: synthesis, characterization and application for imaging and photothermal therapy of breast cancer, Nanoscale, 14 (2022) 9112–9123, doi:https://doi.org/10.1039/D2NR01378A.
[97] B.L. Sanchez-Gaytan, S.-J. Park, Spiky gold Nanoshells, Langmuir 26 (2010) 19170–19174, https://doi.org/10.1021/la1038969.
[98] S.L. Westcott, S.J. Oldenburg, T.R. Lee, N.J. Halas, Formation and adsorption of clusters of gold Nanoparticles onto functionalized silica nanoparticle surfaces, Langmuir 14 (1998) 5396–5401, https://doi.org/10.1021/la980380q.
[99] J. Yang, J. Lee, J. Kang, S.J. Oh, H.-J. Ko, J.-H. Son, K. Lee, J.-S. Suh, Y.-M. Huh, S. Haam, Smart drug-loaded polymer gold Nanoshells for systemic and localized therapy of human epithelial Cancer, Adv. Mater. 21 (2009) 4339–4342, https://doi.org/10.1002/adma.200900334.
[100] P. Alonso-Cristobal, M. Laurenti, E. Lopez-Cabarcos, J. Rubio-Retama, Efficient synthesis of core@shell Fe3O4@Au nanoparticles, Mat. Research Exp. 2 (2015) 075002, https://doi.org/10.1088/2053-1591/2/7/075002.
[101] B.E. Brinson, J.B. Lassiter, C.S. Levin, R. Bardhan, N. Mirin, N.J. Halas, Nanoshells made easy: improving Au layer growth on nanoparticle surfaces, Langmuir 24 (2008) 14166–14171, https://doi.org/10.1021/la802049p.
[102] Z. Liang, Y. Liu, S. Ng, X. Li, L. Lai, S. Luo, S. Liu, The effect of pH value on the formation of gold nanoshells, J. Nanopart. Res. 13 (2011) 3301–3311, https://doi.org/10.1007/s11051-011-0244-z.
[103] J.Y. Kah, N. Phonthammachai, R.Y. Wan, J. Song, T. White, S. Mhaisalkar, I. Ahmadb, C. Shepparda, M. Olivoc, Synthesis of gold nanoshells based on the deposition precipitation process, Gold Bull. 41 (2008) 23–36, https://doi.org/10.1007/BF03215620.
[104] W. Dong, Y. Li, D. Niu, Z. Ma, J. Gu, Y. Chen, W. Zhao, X. Liu, C. Liu, J. Shi, Facile synthesis of monodisperse superparamagnetic Fe_3O_4 Core@hybrid@Au Shell nanocomposite for bimodal imaging and Photothermal therapy, Adv. Mater. 23 (2011) 5392–5397, https://doi.org/10.1002/adma.201103521.
[105] H. Wang, X. Liu, X. Li, W. Lu, L. Jiang, One–pot seedless synthesis of uniform gold Nanoshells and their Photothermal conversion property, ChemistrySelect 1 (2016) 659–663, https://doi.org/10.1002/slct.201600017.
[106] Y. Sun, B. Mayers, Y. Xia, Metal nanostructures with hollow interiors, Adv. Mater. 15 (2003) 641–646, https://doi.org/10.1002/adma.200301639.
[107] Y. Sun, B.T. Mayers, Y. Xia, Template-engaged replacement reaction: a one-step approach to the large-scale synthesis of metal nanostructures with hollow interiors, Nano Lett. 2 (2002) 481–485, https://doi.org/10.1021/nl025531v.
[108] Y. Jin, S. Dong, One-pot synthesis and characterization of novel silver−gold bimetallic nanostructures with hollow interiors and bearing Nanospikes, J. Phys. Chem. B 107 (2003) 12902–12905, https://doi.org/10.1021/jp035400y.
[109] H.-P. Liang, L.-J. Wan, C.-L. Bai, L. Jiang, Gold hollow Nanospheres: tunable surface Plasmon resonance controlled by interior-cavity sizes, J. Phys. Chem. B 109 (2005) 7795–7800, https://doi.org/10.1021/jp045006f.
[110] A.L. Durán-Meza, D.S. Moreno-Gutiérrez, J.F. Ruiz-Robles, A. Bañuelos-Frías, X. F. Segovia-González, A.M. Longoria-Hernández, E. Gomez, J. Ruiz-García, Synthesis and characterization of extremely small gold nanoshells, and comparison of their photothermal conversion capacity with gold nanorods, Nanoscale 8 (2016) 11091–11098, https://doi.org/10.1039/C6NR00027D.
[111] Y. Sun, Y. Xia, Alloying and Dealloying processes involved in the preparation of metal Nanoshells through a galvanic replacement reaction, Nano Lett. 3 (2003) 1569–1572, https://doi.org/10.1021/nl034765r.
[112] P.V. AshaRani, G. Low Kah Mun, M.P. Hande, S. Valiyaveettil, Cytotoxicity and genotoxicity of silver Nanoparticles in human cells, ACS Nano 3 (2009) 279–290, https://doi.org/10.1021/nn800596w.
[113] Y.M. Kwon, Z. Xia, S. Glyn-Jones, D. Beard, H.S. Gill, D.W. Murray, Dose-dependent cytotoxicity of clinically relevant cobalt nanoparticles and ions on macrophages in vitro, Biomed. Mater. 4 (2009) 025018.
[114] A.M. Goodman, Y. Cao, C. Urban, O. Neumann, C. Ayala-Orozco, M.W. Knight, A. Joshi, P. Nordlander, N.J. Halas, The surprising in vivo instability of near-IR-absorbing hollow Au–ag Nanoshells, ACS Nano 8 (2014) 3222–3231, https://doi.org/10.1021/nn405663h.
[115] D. Chen, L. Li, F. Tang, S. Qi, Facile and scalable synthesis of tailored silica "Nanorattle" structures, Adv. Mater. 21 (2009) 3804–3807, https://doi.org/10.1002/adma.200900599.
[116] Y. Choi, S. Hong, L. Liu, S.K. Kim, S. Park, Galvanically replaced hollow Au–ag Nanospheres: study of their surface Plasmon resonance, Langmuir 28 (2012) 6670–6676, https://doi.org/10.1021/la202569q.
[117] L. Wang, S. Patskovsky, B. Gauthier-Soumis, M. Meunier, Porous Au–ag Nanoparticles from galvanic replacement applied as single-particle SERS probe for quantitative monitoring, Small 18 (2022) 2105209, https://doi.org/10.1002/smll.202105209.
[118] K. Cai, W. Zhang, J. Zhang, H. Li, H. Han, T. Zhai, Design of Gold Hollow Nanorods with controllable aspect ratio for multimodal imaging and combined chemo-Photothermal therapy in the second near-infrared window, ACS Appl. Mater. Interfaces 10 (2018) 36703–36710, https://doi.org/10.1021/acsami.8b12758.
[119] H. Wang, D.W. Brandl, F. Le, P. Nordlander, N.J. Halas, Nanorice: a hybrid plasmonic nanostructure, Nano Lett. 6 (2006) 827–832, https://doi.org/10.1021/nl060209w.
[120] Z. Ma, H. Han, S. Tu, J. Xue, Fabrication of shape-controlled hematite particles and growth of gold nanoshells, Colloids Surf. A Physicochem. Eng. Asp. 334 (2009) 142–146. https://www.sciencedirect.com/science/article/pii/S0927775708007073.
[121] C. Wang, P. Tang, M. Ge, X. Xu, F. Cao, J.Z. Jiang, Synthesis and characterization of gold cubic nanoshells using water-soluble GeO_2 templates, Nanotechnology 22 (2011) 155706, https://doi.org/10.1088/0957-4484/22/15/155706.
[122] J.K. Kim, T.-H. Park, D.-J. Jang, Surface-enhanced Raman scattering and photothermal effect of hollow Au nanourchins with well-defined cavities, J. Nanopart. Res. 22 (2020) 305, https://doi.org/10.1007/s11051-020-05034-y.
[123] A. Marchetti, A. Gori, A.M. Ferretti, D.A. Esteban, S. Bals, C. Pigliacelli, P. Metrangolo, Templated out-of-equilibrium self-assembly of branched Au Nanoshells, Small 19 (2023) 2206712, https://doi.org/10.1002/smll.202206712.
[124] B.L. Sanchez-Gaytan, P. Swanglap, T.J. Lamkin, R.J. Hickey, Z. Fakhraai, S. Link, S.-J. Park, Spiky gold Nanoshells: synthesis and enhanced scattering properties, J. Phys. Chem. C 116 (2012) 10318–10324, https://doi.org/10.1021/jp300009b.
[125] H. Wang, G.P. Goodrich, F. Tam, C. Oubre, P. Nordlander, N.J. Halas, Controlled texturing modifies the surface topography and Plasmonic properties of Au Nanoshells, J. Phys. Chem. B 109 (2005) 11083–11087, https://doi.org/10.1021/jp051466c.
[126] H. Park, J. Yang, J. Lee, S. Haam, I.-H. Choi, K.-H. Yoo, Multifunctional Nanoparticles for combined doxorubicin and Photothermal treatments, ACS Nano 3 (2009) 2919–2926, https://doi.org/10.1021/nn900215k.
[127] S.-M. Lee, H. Park, K.-H. Yoo, Synergistic Cancer therapeutic effects of locally delivered drug and heat using multifunctional Nanoparticles, Adv. Mater. 22 (2010) 4049–4053, https://doi.org/10.1002/adma.201001040.
[128] S.J. Oldenburg, S.L. Westcott, R.D. Averitt, N.J. Halas, Surface enhanced Raman scattering in the near infrared using metal nanoshell substrates, J. Chem. Phys. 111 (1999) 4729–4735, https://doi.org/10.1063/1.479235.
[129] M.A. Dobrovolskaia, A.K. Patri, J. Zheng, J.D. Clogston, N. Ayub, P. Aggarwal, B. W. Neun, J.B. Hall, S.E. McNeil, Interaction of colloidal gold nanoparticles with human blood: effects on particle size and analysis of plasma protein binding profiles, nanomedicine: nanotechnology, Biol. Med. 5 (2009) 106–117. https://www.sciencedirect.com/science/article/pii/S1549963408001445.
[130] K. Kozics, M. Sramkova, K. Kopecka, P. Begerova, A. Manova, Z. Krivosikova, Z. Sevcikova, A. Liskova, E. Rollerova, T. Dubaj, V. Puntes, L. Wsolova, P. Simon, J. Tulinska, A. Gabelova, Pharmacokinetics, biodistribution, and biosafety of pegylated gold nanoparticles in vivo, Nano Mat. 11 (2021) 1702, https://doi.org/10.3390/nano11071702.
[131] G. Zhang, Z. Yang, W. Lu, R. Zhang, Q. Huang, M. Tian, L. Li, D. Liang, C. Li, Influence of anchoring ligands and particle size on the colloidal stability and in vivo biodistribution of polyethylene glycol-coated gold nanoparticles in tumor-xenografted mice, Biomaterials 30 (2009) 1928–1936. http://www.sciencedirect.com/science/article/pii/S0142961208010223.
[132] A.-L. Bailly, F. Correard, A. Popov, G. Tselikov, F. Chaspoul, R. Appay, A. Al-Kattan, A.V. Kabashin, D. Braguer, M.-A. Esteve, In vivo evaluation of safety, biodistribution and pharmacokinetics of laser-synthesized gold nanoparticles, Sci. Rep. 9 (2019) 12890, https://doi.org/10.1038/s41598-019-48748-3.
[133] W.H. De Jong, W.I. Hagens, P. Krystek, M.C. Burger, A.J.A.M. Sips, R.E. Geertsma, Particle size-dependent organ distribution of gold nanoparticles after intravenous administration, Biomaterials 29 (2008) 1912–1919. http://www.sciencedirect.com/science/article/pii/S014296120701071X.
[134] M. Semmler-Behnke, W.G. Kreyling, J. Lipka, S. Fertsch, A. Wenk, S. Takenaka, G. Schmid, W. Brandau, Biodistribution of 1.4- and 18-nm gold particles in rats, Small 4 (2008) 2108–2111, https://doi.org/10.1002/smll.200800922.
[135] T. Dubaj, K. Kozics, M. Sramkova, A. Manova, N.G. Bastús, O.H. Moriones, Y. Kohl, M. Dusinska, E. Runden-Pran, V. Puntes, A. Nelson, A. Gabelova, P., Simon, Nanomaterials, in, 2022.
[136] M. Pannerec-Varna, P. Ratajczak, G. Bousquet, I. Ferreira, C. Leboeuf, R. Boisgard, G. Gapihan, J. Verine, B. Palpant, E. Bossy, E. Doris, J. Poupon, E. Fort, A. Janin, In vivo uptake and cellular distribution of gold nanoshells in a preclinical model of xenografted human renal cancer, Gold Bull. 46 (2013) 257–265, https://doi.org/10.1007/s13404-013-0115-8.
[137] T. Nunes, T. Pons, X. Hou, K. Van Do, B. Caron, M. Rigal, M. Di Benedetto, B. Palpant, C. Leboeuf, A. Janin, G. Bousquet, Pulsed-laser irradiation of multifunctional gold nanoshells to overcome trastuzumab resistance in HER2-overexpressing breast cancer, J. Exp. Clin. Cancer Res. 38 (2019) 306, https://doi.org/10.1186/s13046-019-1305-x.
[138] W.D. James, L.R. Hirsch, J.L. West, P.D. O'Neal, J.D. Payne, Application of INAA to the build-up and clearance of gold nanoshells in clinical studies in mice, J. Radioanal. Nucl. Chem. 271 (2007) 455–459, https://doi.org/10.1007/s10967-007-0230-1.
[139] N. Khlebtsov, L. Dykman, Biodistribution and toxicity of engineered gold nanoparticles: a review of in vitro and in vivo studies, Chem. Soc. Rev. 40 (2011) 1647–1671, https://doi.org/10.1039/C0CS00018C.
[140] G. Sonavane, K. Tomoda, K. Makino, Biodistribution of colloidal gold nanoparticles after intravenous administration: effect of particle size, Colloids Surf. B: Biointerfaces 66 (2008) 274–280. http://www.sciencedirect.com/science/article/pii/S0927776508002695.
[141] N. Lewinski, V. Colvin, R. Drezek, Cytotoxicity of Nanoparticles, Small 4 (2008) 26–49, https://doi.org/10.1002/smll.200700595.
[142] S.C. Gad, K.L. Sharp, C. Montgomery, J.D. Payne, G.P. Goodrich, Evaluation of the toxicity of intravenous delivery of Auroshell particles (gold–silica Nanoshells),

Int. J. Toxicol. 31 (2012) 584–594, https://doi.org/10.1177/1091581812465969.
[143] M.A. Dobrovolskaia, A.K. Patri, J. Zheng, J.D. Clogston, N. Ayub, P. Aggarwal, B. W. Neun, J.B. Hall, S.E. McNeil, Interaction of colloidal gold nanoparticles with human blood: effects on particle size and analysis of plasma protein binding profiles, Nanomed. Nanotechnol. Biol. Med. 5 (2009) 106–117. http://linkinghub.elsevier.com/retrieve/pii/S1549963408001445?showall=true.
[144] V. Figueroa, B. Velasco, L.G. Arellano, V. Domínguez-Arca, A. Cambón, A. Pardo, A. Topete, L.C. Rosales-Rivera, J.F.A. Soltero, S. Barbosa, P. Taboada, Role of surface functionalization and biomolecule structure on protein corona adsorption and conformation onto anisotropic metallic nanoparticles, J. Mol. Liq. 398 (2024) 124240. https://www.sciencedirect.com/science/article/pii/S0167732224002964.
[145] L. Arellano, R. Martínez, A. Pardo, I. Diez, B. Velasco, A. Moreda-Piñeiro, P. Bermejo-Barrera, S. Barbosa, P. Taboada, Assessing the effect of surface coating on the stability, degradation, toxicity and cell endocytosis/exocytosis of Upconverting Nanoparticles, J. Colloid Interface Sci. 668 (2024) 575–586. https://www.sciencedirect.com/science/article/pii/S0021979724009226.
[146] A. França, P. Aggarwal, E.V. Barsov, S.V. Kozlov, M.A. Dobrovolskaia, Á. González-Fernández, Macrophage scavenger receptor a mediates the uptake of gold colloids by macrophages in vitro, Nanomedicine 6 (2011) 1175–1188, https://doi.org/10.2217/nnm.11.41.
[147] M.-R. Choi, K.J. Stanton-Maxey, J.K. Stanley, C.S. Levin, R. Bardhan, D. Akin, S. Badve, J. Sturgis, J.P. Robinson, R. Bashir, N.J. Halas, S.E. Clare, A cellular Trojan horse for delivery of therapeutic Nanoparticles into tumors, Nano Lett. 7 (2007) 3759–3765, https://doi.org/10.1021/nl072209h.
[148] S. Madsen, S.-K. Baek, A. Makkouk, T. Krasieva, H. Hirschberg, Macrophages as cell-based delivery Systems for Nanoshells in Photothermal therapy, Ann. Biomed. Eng. 40 (2012) 507–515, https://doi.org/10.1007/s10439-011-0415-1.
[149] A. Antonio, M.O. Sandra, M.S. Bruno, R. María Josefa, F.C. Jael, C. Pierre, S. Katherine, L. Alfonso, M. Rodolfo, S. Álvaro, B.C. Robert, L.C. José, L. C. Aitziber, Multifunctionalized iron oxide nanoparticles for selective drug delivery to CD44-positive cancer cells, Nanotechnology 27 (2016) 065103, https://doi.org/10.1088/0957-4484/27/6/065103.
[150] C.-G. Zhang, W.-J. Zhu, Y. Liu, Z.-Q. Yuan, S.-D. Yang, W.-L. Chen, J.-Z. Li, X.-F. Zhou, C. Liu, X.-N. Zhang, Novel polymer micelle mediated co-delivery of doxorubicin and P-glycoprotein siRNA for reversal of multidrug resistance and synergistic tumor therapy, Sci. Rep. 6 (2016) 23859. http://www.ncbi.nlm.nih.gov/pmc/articles/PMC4814909/.
[151] L. Müller, S. Steiner, L. Rodriguez-Lorenzo, A. Petri-Fink, B. Rothen-Rutishauser, P. Latzin, Effect of engineered nanoparticles on natural killer cells in vitro, Eur. Respir. J. 46 (2015).
[152] L.C. Kennedy, A.S. Bear, J.K. Young, N.A. Lewinski, J. Kim, A.E. Foster, R. A. Drezek, T cells enhance gold nanoparticle delivery to tumors in vivo, Nanoscale Res. Lett. 6 (2011) 1–11, https://doi.org/10.1186/1556-276X-6-283.
[153] C.-Y. Tsai, S.-L. Lu, C.-W. Hu, C.-S. Yeh, G.-B. Lee, H.-Y. Lei, Size-dependent attenuation of TLR9 signaling by gold Nanoparticles in macrophages, J. Immunol. 188 (2012) 68–76. http://www.jimmunol.org/content/188/1/68.abstract.
[154] H.T. Nguyen, H. Shen, The effect of PEGylation on the stimulation of IL-1[small beta] by gold (Au) nanoshell/silica core nanoparticles, J. Mater. Chem. B 4 (2016) 1650–1659, https://doi.org/10.1039/C5TB01553G.
[155] C. Gabay, C. Lamacchia, G. Palmer, IL-1 pathways in inflammation and human diseases, Nat. Rev. Rheumatol. 6 (2010) 232–241, https://doi.org/10.1038/nrrheum.2010.4.
[156] F. Ghiringhelli, L. Apetoh, A. Tesniere, L. Aymeric, Y. Ma, C. Ortiz, K. Vermaelen, T. Panaretakis, G. Mignot, E. Ullrich, J.-L. Perfettini, F. Schlemmer, E. Tasdemir, M. Uhl, P. Genin, A. Civas, B. Ryffel, J. Kanellopoulos, J. Tschopp, F. Andre, R. Lidereau, N.M. McLaughlin, N.M. Haynes, M.J. Smyth, G. Kroemer, L. Zitvogel, Activation of the NLRP3 inflammasome in dendritic cells induces IL-1[beta]-dependent adaptive immunity against tumors, Nat. Med. 15 (2009) 1170–1178, https://doi.org/10.1038/nm.2028.
[157] H.T. Nguyen, K.K. Tran, B. Sun, H. Shen, Activation of inflammasomes by tumor cell death mediated by gold nanoshells, Biomaterials 33 (2012) 2197–2205. http://www.sciencedirect.com/science/article/pii/S0142961211014177.
[158] H. Maeda, The enhanced permeability and retention (EPR) effect in tumor vasculature: the key role of tumor-selective macromolecular drug targeting, Adv. Enzym. Regul. 41 (2001) 189–207. http://www.sciencedirect.com/science/article/pii/S0065257100000133.
[159] S. Sindhwani, A.M. Syed, J. Ngai, B.R. Kingston, L. Maiorino, J. Rothschild, P. MacMillan, Y. Zhang, N.U. Rajesh, T. Hoang, J.L.Y. Wu, S. Wilhelm, A. Zilman, S. Gadde, A. Sulaiman, B. Ouyang, Z. Lin, L. Wang, M. Egeblad, W.C.W. Chan, The entry of nanoparticles into solid tumours, Nat. Mater. 19 (2020) 566–575, https://doi.org/10.1038/s41563-019-0566-2.
[160] Z.R. Goddard, M.J. Marín, D.A. Russell, M. Searcey, Active targeting of gold nanoparticles as cancer therapeutics, Chem. Soc. Rev. 49 (2020) 8774–8789, https://doi.org/10.1039/D0CS01121E.
[161] R.A. Sperling, W.J. Parak, Surface modification, functionalization and bioconjugation of colloidal inorganic nanoparticles, Philos. Trans. R. Soc. A Math. Phys. Eng. Sci. 368 (2010) 1333–1383, https://doi.org/10.1098/rsta.2009.0273.
[162] L. Hong, W. Li, Y. Li, S. Yin, Nanoparticle-based drug delivery systems targeting cancer cell surfaces, RSC Adv. 13 (2023) 21365–21382, https://doi.org/10.1039/D3RA02969G.
[163] D. Kalinowska, I. Grabowska-Jadach, M. Liwinska, M. Drozd, M. Pietrzak, A. Dybko, Z. Brzozka, Studies on effectiveness of PTT on 3D tumor model under microfluidic conditions using aptamer-modified nanoshells, Biosens. Bioelectron. 126 (2019) 214–221. https://www.sciencedirect.com/science/article/pii/S0956566318308870X.
[164] D.P. O'Neal, L.R. Hirsch, N.J. Halas, J.D. Payne, J.L. West, Photo-thermal tumor ablation in mice using near infrared-absorbing nanoparticles, Cancer Lett. 209 (2004) 171–176. http://www.sciencedirect.com/science/article/pii/S0304383504001442.
[165] M.P. Melancon, W. Lu, Z. Yang, R. Zhang, Z. Cheng, A.M. Elliot, J. Stafford, T. Olson, J.Z. Zhang, C. Li, In vitro and in vivo targeting of hollow gold nanoshells directed at epidermal growth factor receptor for photothermal ablation therapy, Mol. Cancer Ther. 7 (2008) 1730–1739, https://doi.org/10.1158/1535-7163.MCT-08-0016.
[166] I. Fratoddi, I. Venditti, C. Cametti, M. Russo, How toxic are gold nanoparticles? The state-of-the-art, Nano Res. 8 (2015) 1771–1799, https://doi.org/10.1007/s12274-014-0697-3.
[167] P. Manivasagan, V.T. Nguyen, S.W. Jun, G. Hoang, S. Mondal, H. Kim, V.H. M. Doan, J. Kim, C.-S. Kim, J. Oh, Anti-EGFR antibody conjugated thiol chitosan-layered gold nanoshells for dual-modal imaging-guided cancer combination therapy, J. Control. Release 311-312 (2019) 26–42. https://www.sciencedirect.com/science/article/pii/S0168365919304717.
[168] C.-C. Wu, Y.-C. Yang, Y.-T. Hsu, T.-C. Wu, C.-F. Hung, J.-T. Huang, C.-L. Chang, Nanoparticle-induced intraperitoneal hyperthermia and targeted photoablation in treating ovarian cancer, Oncotarget 6 (2015) 26861–26875, https://doi.org/10.18632/oncotarget.4766.
[169] A. Topete, M. Alatorre-Meda, E.M. Villar-Alvarez, S. Carregal-Romero, S. Barbosa, W.J. Parak, P. Taboada, V. Mosquera, Polymeric-gold Nanohybrids for combined imaging and Cancer therapy, Adv. Healthc Mater. 3 (2014) 1309–1325, https://doi.org/10.1002/adhm.201400023.
[170] M. Scaranti, E. Cojocaru, S. Banerjee, U. Banerji, Exploiting the folate receptor α in oncology, nature reviews, Clin. Oncol. 17 (2020) 349–359, https://doi.org/10.1038/s41571-020-0339-5.
[171] E. Vives, Present and future of cell-penetrating peptide mediated delivery systems: "is the Trojan horse too wild to go only to Troy?", J. Control. Release 109 (2005) 77–85. https://www.sciencedirect.com/science/article/pii/S0168365905004815.
[172] M. Yu, F. Guo, J. Wang, F. Tan, N. Li, A pH-driven and photoresponsive nanocarrier: remotely-controlled by near-infrared light for stepwise antitumor treatment, Biomaterials 79 (2016) 25–35. https://www.sciencedirect.com/science/article/pii/S014296121500959X.
[173] Y. Jiang, Q. Zhang, X. Liu, Y. Chen, L. Wang, J. Fu, H. Duan, Y. Wang, X. Yang, Au nanoshell-coated superparamagnetic Fe3O4–silica composite nanoparticles with surface-modification of an activatable cell-penetrating peptide for tumor-targeted multimode bioimaging and photothermal therapy, RSC Adv. 6 (2016) 85587–85594, https://doi.org/10.1039/C6RA07708K.
[174] G. Song, S.J. Petschauer, J.A. Madden, C.W. Zamboni, Nanoparticles and the mononuclear phagocyte system: pharmacokinetics and applications for inflammatory diseases, Curr. Rheumatol. Rev. 10 (2014) 22–34, https://doi.org/10.2174/1573403X10666140914160554.
[175] A.J. Tavares, W. Poon, Y.-N. Zhang, Q. Dai, R. Besla, D. Ding, B. Ouyang, A. Li, J. Chen, G. Zheng, C. Robbins, W.C.W. Chan, Effect of removing Kupffer cells on nanoparticle tumor delivery, Proc. Natl. Acad. Sci. 114 (2017) E10871–E10880, https://doi.org/10.1073/pnas.1713390114.
[176] M. Almada, B.H. Leal-Martínez, N. Hassan, M.J. Kogan, M.G. Burboa, A. Topete, M.A. Valdez, J. Juárez, Photothermal conversion efficiency and cytotoxic effect of gold nanorods stabilized with chitosan, alginate and poly(vinyl alcohol), Mater. Sci. Eng. C 77 (2017) 583–593. http://www.sciencedirect.com/science/article/pii/S0928493116321993.
[177] X. He, Y. Yang, Y. Han, C. Cao, Z. Zhang, L. Li, C. Xiao, H. Guo, L. Wang, L. Han, Z. Qu, N. Liu, S. Han, F. Xu, Extracellular matrix physical properties govern the diffusion of nanoparticles in tumor microenvironment, Proc. Natl. Acad. Sci. 120 (2023) e2209260120, https://doi.org/10.1073/pnas.2209260120.
[178] N. Feliu, W.J. Parak, Developing future nanomedicines, Science 384 (2024) 385–386, https://doi.org/10.1126/science.abq3711.
[179] S. Wilhelm, A.J. Tavares, Q. Dai, S. Ohta, J. Audet, H.F. Dvorak, W.C.W. Chan, Analysis of nanoparticle delivery to tumours, Nat Rev Mater 1 (2016) 16014, https://doi.org/10.1038/natrevmats.2016.14.
[180] Q. Dai, S. Wilhelm, D. Ding, A.M. Syed, S. Sindhwani, Y. Zhang, Y.Y. Chen, P. MacMillan, W.C.W. Chan, Quantifying the ligand-coated nanoparticle delivery to Cancer cells in solid tumors, ACS Nano 12 (2018) 8423–8435, https://doi.org/10.1021/acsnano.8b03900.
[181] A. Barhoumi, R. Huschka, R. Bardhan, M.W. Knight, N.J. Halas, Light-induced release of DNA from plasmon-resonant nanoparticles: towards light-controlled gene therapy, Chem. Phys. Lett. 482 (2009) 171–179. http://www.sciencedirect.com/science/article/pii/S000926140901197X.
[182] R. Huschka, O. Neumann, A. Barhoumi, N.J. Halas, Visualizing light-triggered release of molecules inside living cells, Nano Lett. 10 (2010) 4117–4122, https://doi.org/10.1021/nl102293b.
[183] X. Bai, Y. Wang, Z. Song, Y. Feng, Y. Chen, D. Zhang, L. Feng, The basic properties of gold nanoparticles and their applications in tumor diagnosis and treatment, Int. J. Mol. Sci. 21 (2020) 2480, https://doi.org/10.3390/ijms21072480.
[184] M. Hegde, P. Pai, M.G. Shetty, K.S. Babitha, Gold nanoparticle based biosensors for rapid pathogen detection: a review, Environment. Nanotechnol., Monitoring & Manag. 18 (2022) 100756. https://www.sciencedirect.com/science/article/pii/S2215153222001167.
[185] S. Sau, H.O. Alsaab, K. Bhise, R. Alzhrani, G. Nabil, A.K. Iyer, Multifunctional nanoparticles for cancer immunotherapy: a groundbreaking approach for reprogramming malfunctioned tumor environment, J. Control. Release 274

(2018) 24–34. https://www.sciencedirect.com/science/article/pii/S0168365918300464.
[186] X. Hou, X. Wang, R. Liu, H. Zhang, X. Liu, Y. Zhang, Facile synthesis of multifunctional Fe3O4@SiO2@Au magneto-plasmonic nanoparticles for MR/CT dual imaging and photothermal therapy, RSC Adv. 7 (2017) 18844–18850, https://doi.org/10.1039/C7RA00925A.
[187] I. Urries, C. Muñoz, L. Gomez, C. Marquina, V. Sebastian, M. Arruebo, J. Santamaria, Magneto-plasmonic nanoparticles as theranostic platforms for magnetic resonance imaging, drug delivery and NIR hyperthermia applications, Nanoscale 6 (2014) 9230–9240, https://doi.org/10.1039/C4NR01588F.
[188] S. Link, M.A. El-Sayed, Shape and size dependence of radiative, non-radiative and photothermal properties of gold nanocrystals, Int. Rev. Phys. Chem. 19 (2000) 409–453, https://doi.org/10.1080/01442350050034180.
[189] X. Huang, P.K. Jain, I.H. El-Sayed, M.A. El-Sayed, Determination of the minimum temperature required for selective Photothermal destruction of Cancer cells with the use of Immunotargeted gold Nanoparticles, Photochem. Photobiol. 82 (2006) 412–417, https://doi.org/10.1562/2005-12-14-RA-754.
[190] A. Hatef, S. Fortin-Deschênes, E. Boulais, F. Lesage, M. Meunier, Photothermal response of hollow gold nanoshell to laser irradiation: continuous wave, short and ultrashort pulse, Int. J. Heat Mass Transf. 89 (2015) 866–871. https://www.sciencedirect.com/science/article/pii/S0017931015005657.
[191] L. Rouleau, R. Berti, V.W.K. Ng, C. Matteau-Pelletier, T. Lam, P. Saboural, A. K. Kakkar, F. Lesage, E. Rhéaume, J.-C. Tardif, VCAM-1-targeting gold nanoshell probe for photoacoustic imaging of atherosclerotic plaque in mice, Contrast Media & Molecular, Imaging 8 (2013) 27–39, https://doi.org/10.1002/cmmi.1491.
[192] T.-H. Park, D.-W. Jeong, D.-J. Jang, Photothermal structural modification of porous gold nanoshells via pulsed-laser irradiation: effects of laser wavelengths and surface conditions, Phys. Chem. Chem. Phys. 22 (2020) 23333–23341, https://doi.org/10.1039/D0CP03734F.
[193] H. Xiaohua, K. Bin, Q. Wei, A.M. Megan, C.C. Po, K.O. Adegboyega, H.E.-S. Ivan, A.E.-S. Mostafa, Comparative study of photothermolysis of cancer cells with nuclear-targeted or cytoplasm-targeted gold nanospheres: continuous wave or pulsed lasers, Biomedo 15 (2010) 058002, https://doi.org/10.1117/1.3486538.
[194] O. Knights, S. Freear, J.R., McLaughlan, Nanomaterials, in, 2020.
[195] P. Wust, B. Hildebrandt, G. Sreenivasa, B. Rau, J. Gellermann, H. Riess, R. Felix, P.M. Schlag, Hyperthermia in combined treatment of cancer, Lancet Oncol. 3 (2002) 487–497. http://www.sciencedirect.com/science/article/pii/S1470204502008185.
[196] N.R. Datta, S.G. Ordóñez, U.S. Gaipl, M.M. Paulides, H. Crezee, J. Gellermann, D. Marder, E. Puric, S. Bodis, Local hyperthermia combined with radiotherapy and−/or chemotherapy: recent advances and promises for the future, Cancer Treat. Rev. 41 (2015) 742–753. https://www.sciencedirect.com/science/article/pii/S0305737215001048.
[197] R.C. Carrillo-Torres, M.J. Garcia-Soto, S.D. Morales-Chavez, A. Garibay-Escobar, J. Hernandez-Paredes, R. Guzman, M. Barboza-Flores, M.E. Alvarez-Ramos, Hollow Au-ag bimetallic nanoparticles with high photothermal stability, RSC Adv. 6 (2016) 41304–41312, https://doi.org/10.1039/C5RA25821A.
[198] S. Link, M.A. El-Sayed, Optical properties and ultrafast dynamics of metallic nanocrystals, Annu. Rev. Phys. Chem. 54 (2003) 331–366, https://doi.org/10.1146/annurev.physchem.54.011002.103759.
[199] C.M. Aguirre, C.E. Moran, J.F. Young, N.J. Halas, Laser-induced reshaping of Metallodielectric Nanoshells under femtosecond and nanosecond Plasmon resonant illumination, J. Phys. Chem. B 108 (2004) 7040–7045, https://doi.org/10.1021/jp036222b.
[200] A. Elliott, J. Schwartz, J. Wang, A. Shetty, J. Hazle, J.R. Stafford, Analytical solution to heat equation with magnetic resonance experimental verification for nanoshell enhanced thermal therapy, Lasers Surg. Med. 40 (2008) 660–665, https://doi.org/10.1002/lsm.20682.
[201] F.-Y. Cheng, C.-T. Chen, C.-S. Yeh, Comparative efficiencies of photothermal destruction of malignant cells using antibody-coated silica@Au nanoshells, hollow Au/ag nanospheres and Au nanorods, Nanotechnology 20 (2009) 425104, https://doi.org/10.1088/0957-4484/20/42/425104.
[202] V.P. Pattani, J.W. Tunnell, Nanoparticle-mediated photothermal therapy: a comparative study of heating for different particle types, Lasers Surg. Med. 44 (2012) 675–684.
[203] C. Carnovale, G. Bryant, R. Shukla, V. Bansal, Identifying trends in gold nanoparticle toxicity and uptake: size, shape, capping ligand, and biological Corona, ACS, Omega 4 (2019) 242–256, https://doi.org/10.1021/acsomega.8b03227.
[204] A. Woźniak, A. Malankowska, G. Nowaczyk, B.F. Grześkowiak, K. Tuśnio, R. Słomski, A. Zaleska-Medynska, S. Jurga, Size and shape-dependent cytotoxicity profile of gold nanoparticles for biomedical applications, J. Mater. Sci. Mater. Med. 28 (2017) 92, https://doi.org/10.1007/s10856-017-5902-y.
[205] A.M. Gobin, M.H. Lee, N.J. Halas, W.D. James, R.A. Drezek, J.L. West, Near-infrared resonant Nanoshells for combined optical imaging and Photothermal Cancer therapy, Nano Lett. 7 (2007) 1929–1934, https://doi.org/10.1021/nl070610y.
[206] L.E. Strong, J.L. West, Hydrogel-coated near infrared absorbing Nanoshells as light-responsive drug delivery vehicles, ACS Biomater. Sci. Eng. 1 (2015) 685–692, https://doi.org/10.1021/acsbiomaterials.5b00111.
[207] B. Chang, G. Liu, F. Xue, D.G. Rosen, L. Xiao, X. Wang, J. Liu, ALDH1 expression correlates with favorable prognosis in ovarian cancers, Mod. Pathol. 22 (2009) 817–823, https://doi.org/10.1038/modpathol.2009.35.
[208] W. Lu, C. Xiong, G. Zhang, Q. Huang, R. Zhang, J.Z. Zhang, C. Li, Targeted photothermal ablation of murine melanomas with melanocyte-stimulating hormone analog–conjugated hollow gold nanospheres, Clin. Cancer Res. 15 (2009) 876–886, https://doi.org/10.1158/1078-0432.CCR-08-1480.
[209] A.J. Coughlin, J.S. Ananta, N. Deng, I.V. Larina, P. Decuzzi, J.L. West, Gadolinium-conjugated gold Nanoshells for multimodal diagnostic imaging and Photothermal Cancer therapy, Small 10 (2014) 556–565, https://doi.org/10.1002/smll.201302217.
[210] R. Vankayala, C.-C. Lin, P. Kalluru, C.-S. Chiang, K.C. Hwang, Gold nanoshells-mediated bimodal photodynamic and photothermal cancer treatment using ultra-low doses of near infra-red light, Biomaterials 35 (2014) 5527–5538. http://www.sciencedirect.com/science/article/pii/S0142961214003251.
[211] A. Banstola, K. Poudel, F. Emami, S.K. Ku, J.-H. Jeong, J.O. Kim, S. Yook, Localized therapy using anti-PD-L1 anchored and NIR-responsive hollow gold nanoshell (HGNS) loaded with doxorubicin (DOX) for the treatment of locally advanced melanoma, nanomedicine: nanotechnology, Biol. Med. 33 (2021) 102349. https://www.sciencedirect.com/science/article/pii/S1549963420302033.
[212] J.A. Schwartz, A.M. Shetty, R.E. Price, R.J. Stafford, J.C. Wang, R.K. Uthamanthil, K. Pham, R.J. McNichols, C.L. Coleman, J.D. Payne, Feasibility study of particle-assisted laser ablation of brain tumors in Orthotopic canine model, Cancer Res. 69 (2009) 1659–1667, https://doi.org/10.1158/0008-5472.CAN-08-2535.
[213] Z. Li, CD133: a stem cell biomarker and beyond, Exp. Hematol. Oncol. 2 (2013) 1–8, https://doi.org/10.1186/2162-3619-2-17.
[214] H. Liu, D. Chen, L. Li, T. Liu, L. Tan, X. Wu, F. Tang, Multifunctional gold Nanoshells on silica Nanorattles: a platform for the combination of Photothermal therapy and chemotherapy with Low systemic toxicity, Angew. Chem. Int. Ed. 50 (2011) 891–895, https://doi.org/10.1002/anie.201002820.
[215] S. Wang, Z. Dai, H. Ke, E. Qu, X. Qi, K. Zhang, J. Wang, Contrast ultrasound-guided photothermal therapy using gold nanoshelled microcapsules in breast cancer, Eur. J. Radiol. 83 (2014) 117–122. http://www.sciencedirect.com/science/article/pii/S0720048X13005081.
[216] Y. Gao, Y. Li, Y. Wang, Y. Chen, J. Gu, W. Zhao, J. Ding, J. Shi, Controlled synthesis of multilayered gold Nanoshells for enhanced Photothermal therapy and SERS detection, Small 11 (2015) 77–83, https://doi.org/10.1002/smll.201402149.
[217] H. Shen, J. You, G. Zhang, A. Ziemys, Q. Li, L. Bai, X. Deng, D.R. Erm, X. Liu, C. Li, M. Ferrari, Cooperative, nanoparticle-enabled thermal therapy of breast cancer, Adv. Healthcare Mat. 1 (2012) 84–89, https://doi.org/10.1002/adhm.201100005.
[218] B.K. Poudel, B. Gupta, T. Ramasamy, R.K. Thapa, S. Pathak, K.T. Oh, J.-H. Jeong, H.-G. Choi, C.S. Yong, J.O. Kim, PEGylated thermosensitive lipid-coated hollow gold nanoshells for effective combinational chemo-photothermal therapy of pancreatic cancer, Colloids Surf. B: Biointerfaces 160 (2017) 73–83. https://www.sciencedirect.com/science/article/pii/S0927776517305878.
[219] J. Park, J. Park, E.J. Ju, S.S. Park, J. Choi, J.H. Lee, K.J. Lee, S.H. Shin, E.J. Ko, I. Park, C. Kim, J.J. Hwang, J.S. Lee, S.Y. Song, S.-Y. Jeong, E.K. Choi, Multifunctional hollow gold nanoparticles designed for triple combination therapy and CT imaging, J. Control. Release 207 (2015) 77–85. http://www.sciencedirect.com/science/article/pii/S0168365915002254.
[220] S.-J. Yang, J.-A. Pai, M.-J. Shieh, J.L.Y. Chen, K.-C. Chen, Cisplatin-loaded gold nanoshells mediate chemo-photothermal therapy against primary and distal lung cancers growth, Biomed. Pharmacother. 158 (2023) 114146. https://www.sciencedirect.com/science/article/pii/S0753322222015359.
[221] E. Redolfi Riva, A. Desii, E. Sinibaldi, G. Ciofani, V. Piazza, B. Mazzolai, V. Mattoli, Gold Nanoshell/polysaccharide Nanofilm for controlled laser-assisted tissue thermal ablation, ACS Nano 8 (2014) 5552–5563, https://doi.org/10.1021/nn406348v.
[222] G. Shafirstein, D. Bellnier, E. Oakley, S. Hamilton, M. Potasek, K. Beeson, E. Parilov, Interstitial photodynamic therapy-a focused review, Cancers (Basel) 9 (2017) 12, https://doi.org/10.3390/cancers9020012.
[223] D.K. Ledezma, P.B. Balakrishnan, A. Shukla, J.A. Medina, J. Chen, E. Oakley, C. M. Bollard, G. Shafirstein, M. Miscuglio, R. Fernandes, Interstitial Photothermal therapy generates durable treatment responses in neuroblastoma, Adv. Healthc. Mater. 11 (2022) 2201084, https://doi.org/10.1002/adhm.202201084.
[224] D. Paithankar, B.H. Hwang, G. Munavalli, A. Kauvar, J. Lloyd, R. Blomgren, L. Faupel, T. Meyer, S. Mitragotri, Ultrasonic delivery of silica–gold nanoshells for photothermolysis of sebaceous glands in humans: nanotechnology from the bench to clinic, J. Control. Release 206 (2015) 30–36. http://www.sciencedirect.com/science/article/pii/S0168365915001510.
[225] H.J. Kim, S.-M. Lee, K.-H. Park, C.H. Mun, Y.-B. Park, K.-H. Yoo, Drug-loaded gold/iron/gold plasmonic nanoparticles for magnetic targeted chemo-photothermal treatment of rheumatoid arthritis, Biomaterials 61 (2015) 95–102. https://www.sciencedirect.com/science/article/pii/S0142961215004688.
[226] P. Manivasagan, F. Khan, G. Hoang, S. Mondal, H. Kim, V. Hoang, Minh Doan, Y.-M. Kim, J. Oh, Thiol chitosan-wrapped gold nanoshells for near-infrared laser-induced photothermal destruction of antibiotic-resistant bacteria, Carbohydr. Polym. 225 (2019) 115228. https://www.sciencedirect.com/science/article/pii/S0144861719308951.
[227] P. Manivasagan, F. Khan, D. Rajan Dhatchayeny, S. Park, A. Joe, H.-W. Han, S.-H. Seo, T. Thambi, V.H. Giang Phan, Y.-M. Kim, C.-S. Kim, J. Oh, E.-S. Jang, Antibody-conjugated and streptomycin-chitosan oligosaccharide-modified gold nanoshells for synergistic chemo-photothermal therapy of drug-resistant bacterial infection, J. Adv. Res. 48 (2023) 87–104. https://www.sciencedirect.com/science/article/pii/S2090123222001904.
[228] J. He, Y. Qiao, H. Zhang, J. Zhao, W. Li, T. Xie, D. Zhong, Q. Wei, S. Hua, Y. Yu, K. Yao, H.A. Santos, M. Zhou, Gold–silver nanoshells promote wound healing from drug-resistant bacteria infection and enable monitoring via surface-

enhanced Raman scattering imaging, Biomaterials 234 (2020) 119763. https://www.sciencedirect.com/science/article/pii/S0142961220300090.
[229] O. Khantamat, C.-H. Li, F. Yu, A.C. Jamison, W.-C. Shih, C. Cai, T.R. Lee, Gold Nanoshell-decorated silicone surfaces for the near-infrared (NIR) Photothermal destruction of the pathogenic Bacterium E. Faecalis, ACS Appl. Mater. Interfaces 7 (2015) 3981–3993, https://doi.org/10.1021/am506516r.
[230] A.D. Waldman, J.M. Fritz, M.J. Lenardo, A guide to cancer immunotherapy: from T cell basic science to clinical practice, Nat. Rev. Immunol. (2020), https://doi.org/10.1038/s41577-020-0306-5.
[231] R.S. Wallis, A. O'Garra, A. Sher, A. Wack, Host-directed immunotherapy of viral and bacterial infections: past, present and future, Nat. Rev. Immunol. 23 (2023) 121–133, https://doi.org/10.1038/s41577-022-00734-z.
[232] C. Franklin, E. Livingstone, A. Roesch, B. Schilling, D. Schadendorf, Immunotherapy in melanoma: recent advances and future directions, Eur. J. Surgical Oncol. (EJSO) 43 (2017) 604–611. https://www.sciencedirect.com/science/article/pii/S0748798316308666.
[233] D. Marin, Y. Li, R. Basar, H. Rafei, M. Daher, J. Dou, V. Mohanty, M. Dede, Y. Nieto, N. Uprety, S. Acharya, E. Liu, J. Wilson, P. Banerjee, H.A. Macapinlac, C. Ganesh, P.F. Thall, R. Bassett, M. Ammari, S. Rao, K. Cao, M. Shanley, M. Kaplan, C. Hosing, P. Kebriaei, L.J. Nastoupil, C.R. Flowers, S.M. Moseley, P. Lin, S. Ang, U.R. Popat, M.H. Qazilbash, R.E. Champlin, K. Chen, E.J. Shpall, K. Rezvani, Safety, efficacy and determinants of response of allogeneic CD19-specific CAR-NK cells in CD19+ B cell tumors: a phase 1/2 trial, Nat. Med. 30 (2024) 772–784, https://doi.org/10.1038/s41591-023-02785-8.
[234] Z.P. Lin, L.N.M. Nguyen, B. Ouyang, P. MacMillan, J. Ngai, B.R. Kingston, S. M. Mladjenovic, W.C.W. Chan, Macrophages actively transport Nanoparticles in tumors after extravasation, ACS Nano 16 (2022) 6080–6092, https://doi.org/10.1021/acsnano.1c11578.
[235] S.-K. Baek, A.R. Makkouk, T. Krasieva, C.-H. Sun, S.J. Madsen, H. Hirschberg, Photothermal treatment of glioma; an in vitro study of macrophage-mediated delivery of gold nanoshells, J. Neuro-Oncol. 104 (2011) 439–448, https://doi.org/10.1007/s11060-010-0511-3.
[236] H. Kim, Y. Baek, T. Ha, D. Choi, W.J. Lee, Y. Cho, J. Park, S. Kim, J. Doh, Gold nanoparticle-carrying T cells for the combined Immuno-Photothermal therapy, Small n/a (2023) 2301377, https://doi.org/10.1002/smll.202301377.
[237] S.H. Kang, Y.K. Lee, I.S. Park, I.-K. Park, S.M. Hong, S.Y. Kwon, Y.H. Choi, S. J. Madsen, H. Hirschberg, S.J. Hong, Biomimetic gold Nanoshell-loaded macrophage for Photothermal biomedicine, Biomed. Res. Int. 2020 (2020) 5869235, https://doi.org/10.1155/2020/5869235.
[238] M. Xuan, J. Shao, L. Dai, J. Li, Q. He, Macrophage cell membrane camouflaged Au Nanoshells for in vivo prolonged circulation life and enhanced Cancer Photothermal therapy, ACS Appl. Mater. Interfaces 8 (2016) 9610–9618, https://doi.org/10.1021/acsami.6b00853.
[239] X. Huang, N. Kong, X. Zhang, Y. Cao, R. Langer, W. Tao, The landscape of mRNA nanomedicine, Nat. Med. 28 (2022) 2273–2287, https://doi.org/10.1038/s41591-022-02061-1.
[240] R. Huschka, J. Zuloaga, M.W. Knight, L.V. Brown, P. Nordlander, N.J. Halas, Light-induced release of DNA from gold Nanoparticles: Nanoshells and Nanorods, J. Am. Chem. Soc. 133 (2011) 12247–12255, https://doi.org/10.1021/ja204578e.
[241] H. Asanuma, Z. Jiang, K. Ikeda, K. Uosaki, H.-Z. Yu, Selective dehybridization of DNA–Au nanoconjugates using laser irradiation, Phys. Chem. Chem. Phys. 15 (2013) 15995–16000, https://doi.org/10.1039/C3CP52771A.
[242] F. Thibaudau, Ultrafast Photothermal release of DNA from gold Nanoparticles, J. Phy. Chem. Lett. 3 (2012) 902–907, https://doi.org/10.1021/jz3001213.
[243] A.M. Goodman, N.J. Hogan, S. Gottheim, C. Li, S.E. Clare, N.J. Halas, Understanding resonant light-triggered DNA release from Plasmonic Nanoparticles, ACS Nano 11 (2017) 171–179, https://doi.org/10.1021/acsnano.6b06510.
[244] R. Huschka, A. Barhoumi, Q. Liu, J.A. Roth, L. Ji, N.J. Halas, Gene silencing by gold Nanoshell-mediated delivery and laser-triggered release of antisense oligonucleotide and siRNA, ACS Nano 6 (2012) 7681–7691, https://doi.org/10.1021/nn301135w.
[245] S. Siddique, J.C.L. Chow, Gold Nanoparticles for drug delivery and Cancer therapy, Appl. Sci. 10 (2020) 3284, https://doi.org/10.3390/app10113824.
[246] J. You, G. Zhang, C. Li, Exceptionally high payload of doxorubicin in hollow gold Nanospheres for near-infrared light-triggered drug release, ACS Nano 4 (2010) 1033–1041, https://doi.org/10.1021/nn901181c.
[247] E.S. Levy, D.P. Morales, J.V. Garcia, N.O. Reich, P.C. Ford, Near-IR mediated intracellular uncaging of NO from cell targeted hollow gold nanoparticles, Chem. Commun. (2015), https://doi.org/10.1039/C5CC07989F.
[248] A.L. Oei, H.P. Kok, S.B. Oei, M.R. Horsman, L.J.A. Stalpers, N.A.P. Franken, J. Crezee, Molecular and biological rationale of hyperthermia as radio- and chemosensitizer, Adv. Drug Deliv. Rev. 163-164 (2020) 84–97, https://doi.org/10.1016/j.addr.2020.01.003.
[249] R.C. Rietbroek, D.M. Katschinski, M.H.E. Reijers, H.I. Robins, A. Geerdink, K. Tutsch, F. D'Oleire, J. Haveman, Lack of thermal enhancement for taxanes in vitro, Int. J. Hyperth. 13 (1997) 525–533, https://doi.org/10.3109/02656739709023551.
[250] A.M. Goodman, O. Neumann, K. Nørregaard, L. Henderson, M.-R. Choi, S.E. Clare, N.J. Halas, Near-infrared remotely triggered drug-release strategies for cancer treatment, Proc. Natl. Acad. Sci. 114 (2017) 12419–12424, https://doi.org/10.1073/pnas.1713137114.
[251] E. Villar-Alvarez, I. Golán-Cancela, A. Pardo, B. Velasco, J. Fernández-Vega, A. Cambón, A. Al-Modlej, A. Topete, S. Barbosa, J.A. Costoya, P. Taboada, Inhibiting HER3 Hyperphosphorylation in HER2-Overexpressing Breast Cancer through Multimodal Therapy with Branched Gold Nanoshells, Small n/a (2023) 2303934, https://doi.org/10.1002/smll.202303934.
[252] K. Kobayashi, N. Usami, E. Porcel, S. Lacombe, C. Le Sech, Enhancement of radiation effect by heavy elements, Mutation Research/Reviews in Mutation Research 704 (2010) 123–131, https://doi.org/10.1016/j.mrrev.2010.01.002.
[253] D.R. Cooper, D. Bekah, J. Nadeau, Gold Nanoparticles and their alternatives for radiation therapy enhancement, Front Chem. 2 (2014), https://doi.org/10.3389/fchem.2014.00086.
[254] P. Diagaradjane, A. Shetty, J.C. Wang, A.M. Elliott, J. Schwartz, S. Shentu, H. C. Park, A. Deorukhkar, R.J. Stafford, S.H. Cho, J.W. Tunnell, J.D. Hazle, S. Krishnan, Modulation of in vivo tumor radiation response via gold Nanoshell-mediated vascular-focused hyperthermia: characterizing an integrated Antihypoxic and localized vascular disrupting targeting strategy, Nano Lett. 8 (2008) 1492–1500, https://doi.org/10.1021/nl080496z.
[255] R.L. Atkinson, M. Zhang, P. Diagaradjane, S. Peddibhotla, A. Contreras, S. G. Hilsenbeck, W.A. Woodward, S. Krishnan, J.C. Chang, J.M. Rosen, Thermal enhancement with optically activated gold nanoshells sensitizes breast cancer stem cells to radiation therapy, Sci. Transl. Med. 2 (2010) 55ra79, https://doi.org/10.1126/scitranslmed.3001447.
[256] K.H. Tang, S. Ma, T.K. Lee, Y.P. Chan, P.S. Kwan, C.M. Tong, I.O. Ng, K. Man, K. F. To, P.B. Lai, CD133(+) liver tumor-initiating cells promote tumor angiogenesis, growth, and self-renewal through neurotensin/interleukin-8/CXCL1 signaling, Hepatology 55 (2012), https://doi.org/10.1002/hep.24739.
[257] R. Dent, M. Trudeau, K.I. Pritchard, W.M. Hanna, H.K. Kahn, C.A. Sawka, L. A. Lickley, E. Rawlinson, P. Sun, S.A. Narod, Triple-negative breast Cancer: clinical features and patterns of recurrence, American association for, Cancer Res. 13 (2007) 4429–4434, https://doi.org/10.1158/1078-0432.CCR-06-3045.
[258] P.N. Prasad, Light-activated therapy: Photodynamic therapy, in: Introduction to Biophotonics, John Wiley & Sons, Inc., 2004, pp. 433–463, https://doi.org/10.1002/0471465380.ch12.
[259] P. Agostinis, K. Berg, K.A. Cengel, T.H. Foster, A.W. Girotti, S.O. Gollnick, S. M. Hahn, M.R. Hamblin, A. Juzeniene, D. Kessel, M. Korbelik, J. Moan, P. Mroz, D. Nowis, J. Piette, B.C. Wilson, J. Golab, Photodynamic therapy of cancer: an update, CA Cancer J. Clin. 61 (2011) 250–281, https://doi.org/10.3322/caac.20114.
[260] S. Miraglia, W. Godfrey, A.H. Yin, K. Atkins, R. Warnke, J.T. Holden, R.A. Bray, E. K. Waller, D.W. Buck, A novel five-transmembrane hematopoietic stem cell antigen: isolation, characterization, and molecular cloning, Blood 90 (1997), https://doi.org/10.1182/blood.V90.12.5013.
[261] A. Topete, M. Alatorre-Meda, P. Iglesias, E.M. Villar-Alvarez, S. Barbosa, J. A. Costoya, P. Taboada, V. Mosquera, Fluorescent drug-loaded, polymeric-based, branched gold Nanoshells for localized multimodal therapy and imaging of Tumoral cells, ACS Nano 8 (2014) 2725–2738, https://doi.org/10.1021/nn406425h.
[262] H. Mohseni, A. Imanparast, S.S. Salarabadi, A. Sazgarnia, In vitro evaluation of the intensifying photodynamic effect due to the presence of plasmonic hollow gold nanoshells loaded with methylene blue on breast and melanoma cancer cells, Photodiagn. Photodyn. Ther. 40 (2022) 103065, https://doi.org/10.1016/j.pdpdt.2022.103065.
[263] D. Crosby, S. Bhatia, K.M. Brindle, L.M. Coussens, C. Dive, M. Emberton, S. Esener, R.C. Fitzgerald, S.S. Gambhir, P. Kuhn, T.R. Rebbeck, S. Balasubramanian, Early detection of cancer, Science 375 (2010) eaay9040, https://doi.org/10.1126/science.aay9040.
[264] J.C.Y. Kah, T.H. Chow, B.K. Ng, S.G. Razul, M. Olivo, C.J.R. Sheppard, Concentration dependence of gold nanoshells on the enhancement of optical coherence tomography images: a quantitative study, Appl. Opt. 48 (2009) D96–D108, https://doi.org/10.1364/AO.48.000D96.
[265] S.H. Syed, A.J. Coughlin, M.D. Garcia, S. Wang, J.L. West, K.V. Larin, I.V. Larina, Optical coherence tomography guided microinjections in live mouse embryos: high-resolution targeted manipulation for mouse embryonic research, Biomedo 20 (2015) 051020, https://doi.org/10.1117/1.JBO.20.5.051020.
[266] T. Muñoz-Ortiz, J. Hu, D.H. Ortgies, S. Shrikhande, P. Zamora-Perez, M. Granado, D. González-Hedström, M. de la Fuente-Fernández, Á.L. García-Villalón, L. Andrés-Delgado, E. Martín Rodríguez, R. Aguilar, F. Alfonso, J. García Solé, P. Rivera Gil, D. Jaque, F. Rivero, Molecular imaging of infarcted heart by biofunctionalized gold Nanoshells, Adv. Healthc. Mater. 10 (2021) 2002186, https://doi.org/10.1002/adhm.202002186.
[267] C. Loo, A. Lowery, N. Halas, J. West, R. Drezek, Immunotargeted Nanoshells for integrated Cancer imaging and therapy, Nano Lett. 5 (2005) 709–711, https://doi.org/10.1021/nl050127s.
[268] K. Nishida, G. Deka, N.I. Smith, S.-W. Chu, K. Fujita, Nonlinear scattering of near-infrared light for imaging Plasmonic Nanoparticles in deep tissue, ACS Photonics 7 (2020) 2139–2146, https://doi.org/10.1021/acsphotonics.0c00607.
[269] P. Xu, R. Wang, W. Yang, Y. Liu, D. He, Z. Ye, D. Chen, Y. Ding, J. Tu, Y. Shen, A DM1-doped porous gold nanoshell system for NIR accelerated redox-responsive release and triple modal imaging guided photothermal synergistic chemotherapy, J Nanobiotechnol. 19 (2021) 77, https://doi.org/10.1186/s12951-021-00824-5.
[270] W. Lu, Q. Huang, G. Ku, X. Wen, M. Zhou, D. Guzatov, P. Brecht, R. Su, A. Oraevsky, L.V. Wang, C. Li, Photoacoustic imaging of living mouse brain vasculature using hollow gold nanospheres, Biomaterials 31 (2010) 2617–2626. http://www.sciencedirect.com/science/article/pii/S0142961209013660.
[271] T. Mitcham, K. Dextraze, H. Taghavi, M. Melancon, R. Bouchard, Photoacoustic imaging driven by an interstitial irradiation source, Photoacoustics 3 (2015) 45–54. http://www.sciencedirect.com/science/article/pii/S2213597915000051.

[272] L.D.B. Manuel, V.D. Vincely, C.L. Bayer, K.M. McPeak, Monodisperse Sub-100 nm Au Nanoshells for Low-Fluence deep-tissue photoacoustic imaging, Nano Lett. 23 (2023) 7334–7340, https://doi.org/10.1021/acs.nanolett.3c01696.
[273] L. Min-Ho, V. Nammalvar, A. Gobin, J. Barton, J. West, R. Drezek, Nanoshells as contrast agents for scatter-based optical imaging, 3rd IEEE international symposium on biomedical imaging: Nano to macro, Arlington, VA, 2006, pp. 371–374, https://doi.org/10.1109/ISBI.2006.1624930.
[274] P. Libby, The changing landscape of atherosclerosis, Nature 592 (2021) 524–533, https://doi.org/10.1038/s41586-021-03392-8.
[275] T.-F. Yu, K. Wang, L. Yin, W.-Z. Li, C.-P. Li, W. Zhang, J. Tian, W. He, A molecular probe carrying anti-tropomyosin 4 for early diagnosis of cerebral ischemia/reperfusion injury, Neural Regen. Res. 18 (2023), https://doi.org/10.4103/1673-5374.357907.
[276] Y. Mantri, J.V. Jokerst, Engineering Plasmonic Nanoparticles for enhanced photoacoustic imaging, ACS Nano 14 (2020) 9408–9422, https://doi.org/10.1021/acsnano.0c05215.
[277] L. Xiang, X. Da, H. Gu, D. Yang, L. Zeng, S. Yang, International symposium on biophotonics, Nanophotonics and Metamat. 2006 (2006) 76–79.
[278] L. Meng-Lin, C.W. James, A.S. Jon, L.G.-S. Kelly, D.V.M. George Stoica, V. W. Lihong, In-vivo photoacoustic microscopy of nanoshell extravasation from solid tumor vasculature, Biomedo 14 (2009) 010507, https://doi.org/10.1117/1.3081556.
[279] W.R. Zipfel, R.M. Williams, R. Christie, A.Y. Nikitin, B.T. Hyman, W.W. Webb, Live tissue intrinsic emission microscopy using multiphoton-excited native fluorescence and second harmonic generation, Proc. Natl. Acad. Sci. 100 (2003) 7075–7080, https://doi.org/10.1073/pnas.0832308100.
[280] N.J. Durr, T. Larson, D.K. Smith, B.A. Korgel, K. Sokolov, A. Ben-Yakar, Two-photon luminescence imaging of Cancer cells using molecularly targeted gold Nanorods, Nano Lett. 7 (2007) 941–945, https://doi.org/10.1021/nl062962v.
[281] H. Wang, T.B. Huff, D.A. Zweifel, W. He, P.S. Low, A. Wei, J.-X. Cheng, In vitro and in vivo two-photon luminescence imaging of single gold nanorods, Proc. Natl. Acad. Sci. 102 (2005) 15752–15756, https://doi.org/10.1073/pnas.0504892102.
[282] N. Gao, Y. Chen, L. Li, Z. Guan, T. Zhao, N. Zhou, P. Yuan, S.Q. Yao, Q.-H. Xu, Shape-dependent two-photon photoluminescence of single gold Nanoparticles, J. Phys. Chem. C (2014), https://doi.org/10.1021/jp502038v.
[283] H. Park, J. Yang, S. Seo, K. Kim, J. Suh, D. Kim, S. Haam, K.-H. Yoo, Multifunctional Nanoparticles for Photothermally controlled drug delivery and magnetic resonance imaging enhancement, Small 4 (2008) 192–196, https://doi.org/10.1002/smll.200700807.
[284] A. Pardo, S. Yáñez, Y. Piñeiro, R. Iglesias-Rey, A. Al-Modlej, S. Barbosa, J. Rivas, P. Taboada, Cubic anisotropic co- and Zn-substituted ferrite Nanoparticles as multimodal magnetic agents, ACS Appl. Mater. Interfaces 12 (2020) 9017–9031, https://doi.org/10.1021/acsami.9b20496.
[285] A. Pardo, B. Pelaz, J. Gallo, M. Bañobre-López, W.J. Parak, S. Barbosa, P. del Pino, P. Taboada, Synthesis, characterization, and evaluation of superparamagnetic doped ferrites as potential therapeutic Nanotools, Chem. Mater. 32 (2020) 2220–2231, https://doi.org/10.1021/acs.chemmater.9b04848.
[286] E. Polo, P. del Pino, A. Pardo, P. Taboada, B. Pelaz, Magnetic Nanoparticles for Cancer therapy and bioimaging, in: G. Gonçalves, G. Tobias (Eds.), Nanooncology: Engineering Nanomaterials for cancer Therapy and Diagnosis, Springer International Publishing, Cham, 2018, pp. 239–279, https://doi.org/10.1007/978-3-319-89878-0_7.
[287] G. Brennan, N.D. Thorat, M. Pescio, S. Bergamino, J. Bauer, N. Liu, S.A.M. Tofail, C. Silien, Spectral drifts in surface textured Fe3O4-Au, core–shell nanoparticles enhance spectra-selective photothermal heating and scatter imaging, Nanoscale 12 (2020) 12632–12638, https://doi.org/10.1039/D0NR01463J.
[288] S. Rahmati, A.E. David, A review of design criteria for cancer-targeted, nanoparticle-based MRI contrast agents, Appl. Mater. Today 37 (2024) 102087, https://doi.org/10.1016/j.apmt.2024.102087.
[289] R. Lapusan, R. Borlan, M. Focsan, Advancing MRI with magnetic nanoparticles: a comprehensive review of translational research and clinical trials, Nanoscale Adv. (2024), https://doi.org/10.1039/D3NA01064C.
[290] Y. Kadria-Vili, O. Neumann, Y. Zhao, P. Nordlander, G.V. Martinez, J.A. Bankson, N.J. Halas, Gd2O3-mesoporous silica/gold nanoshells: a potential dual T1/T2 contrast agent for MRI-guided localized near-IR photothermal therapy, Proc. Natl. Acad. Sci. 119 (2022) e2123527119, https://doi.org/10.1073/pnas.2123527119.
[291] J.C. Park, S. Yeo, M. Kim, G.T. Lee, J.H. Seo, Synthesis and characterization of novel lanthanide-doped magnetite@Au core@shell nanoparticles, Mater. Lett. 181 (2016) 272–277, https://doi.org/10.1016/j.matlet.2016.06.050.
[292] Y.-C. Lin, E. Perevedentseva, Z.-R. Lin, C.-C. Chang, H.-H. Chen, S.-M. Yang, M.-D. Lin, A. Karmenyan, G. Speranza, L. Minati, C. Nebel, C.-L. Cheng, Multimodal bioimaging using nanodiamond and gold hybrid nanoparticles, Sci. Rep. 12 (2022) 5331, https://doi.org/10.1038/s41598-022-09317-3.
[293] C. de la Encarnación, E. Lenzi, M. Henriksen-Lacey, B. Molina, K. Jenkinson, A. Herrero, L. Colás, P. Ramos-Cabrer, J. Toro-Mendoza, I. Orue, J. Langer, S. Bals, D. Jimenez de Aberasturi, L.M. Liz-Marzán, Hybrid magnetic–plasmonic nanoparticle probes for multimodal bioimaging, J. Phys. Chem. C 126 (2022) 19519–19531, https://doi.org/10.1021/acs.jpcc.2c06299.
[294] M. Holzinger, A. Le Goff, S. Cosnier, Nanomaterials for biosensing applications: a review, Front. Chem. 2 (2014), https://doi.org/10.3389/fchem.2014.00063.
[295] S. Zeng, K.-T. Yong, I. Roy, X.-Q. Dinh, X. Yu, F. Luan, A review on functionalized gold Nanoparticles for biosensing applications, Plasmonics 6 (2011) 491–506, https://doi.org/10.1007/s11468-011-9228-1.
[296] Y. Sun, Y. Xia, Synthesis of gold Nanoshells and their use in sensing applications, MRS Online Proceedings Library (OPL) 776 (2003) Q2.7. https://www.cambridge.org/core/article/synthesis-of-gold-nanoshells-and-their-use-in-sensing-applications/302C4555124499998C1474CDE16F0544.
[297] M. Perfezou, A. Turner, A. Merkoci, Cancer detection using nanoparticle-based sensors, Chem. Soc. Rev. 41 (2012) 2606–2622, https://doi.org/10.1039/C1CS15134G.
[298] G. Raschke, S. Brogl, A.S. Susha, A.L. Rogach, T.A. Klar, J. Feldmann, B. Fieres, N. Petkov, T. Bein, A. Nichtl, K. Kürzinger, Gold Nanoshells improve single nanoparticle molecular sensors, Nano Lett. 4 (2004) 1853–1857, https://doi.org/10.1021/nl049038q.
[299] L.R. Hirsch, J.B. Jackson, A. Lee, N.J. Halas, J.L. West, A whole blood immunoassay using gold Nanoshells, Anal. Chem. 75 (2003) 2377–2381, https://doi.org/10.1021/ac0262210.
[300] H. He, X. Xu, H. Wu, Y. Jin, Enzymatic Plasmonic engineering of ag/Au bimetallic Nanoshells and their use for sensitive optical glucose sensing, Adv. Mater. 24 (2012) 1736–1740, https://doi.org/10.1002/adma.201104678.
[301] J.B. Jackson, N.J. Halas, Surface-enhanced Raman scattering on tunable plasmonic nanoparticle substrates, Proc. Natl. Acad. Sci. 101 (2004) 17930–17935. http://www.pnas.org/content/101/52/17930.abstract.
[302] K.N. Heck, B.G. Janesko, G.E. Scuseria, N.J. Halas, M.S. Wong, Using catalytic and surface-enhanced Raman spectroscopy-active gold Nanoshells to understand the role of basicity in glycerol oxidation, ACS Catal. 3 (2013) 2430–2435, https://doi.org/10.1021/cs400643f.
[303] C. Liu, H. Wang, S. Xu, H. Li, Y. Lu, C., Zhu, Chemosensors, in, 2023.
[304] G.V.P. Kumar, S. Shruthi, B. Vibha, B.A.A. Reddy, T.K. Kundu, C. Narayana, Hot spots in ag Core−Au Shell Nanoparticles potent for surface-enhanced Raman scattering studies of biomolecules, J. Phys. Chem. C 111 (2007) 4388–4392, https://doi.org/10.1021/jp068253n.
[305] T.B. Hope, B.C. Christopher, A.G. Theresa, L.C. Gerard, Proc.SPIE, 2008 686904, https://doi.org/10.1117/12.763888.
[306] J. Jiang, C. Auchinvole, K. Fisher, C.J. Campbell, Quantitative measurement of redox potential in hypoxic cells using SERS nanosensors, Nanoscale 6 (2014) 12104–12110, https://doi.org/10.1039/C4NR01263A.
[307] R.E. Wilson Jr., R. O'Connor, C.E. Gallops, E.A. Kwizera, B. Noroozi, B.I. Morshed, Y. Wang, X. Huang, Immunomagnetic capture and multiplexed surface marker detection of circulating tumor cells with magnetic multicolor surface-enhanced Raman scattering Nanotags, ACS Appl. Mater. Interfaces 12 (2020) 47220–47232, https://doi.org/10.1021/acsami.0c12395.
[308] S. Bock, Y.-S. Choi, M. Kim, Y. Yun, X.-H. Pham, J. Kim, B. Seong, W. Kim, A. Jo, K.-M. Ham, S.G. Lee, S.H. Lee, H. Kang, H.S. Choi, D.H. Jeong, H. Chang, D.-E. Kim, B.-H. Jun, Highly sensitive near-infrared SERS nanoprobes for in vivo imaging using gold-assembled silica nanoparticles with controllable nanogaps, J Nanobiotechnol. 20 (2022) 130, https://doi.org/10.1186/s12951-022-01327-7.
[309] W. Zhao, D. Zhang, T. Zhou, J. Huang, Y. Wang, B. Li, L. Chen, J. Yang, Y. Liu, Aptamer-conjugated magnetic Fe3O4@Au core-shell multifunctional nanoprobe: a three-in-one aptasensor for selective capture, sensitive SERS detection and efficient near-infrared light triggered photothermal therapy of Staphylococcus aureus, Sensors Actuators B Chem. 350 (2022) 130879. https://www.sciencedirect.com/science/article/pii/S0925400521014477.
[310] O. Anca, J. Ancuta, M. Cristian, B.-N. Ioana, Theranostic Nanoparticles and Their Spectrum in Cancer, in: A. Sorin Marius, A. Kalsoom, F. Irina, K. Sher Bahadar, A. Fayaz, M.A. Abdullah (Eds.) Engineered Nanomaterials, IntechOpen, Rijeka, 2019, https://doi.org/10.5772/intechopen.88097 pp. Ch. 7.
[311] E. Villar-Alvarez, A. Cambón, A. Pardo, V.X. Mosquera, A. Bouzas-Mosquera, A. Topete, S. Barbosa, P. Taboada, V. Mosquera, Gold Nanorod-based Nanohybrids for combinatorial therapeutics, ACS Omega 3 (2018) 12633–12647, https://doi.org/10.1021/acsomega.8b01591.
[312] E. Villar-Alvarez, A. Cambón, A. Pardo, L. Arellano, A.V. Marcos, B. Pelaz, P. del Pino, A. Bouzas Mosquera, V.X. Mosquera, A. Almodlej, G. Prieto, S. Barbosa, P. Taboada, Combination of light-driven co-delivery of chemodrugs and plasmonic-induced heat for cancer therapeutics using hybrid protein nanocapsules, J Nanobiotechnol. 17 (2019) 106, https://doi.org/10.1186/s12951-019-0538-3.
[313] S. Barbosa, A. Topete, M. Alatorre-Meda, E.M. Villar-Alvarez, A. Pardo, C. Alvarez-Lorenzo, A. Concheiro, P. Taboada, V. Mosquera, Targeted combinatorial therapy using gold Nanostars as Theranostic platforms, J. Phys. Chem. C 118 (2014) 26313–26323, https://doi.org/10.1021/jp505979e.
[314] B. Campos, C.C. Herold-Mende, Insight into the complex regulation of CD133 in glioma, Int. J. Cancer 128 (2011), https://doi.org/10.1002/ijc.25687.
[315] H. Jang, Y.-K. Kim, H. Huh, D.-H. Min, Facile synthesis and Intraparticle self-catalytic oxidation of dextran-coated hollow Au–ag Nanoshell and its application for chemo-thermotherapy, ACS Nano 8 (2014) 467–475, https://doi.org/10.1021/nn404833b.
[316] J. Ibarra, D. Encinas-Basurto, M. Almada, J. Juárez, M.A. Valdez, S. Barbosa, P. Taboada, Gold Nanorods with mesoporous silica Shell: a promising platform for cisplatin delivery, Micromachines 14 (2023) 1031, https://doi.org/10.3390/mi14051031.
[317] J.M. Stern, V.V. Kibanov Solomonov, E. Sazykina, J.A. Schwartz, S.C. Gad, G. P. Goodrich, Initial evaluation of the safety of Nanoshell-directed Photothermal therapy in the treatment of prostate disease, Int. J. Toxicol. 35 (2015) 38–46, https://doi.org/10.1177/1091581815600170.
[318] A. Pardo, R. Pujales, M. Blanco, E.M. Villar-Alvarez, S. Barbosa, P. Taboada, V. Mosquera, Analysis of the influence of synthetic paramaters on the structure and physico-chemical properties of non-spherical iron oxide nanocrystals and their biological stability and compatibility, Dalton Trans. 45 (2016) 797–810, https://doi.org/10.1039/C5DT03923A.

[319] A. Pardo, M. Gomez-Florit, M.D. Davidson, M.Ö. Öztürk-Öncel, R.M. A. Domingues, J.A. Burdick, M.E. Gomes, Hierarchical Design of Tissue-Mimetic Fibrillar Hydrogel Scaffolds, Adv. Healthc. Mater. n/a (2024) 2303167, https://doi.org/10.1002/adhm.202303167.

[320] S.M. Bakht, A. Pardo, M. Gómez-Florit, R.L. Reis, R.M.A. Domingues, M.E. Gomes, Engineering next-generation bioinks with nanoparticles: moving from reinforcement fillers to multifunctional nanoelements, J. Mater. Chem. B 9 (2021) 5025–5038, https://doi.org/10.1039/D1TB00717C.

[321] C. Alvarez-Lorenzo, M. Zarur, A. Seijo-Rabina, B. Blanco-Fernandez, I. Rodríguez-Moldes, A. Concheiro, Physical stimuli-emitting scaffolds: the role of piezoelectricity in tissue regeneration, Mat. Today Bio. 22 (2023) 100740, https://doi.org/10.1016/j.mtbio.2023.100740.

[322] C. Stenner, L.-H. Shao, N. Mameka, J. Weissmüller, Piezoelectric gold: strong charge-load response in a metal-based hybrid nanomaterial, Adv. Funct. Mater. 26 (2016) 5174–5181, https://doi.org/10.1002/adfm.201600938.